MAXIMIZING THE COVERAGE AND UTILITY OF MULTIBEAM BACKSCATTER FOR SEAFLOOR CLASSIFICATION

by

Aluizio Maciel de Oliveira Junior

B.Sc.Eng. Electronics, Navy School, Brazil, 1994
Extension, Hydrography, Directorate of Hydrography and Navigation, Brazil, 1998

A Thesis Submitted in Partial Fulfillment of
the Requirements for the Degree of

Master of Science in Engineering

In the Graduate Academic Unit of Geodesy and Geomatics Engineering

Supervisor: John E. Hughes Clarke, Ph.D., Geodesy and Geomatics Engineering

Examining Board: Marcelo Santos, Ph.D., Geodesy and Geomatics Engineering

External Examiner: Robert C. Courtney, Ph.D., Geological Survey of Canada

This thesis is accepted by the Dean of Graduate Studies

THE UNIVERSITY OF NEW BRUNSWICK

July, 2007

DEDICATION

For my love, my wife Isabela.

ABSTRACT

This thesis is focused on the backscatter strength data collected by the Brazilian Navy with the Simrad EM1000 multibeam echosounder installed onboard the Hydrographic ship Taurus. Data have been collected since 1999 as part of the national hydrographic mapping program. During this period, the echosounder was operating primarily in the equiangle beam spacing (EABS) +/-75^{o} angular sector, with survey lines spacing achieving 200% coverage.

Although bathymetric data have been already processed for chart production, valuable backscatter has not been analysed until this present study. Backscatter is a useful tool for the task of seafloor classification, as long as it is compensated for the radiometric and geometric artefacts.

With the aid of Ocean Mapping Group (OMG) software, data artefacts related to the angular response effect and beam-to-beam variations have been normalized. This research developed additional algorithms capable of reducing artefacts related to within-beam directivity pattern. This processing enhanced the quality of external amplitude traces logged beyond the -3 dB limits of the outermost beams. Through this approach, the usable backscatter coverage has been expanded by 28%.

Taking advantage of the expanded coverage, outermost beams are now used to replace the noisy inner beams of adjacent lines during mosaicking construction. This alternative mosaicking method, using higher weights for outer beams, delivers backscatter mosaics with reduced along-track printed artefacts. As a complementary addition to backscatter mosaics enhancements, a parallel study has been undertaken, which uses digital image analysis techniques to reduce the remaining along-track

artefacts printed in the same direction of the survey lines. This technique uses two-dimensional Fourier transform to bring the mosaic to the frequency domain where structured directional noise can be filtered out.

Building on the increased coverage and removal of within-beam pattern artefacts, power spectral analysis algorithms were implemented to explore the lower grazing angle data. A dynamically-located classification box scheme identifies and uses the most valuable region of the swath for statistical and power spectral analysis. The resulting maps of these variables cover the entire survey area and add further degrees of freedom towards successful seafloor segmentation.

Finally, the same software that has been implemented for the EM1000 multibeam was also adopted to work specifically on the outermost beams of the newer EM710 multibeam. The EM710 data have been collected by the CCGS Matthew operating in the equidistance beam spacing (EDBS) +/-65^{o} mode (with only one swath per ping cycle at this time). But, this newer sonar is going to operate with multiple across-track swaths per ping cycle, which gets around the bathymetric requirement of narrowing the angular sector to achieve better along-track spacing. Therefore, improvements described here for the EM1000 wide angular sector (+/-75^{o}) can be also useful for the EM710 echosounder in the future surveys.

ACKNOWLEDGEMENTS

Firstly, I would like to thank the Brazilian Navy for the funds provided for this course, which enhanced my knowledge about Hydrography, Oceanography and Geology. In addition, the thesis research brought me detailed information about multibeam backscatter and seafloor classification. I wish these studies will be useful in my future works serving the Navy.

I also thank the following people who helped me during these two years of research:

- Capt. Norberto Bento, Cmd. Edson Magno and LCmd. Izabel King (Centro de Hidrografia da Marinha) for the EM1000 data provided for my research and technical information exchanged;
- LCom. Jim Bradford (Canadian Navy Route Survey Group) and Mike Lamplugh (Canadian Hydrographic Service) for the opportunity to go onboard the CCGS Matthew, where newer EM710 multibeam echosounder has been operated;
- Dr. John Hughes Clarke (Ocean Mapping Group) for the opportunity of working with the EM3002 multibeam echosounder in the Heron launch during the Hydrocamp 2006;
- Dr. Alberto Figueiredo (Universidade Federal Fluminense), Cmd. Alberto Costa Neves (Navio Hidrográfico Sírius) and LCmd. Isabel Peres (Diretoria de Hidrografia da Marinha) for the Amazon River Delta information provided, which helped my work with GGE 6022 course;

- Felipe Nievinski (UNB Geodesy Group) for the help with Matlab programming in GGE 5013 course; and
- Steve Brucker (Ocean Mapping Group) and Daniel Cid (Q1 Labs) for the assistance with Linux and OMG software installations in my laptop.

I also thank the following groups for their friendship: Geodesy and Geomatics Department and Ocean Mapping Group (including professors, secretaries and students); fellows from other Navies (Chile, Portugal and Spain); and Brazilian community in Fredericton.

Thanks to my mother Maria, my parents-in-law Daisy and Mário, my family and friends that have been cheering for my success from Brazil.

Special thanks to my supervisor Dr. John Hughes Clarke who guided me with his wisdom to clarify my doubts about the complex backscatter subject. Also thanks to my co-supervisor Dr. Marcelo Santos who provided intelligent advises during my work.

Finally, thanks for my lovely wife Isabela and our dog Brenda. You kept our home warm even during the long and cold winters of Fredericton, which is a very nice city. Isabela has been my strongest enforcement since we met in 1993.

TABLE OF CONTENTS

LIST OF FIGURES

Chapter 1: INTRODUCTION

The main problem studied in this thesis concerns the reduction of the backscatter artefacts present in the Brazilian Navy EM1000 multibeam echosounder data and solutions for mosaicking and seafloor classification tasks using these data.

There have been extensive studies concerning backscatter artefacts reduction. But, each sonar system has its particular characteristics, which produces different artefacts. Beaudoin et al. [2002] analysed the Reson 8101 system, where radiometric (transmit power and receiver gain) and geometric (slant range to horizontal range) artefacts were the main problems. In Intelmann et al. [2006], the Reson 8101 software was expanded to work also for the Reson 8125 and beam-pattern and angular response effects were included in the processing. The Simrad systems also have their particularities already studied. Hughes Clarke et al. [1996] detailed the various bathymetric and backscatter artefacts for the EM100 and EM1000 sonars. Hellequin et al. [1997; 2003] also analysed the EM1000 sonars and particularly discussed limitations while processing near-nadir beams in the equidistance beam spacing (EDBS) mode. They implemented a heuristic model to extract the array directivity pattern, which was used for artefact reduction. Augustin and Lurton [2005] analysed multi-sector artefacts for the EM300 and applied filters to remove speckle noise. Llewellyn [2006] also described EM300 multi-sector issue, but for the ice window installation of the Canadian Coast Guard Ship Amundsen. Therefore, any sonar has particular issues to be addressed.

For the case of the Brazilian Navy EM1000 sonar, the system has been primarily operated for 7 years in the equiangle beam spacing (EABS) mode. A decision was taken

to use +/-75° angular sector (~7.5x the water depth) and 200% coverage. This configuration allowed a swath coverage nearly twice as wide as most other hydrographic agencies, which have been using primarily narrower (+/-60°) angular sectors. Figure 1.1 illustrates this geometry, where one can also observe that wider sector causes along-track coverage loss due to two-way travel time limitations.

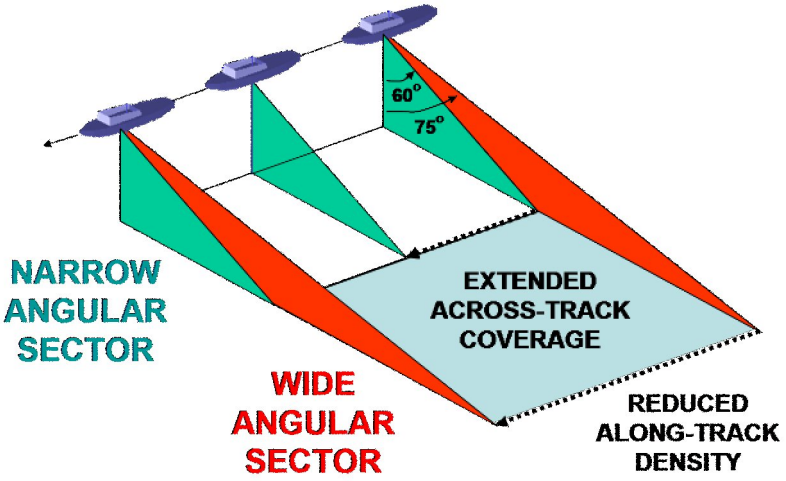

Figure 1.1 Comparison between wide angular sector (+/-75°) used by the Brazilian Navy and the narrow angular sector (+/-60°) normally used by other hydrographic agencies. Swath across-track coverage extends nearly twice as far. The detrimental aspect, of course, is the loss in the along-track sounding density.

The Brazilian Navy purpose for using EABS (+/-75°) was to maintain an enhanced beam density in the inner regions while simultaneously using the sparse outer beams distribution as a means of detecting refraction problems during survey. This provides an indicator for when it might be necessary to obtain new sound velocity casts.

A serendipitous by-product of this policy, however, was the collection of additional extra valuable backscatter information that is suitable for power spectral classification methods. To be used for this purpose, however, the data need to be properly reduced for geometric and radiometric artefacts. Prior to this study, only secondary importance was

placed on the processing of the backscatter that had been collected. Maps have been produced with backscatter information provided in the Simrad sonar image telegrams, which normally has simplistic corrections applied during data acquisition. Therefore, further detailed analysis is necessary to properly reduce the many artefacts.

In order to better apply this backscatter data, the principal effort of this thesis is to identify and reduce the main artefacts for the specific configuration (wide angular sector EABS +/-75^{o} mode with 200% coverage) used by the Brazilian Navy with the Hydrographic Ship Taurus.

As commented, Hellequin et al. [1997; 2003] presented detailed information about the EM1000 system artefacts, in particular analyzing an example of EDBS data. They used an approach for artefacts reduction that includes the following main steps: 1) restoring Lambert's law, 2) heuristic model fitting, 3) extracting directivity patterns and 4) reducing directivity for each beam/emission angle.

Here in this study, the implemented approach worked to build upon the software (getBeamPatt) already being used in the Ocean Mapping Group (OMG), which was able to reduce artefacts related to the angular response and beam-to-beam amplitude oscillations.

For that, new software termed "traceBP" has been implemented. It uses the following steps: 1) extracts time series amplitudes within each beam and arranges them with relation to their incidence angles, 2) Least squares fitting is used to generate a suitable function that best describes the inside-beam pattern variation about each beam boresite and 3) This function is then used for trace amplitudes normalization.

Processing results showed that outermost beams, in particular, exhibit amplitude variations greater than 10 dB. This indicates that, for these beams, backscatter is logged beyond the -3 dB beam limits. As EABS +/-75^{o} mode has been used, this extended data covers an area corresponding to approximately 28% of the entire swath. Other beams present backscatter oscillation usually smaller than 3 dB, but can have greater variations if a neighboring beam loses the seafloor tracking.

Processed backscatter, including the extended range of the outermost beam traces, was used for mosaic creation. Backscatter mosaicking deals with the problem of deciding the value to represent image pixels from backscatter amplitudes when they occupy the same geographical position. Several approaches can be used for mosaicking. Augustin et al. [1996] described their technique to mosaic the EM12 along-track samples. They averaged the over-sampled outer beams, which have elongated footprints. Fonseca and Calder [2005] used a priority table based on distance between samples and ship's track and a blending algorithm to minimize seams. Caris HIPS/SIPS software [2005] uses three methods: auto-seam (higher priority for near-nadir beams), shine-thru (higher priority for the greater amplitudes) and overwrite (higher priority for the most recent in time). Intelmann et al. [2006] decided to not use the backscatter traces logged beyond the centre of the outermost beams during mosaicking process.

In this study, an alternative method has been implemented to replace the noisy inner beams amplitudes by the outer beams (including the outermost beam traces). For that, the traditional weighting function (auto-seam) normally used in commercial packages has been applied in the reverse way. This modification permits a significant improvement in

the backscatter mosaic quality. This is primarily achieved through the considerable reduction of along-track artefacts when compared to the traditional weighting method.

A parallel study has been done with digital image analysis working on the georeferenced mosaics. Parker [1997] describes the structured noise, which is similar to the nadir residuals commonly observed in the backscatter mosaics. Existing Fourier transform (2D-FFT) software [Parker, 1997] was used to convert mosaics to the frequency domain. Working in this domain, one algorithm termed "bsfilter" (backscatter filter) was implemented here to reduce the spectral noise concentrated in angular sectors (perpendicular to the survey line direction).

The final step in the new processing sequence was the implementation of seafloor characterization. Previous works attempted a variety of approaches for this task, as the examples listed:

1. Textural methods such as gray-level co-occurrence matrices (GLCM) [Pace and Dyer, 1979; Haralick, 1979; Reed and Hussong, 1989; Imen et al., 2005];
2. Angular response characterization [deMoustier and Alexandrou, 1991; Matsumoto et al., 1993; Hughes Clarke, 1994];
3. Fractal analysis [Linnett et al., 1991; Carmichael et al., 1996];
4. Probability density function (PDF) [Stanton, 1984; de Moustier, 1986; Alexandrou et al., 1992; Stewart et al. 1994]; and
5. Power spectral methods [Pace and Gao, 1988; Tamsett, 1993; Lurton et al., 1994; Hughes Clarke, 2004].

The OMG has already developed an algorithm termed “classSS”, which produces statistical and power spectral analyses for sidescan sonar [Hughes Clarke, 2004]. In this thesis research, the OMG algorithm was adapted to cope with the higher grazing angles common in multibeam sonars. Software implemented can detect outer pixels range and auto-adjust for depth oscillations. In addition, the user can choose the classification outer angular limits (to explore the extended outer traces range) and inner angular limits (to avoid the noisy nadir region). Classification products include statistical and power spectral maps covering the entire survey area. These extra maps augment the degrees of freedom for the classification task. They permit the better segmentation of different seafloor types, particularly those ones presenting the same mean backscatter strength.

Software developments created for the EM1000 sonar were also adopted to work with the EM710. For that, dataset was collected by the Canadian Coast Guard Ship (CCGS) Matthew in the EDBS +/-65^{o} mode at Esquimalt area, close to Halifax harbour, in May 2006. The actual sonar configuration has 0.5^{o} x 1.0^{o} transmit-receive beam width and only one swath per ping cycle. But, this newer sonar (EM710) is starting to operate with multiple swaths per ping cycle. Therefore, future surveys can use the wider angular sector (+/-75^{o}) without compromising the along-track ping density required for bathymetric purposes.

Chapter 2: EM1000 BACKSCATTER PROCESSING

Multibeam backscatter has been used extensively as a source for seafloor classification. The backscattered energy that returns to the ship depends both on the seafloor physical properties themselves and also on the sonar configuration, water column propagation and measurement geometry. These last geometric and radiometric modulations on the backscatter intensity must be reduced, such that the backscatter strength represents only inherent properties of the seafloor. Thus, might become a useful signal for the task of seafloor characterization.

In this chapter, the entire EM1000 backscatter processing adopted is described. For that, the following subjects are discussed:

- Quick overview of the EM1000 general specifications that are necessary for the comprehension of further backscatter analysis.
- Characteristics of "raw" backscatter data delivered in the Simrad sonar image telegram. The simplistic compensations applied during data acquisition are explained.
- Backscatter formats recorded in the sonar image and depth telegrams.
- OMG software (getBeamPattern.c) used for data processing and related improvements bound to the angular response effects and beam-to-beam average amplitude variations.
- New software (traceBP.c) implemented for this thesis and reduction of artefacts related to the inside-beams directivity pattern.
- Solution used to fill the inter-pings gaps (beam-hopping) of outermost beams.
- Comparison between backscatter patterns mapped during different surveys.

2.1 EM1000 system specifications

An EM1000 multibeam echosounder was installed in the Hydrographic ship Taurus (Figure 2.1) in 1998.

Figure 2.1 Brazilian hydrographic ship Taurus had the EM1000 system installed in 1998.

The transducer is mounted fixed in prominent structure in the keel (Figure 2.2), which increased ship's draft by 0.5 m. Now, the draft is approximately 3.5 m with small variations depending on ship's loading. The transducer has an arcuate shape with 128 ceramic staves (each stave has 5 along-track elements). The transmit (TX) acoustic fan has a maximum of +/- 85^{o} across-track angular sector (wider than receive sector to allow for roll) and 3.3^{o} along-track beamwidth. Receive (RX) beams have both across-track and along-track beam width of 3.3^{o}. The product between transmit and receive beams generates an effective along-track beam width of 2.4^{o}.

Figure 2.2 EM1000 transducer installed in a fixed-mounted way in the prominent structure (0.5 m height) at the keel of the Hydrographic Ship Taurus.

The sonar operates at 95 KHz frequency and can use many different modes. The list of modes available includes the shallow (0.2 ms pulse length), medium (0.7 ms) and deep (2.0 ms) options. In this study, only shallow mode data have been analysed reflecting the current predominant focus of the Brazilian Navy on the inner continental shelf (<100 m depth), where the major navigation issues exist.

Shallow mode has 60 roll-stabilized beams, which can be spaced in the equiangle beam spacing (EABS) or in the equidistance beam spacing (EDBS) as presented in Figure 2.3.

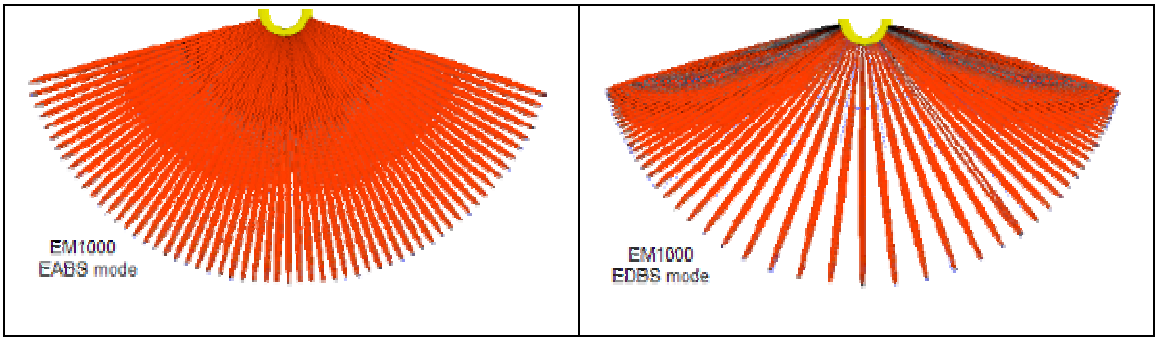

Figure 2.3 The EM1000 shallow modes: (left) equiangle beam spacing mode and (right) equidistance beam spacing mode [from Hughes Clarke, 2005a].

Previous works [Hellequin et al., 1997; 2003] described the processes involved in EM1000 backscatter artefact cleaning for the case of equidistance beam spacing (EDBS). In this beam spacing mode, particular attention needed to be paid to the fact that the inner beams were spaced much wider than their -3 dB beam widths. Figure 2.4 shows the coverage of each of the 60 beams for the EDBS mode.

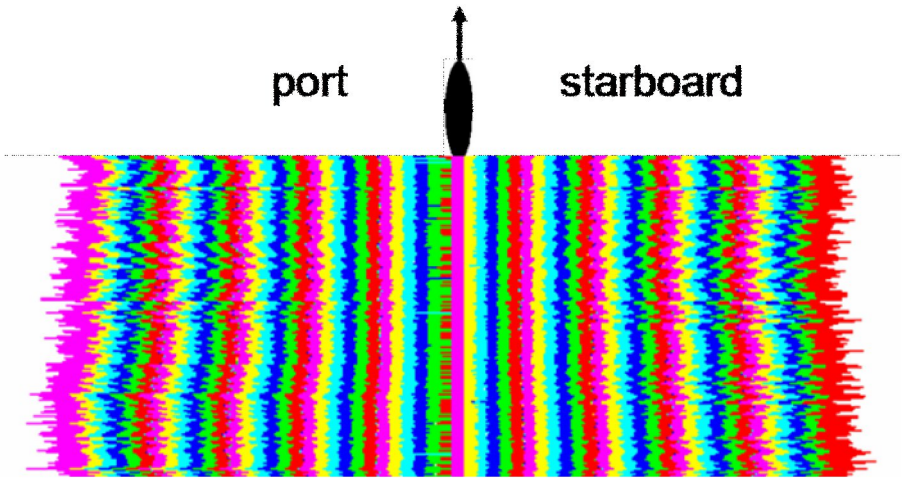

Figure 2.4 Equidistance beam spacing (EDBS) +/-75^{o} mode and the correspondent coverage for each of the 60 beams.

With the EABS data collected herein, the main focus of the backscatter artefact cleaning is to cope with the outer beams artefacts. These resulted from the system logging additional backscatter data beyond the half beam width of the outermost beam. A pleasant by-product of this extra logging is that the effective backscatter swath width markedly increased. Figure 2.5 presents the coverage of each of the 60 beams within EABS mode. The outermost beams importance is visually evident as they represent up to 28% of the entire coverage.

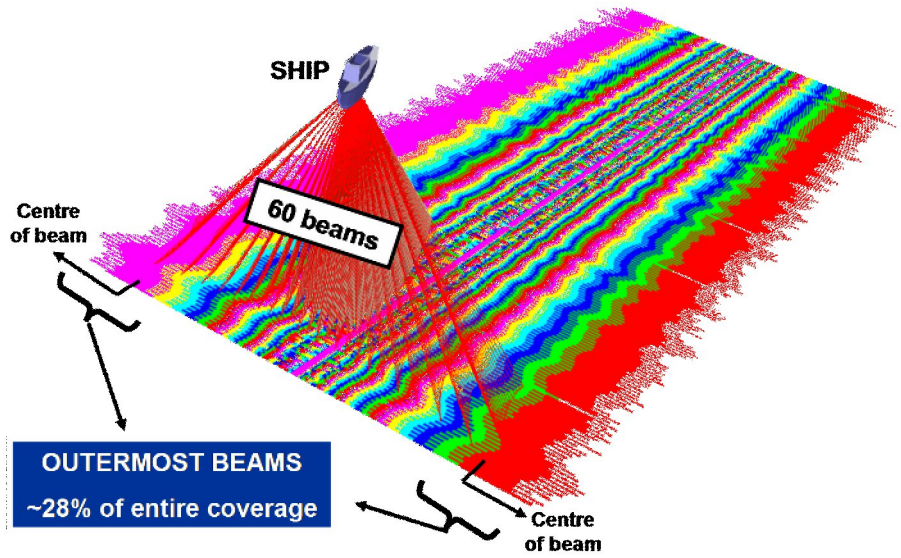

Figure 2.5 The 60 beams coverage areas and the extended area of the outermost beams.

During the acquisition of the raw intensity time series for each beam, data well before and beyond the projection of the half-beam width (-3 dB limit) are recorded. When the data are subsequently stored, overlapping inner beams have redundant data and thus usually only the data within the -3 dB limits are generally retained. If, however, an inner beam is dropped, the beam traces on either side are lengthened just enough into the intervening time gap to ensure a continuous coverage. For the outermost beams, however, for which there is never an adjacent beam outboard, the full beam trace outboard is retained, resulting in potentially a much wider available backscatter swath.

The reception beamspacing is systematically shifted between pings to achieve a more even sounding spacing. This is achieved by the receiver beamspacing having alternately offset (½ a beam width) beam steering angles for subsequent pings. This effect is termed "beam hopping" and is highlighted in Figure 2.6.

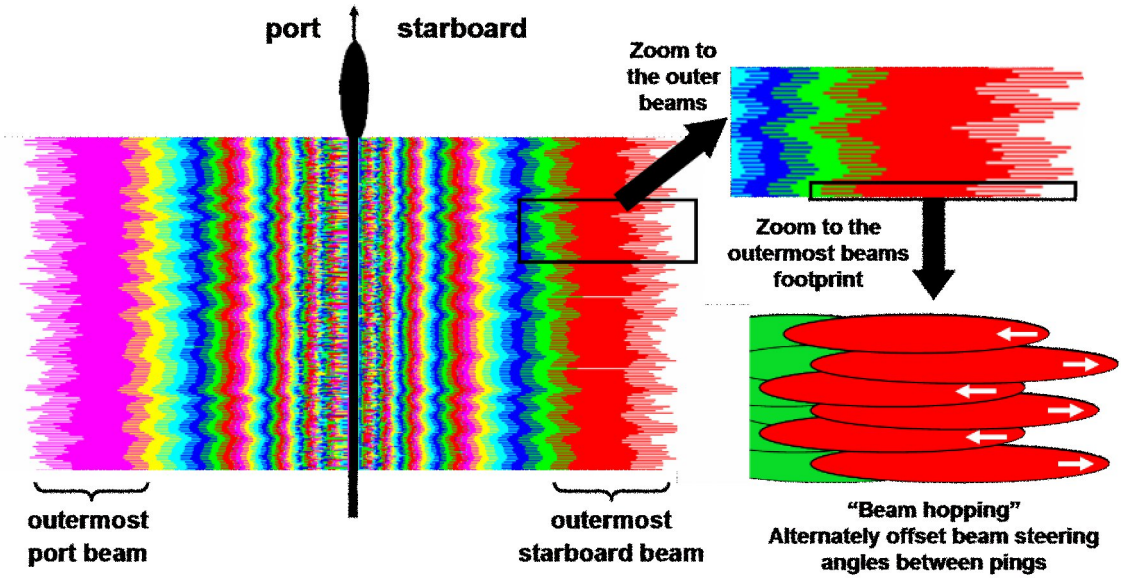

Figure 2.6 Beam hopping effect of the outermost beams is highlighted. Notice the gap between successive pings.

True coverage in the seafloor depends on various parameters [Miller et al., 1997]:

1. Ping rate, which depends on the depth and angular sector. Each transmitted swath has to propagate the entire two-way-travel (ship-seafloor-ship distance) before the next swath can be executed.
2. Vessel speed must be adjusted in accordance with ping rate to keep adequate along-track coverage. If vessel speeds up, gaps are generated in the survey coverage.
3. Roll movements (if not compensated) can cause lateral displacements in the swath.
4. Pitch movements (if not compensated) can cause uneven swath distribution in the along-track direction. Its compensation usually is able to reduce this problem in the near-nadir beams, but outer beams are under-compensated.

5. Yaw movements (if not compensated) rotates the entire swath around the ship's vertical axis. Ideally, inter-ping yaw has to be smaller than half the transmit beam width (without roll and pitch problems).
6. Heave movements (if not compensated) increase (ship upwards) or decrease (ship downwards) the entire swath width. Heave problems have greater importance when the water depth is shallower.

2.2 Simrad recorded "raw" amplitudes

The EM1000 echosounder stores the bottom backscatter strength data both in the sonar image and depth telegrams. Amplitudes receive corrections during acquisition, then "raw" is used to indicate that they are not purely raw. Recorded data format and scales used for backscatter conversion are presented in Figure 2.7.

- Scale (a) represents the way backscatter amplitudes are stored, which uses signed char binary format, ranging from -128 DN (digital numbers) to +127DN.
- Scale (b) presents the corresponding backscatter strength values in the log scale. Ranges are now from -64 dB to +63.5 dB with 0.5 dB resolution.
- Scale (c) is used for image gray-level representation, which uses unsigned char binary format, ranging from 0 DN to 255 DN. As backscatter strength value should always be smaller than 0 dB (dashed line), the signed/unsigned char representation should be irrelevant. However, if there are sonar calibration problems (or coherent reflectors), eventual amplitudes higher than 0 dB can occur. This can cause wrap around in the visible gray-level scale.

- Scale (d) represents the backscatter coefficient, which uses linear scale. It corresponds to the ratio of backscattered and incidence intensities.

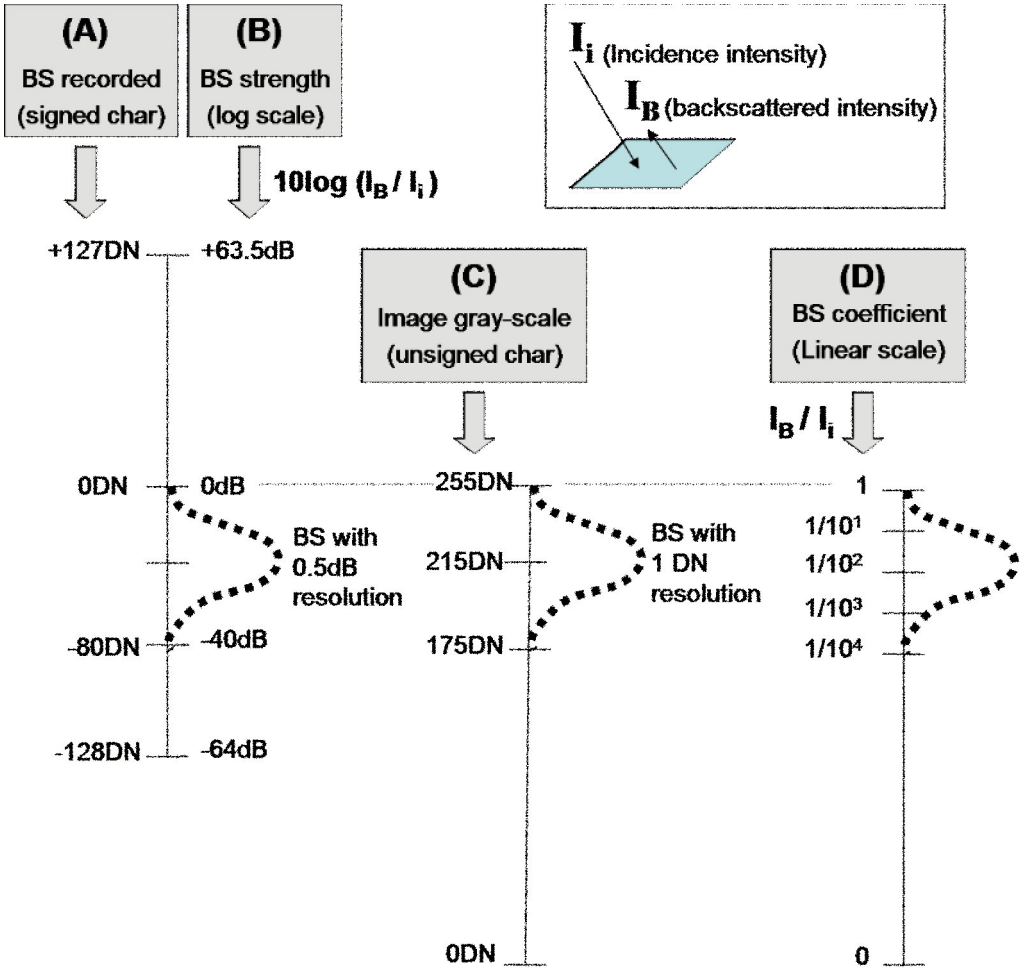

Figure 2.7 Backscatter is recorded and represented using several scales. (Scale A) shows the way data is recorded by Simrad. (Scale B) has the corresponding values in log scale. (Scale C) is the way data is represented in gray-level images. (Scale D) is the corresponding values in linear scale.

The EM1000 system applies some signal corrections to obtain the backscatter values. For that, the sonar equation (Equation 2.1) is used to explain the processes of acoustic wave propagation.

$$EL = SL - 2TL + BS \tag{2.1}$$

Where:

EL - Echo Level (received energy)

SL - Source Level (transmitted energy)

TL - Transmission Loss (propagation)

BS - Backscatter Strength (target)

The next two sections will describe the simplified processes used by the sonar to compensate for the transmission loss and backscatter strength effects during data acquisition [Hammerstad, 2000]. In summary, the algorithm analyses the previous pings and calculates the expected bottom backscatter strength (at normal (BSn) and oblique incidence (BSo)) and the minimum slant range (or range to normal incidence (Ri)) for the next pings. The flat seafloor assumption is taken w.r.t. minimum slant range position (Figure 2.8). With expected values for the next pings already calculated, preamplifiers linked to each one of the 128 transducer staves are able to apply the amplitude corrections (time-varying-gain TVG) to normalize the signal during reception.

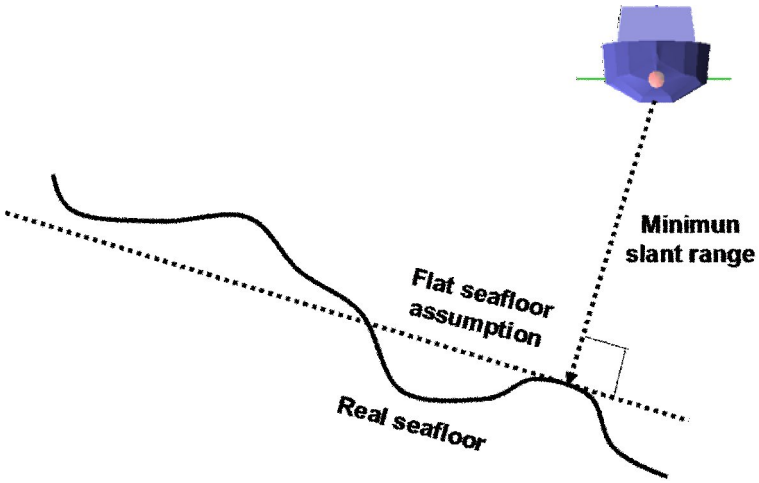

Figure 2.8 Sonar algorithm builds a flat seafloor model, which is placed in the perpendicular to the minimum slant range position. In fact, real seafloor has irregular shape.

Next sections also present some recommendations about more accurate corrections, which should be applied for reducing the geometric and radiometric artefacts that remain in the Simrad "raw" backscatter strength data. The main objective is to isolate only the seafloor properties contribution, therefore producing useful information for the seafloor characterization task.

2.2.1 Transmission loss (TL) compensation

Transmission loss is multiplied by two in the sonar equation to express the energy lost during propagation from the transducer to the target (seafloor) and also in the way backwards, which is termed as two-way travel of the acoustic wave. Transmission loss includes the contributions from two different phenomena: spherical spreading and attenuation.

Firstly, spherical spreading corresponds to the diffusion of the emitted energy on a growing geometrical surface [Augustin et al., 1996]. Intensity decreases (in each direction) in a rate proportional to the spherical surface area, which is equivalent to the power of two of the propagated distance (R). Therefore, two-way travel spherical spreading can be expressed by:

1. For the incoherent scattered case, when the target re-radiates energy spherically, the linear formula is $1/(R^2 \times R^2)$ and the logarithmic formula is -40logR. This model is assumed for high frequency scatters such as this data; or
2. For the coherent reflected case, when energy is reflected like a plane wave (eg. seismics large pulse length is bigger than surface roughness), the linear

formula is $1/(2R^2)$ and the logarithmic formula is -20log(2R). This model is normally only assumed for low frequency reflectors such as seismics.

Secondly, attenuation occurs because sea water is a dissipative medium that absorbs part of the energy of the acoustic wave [Lurton, 2002]. The main causes of attenuation are water viscosity and chemical reactions bound to the relaxation of the boric acid molecules below 10 KHz and magnesium sulphate molecules below 1 MHz. Attenuation can be expressed as $-2\alpha R$ for the two-way propagation.

The term α is the absorption coefficient. According to the model implemented by Francois and Garrison [1982], the absorption coefficient can be calculated from sonar frequency and propagation medium properties (temperature, salinity, depth and pH). α is usually expressed in units of dB/Km.

Figure 2.9 illustrates the Francois and Garrison model. The corresponding absorption coefficient values expected for the EM1000 echosounder (95 KHz) are highlighted. As observed in the plot, absorption coefficient for fresh water is only ~3dB/Km while for salt water is ~30 dB/Km. It represents a value $\sim 10^{2.7}$ (or ~500) times bigger in the linear scale. Therefore, surveys executed close to estuarine zones need to account for this variation. If overestimated attenuation is considered in the fresh water, resulting backscatter estimates will be artificially strong.

The EM1000 system compensates the transmission loss effect during data acquisition. But, it assumes a fixed value for the absorption coefficient, which is a simplification because watercolumn properties are constantly changing. The absorption coefficient value is chosen and inserted in the operator unit before the survey. The Brazilian Navy has been using the Simrad's default value (30 dB/Km) until now. Typical

waters in Brazil are in the range of 15° to 25° Celsius, with salinities approximately 35psu. Thus, real absorption coefficient should be ~34-35 dB/Km, which causes a systematic underestimation of the true backscatter. This underestimation gets worse as the water gets deeper. Therefore, further processing should include more precise values for the absorption coefficient, which would require constant measurements of watercolumn properties during survey. Watercolumn CTD (conductivity-temperature-depth) profiles already being executed for the refraction corrections should be adapted to accommodate the absorption coefficient calculations. This process is now automatically implemented in the newer EM sonar series software.

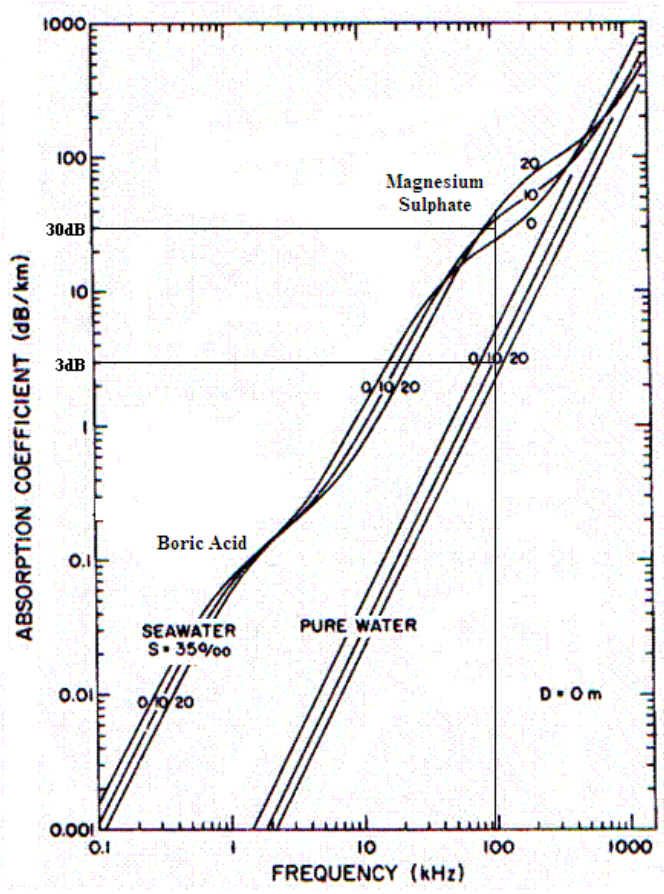

Figure 2.9 Absorption coefficient (α) according to the model developed by Francois and Garrison [1982]. Attenuation for the two-way travel can be calculated by the formula -2αR. The EM1000 multibeam (95 KHz) situation is highlighted. Notice that absorption coefficient for salt water (30dB/Km) is ~500 times bigger (linear scale) than fresh water (3dB/Km).

2.2.2 Backscatter strength (BS) compensation

Backscatter strength depends on the seabed properties and on the seabed area that is ensonified by each sample [Urick, 1983]. The Equation 2.2 aggregates both effects.

$$BS = BS_B + 10\log A \tag{2.2}$$

Where:

BS – Backscatter Strength

BS_B – Bottom Backscatter Strength

A – Instantaneous ensonified area

Bottom backscatter strength is defined as the ratio of the backscattered intensity (taken 1 m from the target) to the incident wave intensity (per unit area per unit solid angle). Normally, it is expressed in decibels and calculated by the logarithmic formula $10\log (I_B/I_I)$. The quotient expresses the ratio of the backscattered (I_B) and incident (I_I) intensities in the linear scale, which is termed as backscatter coefficient. Bottom backscatter strength is a function of the sediment type and grazing angle, as showed in the illustrative plotting in Figure 2.10. Therefore, bottom backscatter strength has higher values when sediment type is harder and grazing angles gets closer to the vertical. The grazing angle effect is normally known as the angular response effect.

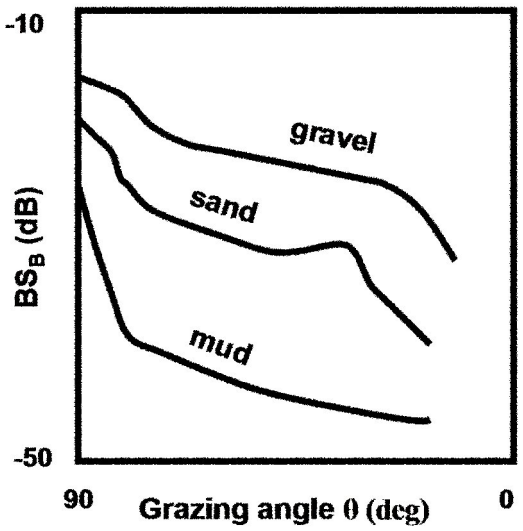

Figure 2.10 Typical Bottom Backscatter Strength (BS_B) dependence on sediment type and on ensonification grazing angle [edited from Hughes Clarke, 2005].

Simrad tries to compensate the angular response effect following the steps presented in Figure 2.11. The objective is to have a sediment type represented by the same backscatter strength value, independently of the ensonification angle.

For that, the previous pings are used to estimate the bottom backscatter strength within normal incidence (BSn) and oblique incidence at crossover angle (BSo). Crossover angle can be modified in the operator unit, but the Brazilian Navy has been using the default value (65^o grazing angle or 25^o incidence angle). With BSn and BSo already estimated, a linear curve is build for the inner region ($90^o > \theta > 65^o$) and a Lambertian curve is used for the outer region ($65^o > \theta > 0^o$). These curves are represented by dashed thick lines in the Figure 2.11. The curves generate the correction values (indicated by arrows) used for next pings normalization. Nevertheless, the next ping could present different shapes, like that ones indicated by curves (1) and (2). Therefore, in the outer beams region (lower grazing angles) for example, curve (1) would be over-compensated, while curve (2) would be under-compensated.

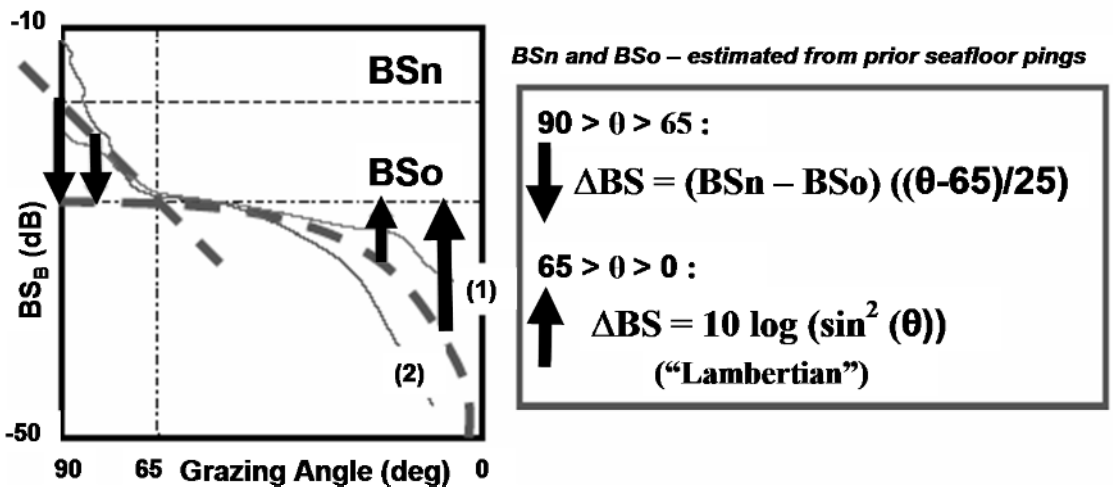

Figure 2.11 Simrad compensates the angular response effect. By estimating BSn and BSo values from previous pings, Simrad model draws the dashed lines and considers they are the appropriate model for normalizing next pings to the crossover level. Model assumes a linear behavior for nadir region (90 > θ > 65) and Lambertian behavior for the oblique incidence region (65 > θ > 0). Nevertheless, next pings could present different shapes, like that ones indicated by curves (1) and (2). Therefore, corrections applied would under-compensate or over-compensate backscatter curves. [from Hughes Clarke, 2005].

After describing the problems bound to the bottom backscatter strength and its angular response normalization, the second factor that matters for the backscatter strength is the instantaneous ensonified area.

The imaging geometry regulates the ensonified area problem. Figure 2.12 shows that beams closer to normal incidence (incidence angle smaller than ~10^o) have their across-track instantaneous footprint limited by the receive beam width. Otherwise, beams within oblique incidence have their across-track footprint calculated with the pulse length. Therefore, Simrad uses the Equation 2.3 for normal incidence and Equation 2.4 for oblique incidence situations.

Normal Incidence $$A = \frac{\theta_R R}{\cos\theta}\theta_T R \quad (2.3)$$

Oblique Incidence $$A = \frac{\tau\, c/2}{\sin\theta}\theta_T R \quad (2.4)$$

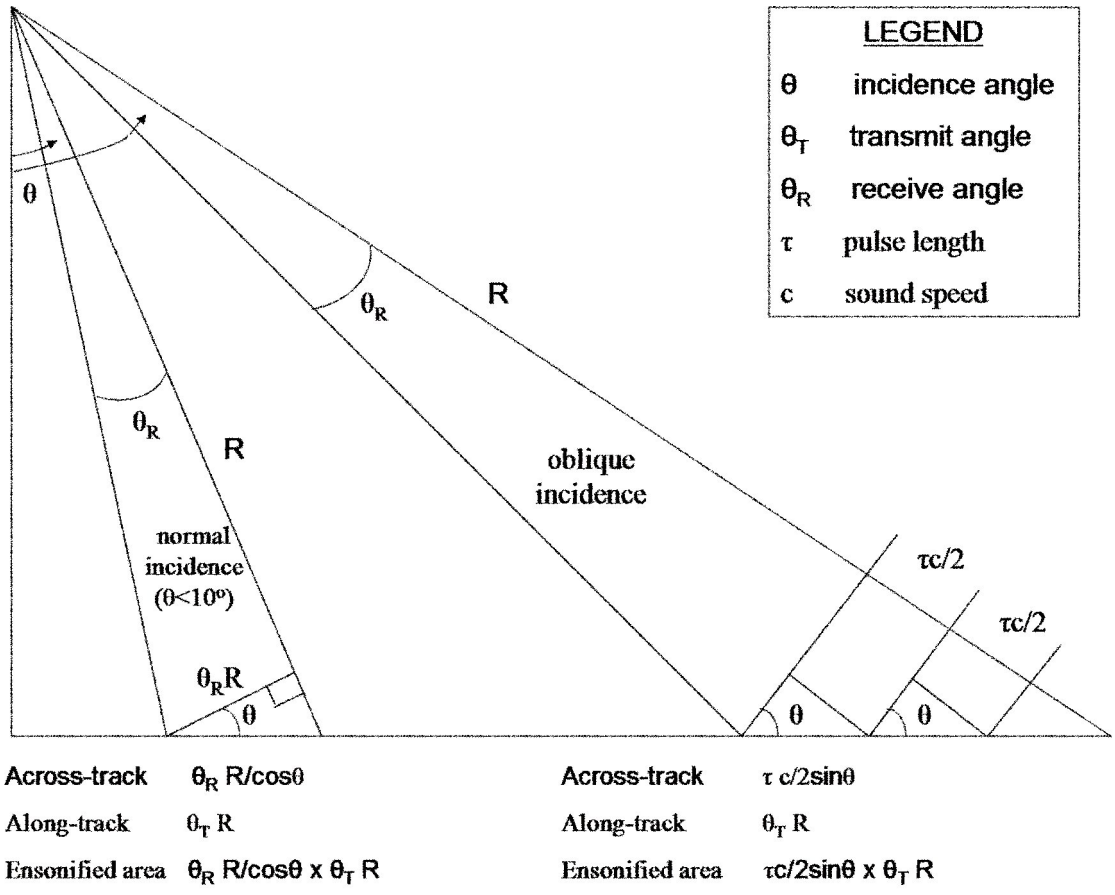

Figure 2.12 Imaging geometry and instantaneous ensonified areas. Normal and oblique incidence situations.

The Simrad algorithm considers the imaging geometry to compensate the area influence to the backscatter strength. However, as described before, previous pings are only able to construct a flat topographic model of the seafloor. Therefore, topographic

variations away from the flat approximation are not considered, which produces imprecise results.

Ideally, post-processing should retrieve bathymetric data to generate the seafloor topographic model to be used for correcting the ensonified area.

2.3 Amplitude traces and reflectivity

EM1000 echosounders record the backscatter amplitudes that are pre-processed during data acquisition. Amplitudes are logged both in the sonar image telegram and in the depth telegram. The sonar image telegram stores the full time-series amplitudes (or trace amplitudes) corresponding to each instantaneous ensonification of the seafloor. The depth telegram only records an average of higher amplitudes taken inside each beam, which is termed as reflectivity. Also, the reflectivity value has not been reduced for the angular response effect (BSn-BSo and BSo-Lambertian corrections). As such, the values should more closely represent true backscatter strength.

Figure 2.13 presents backscatter images and average backscatter plots both for the full sidescan trace (top) and for the beam average reflectivity (bottom). Comparing the two images, one can notice that trace amplitudes are able to produce a more detailed image of the seafloor backscatter, while the reflectivity image blurs some facies because of its lower resolution. Moreover, the centre of outermost beams has been highlighted (along-track lines). It can demonstrate the extended swath range (beyond the -3 dB limits of outermost beams) achieved while using trace sidescan record. Comparing the average backscatter plots, values have inverted pattern because trace amplitudes receive Simrad corrections (for angular response effect) and reflectivity do not.

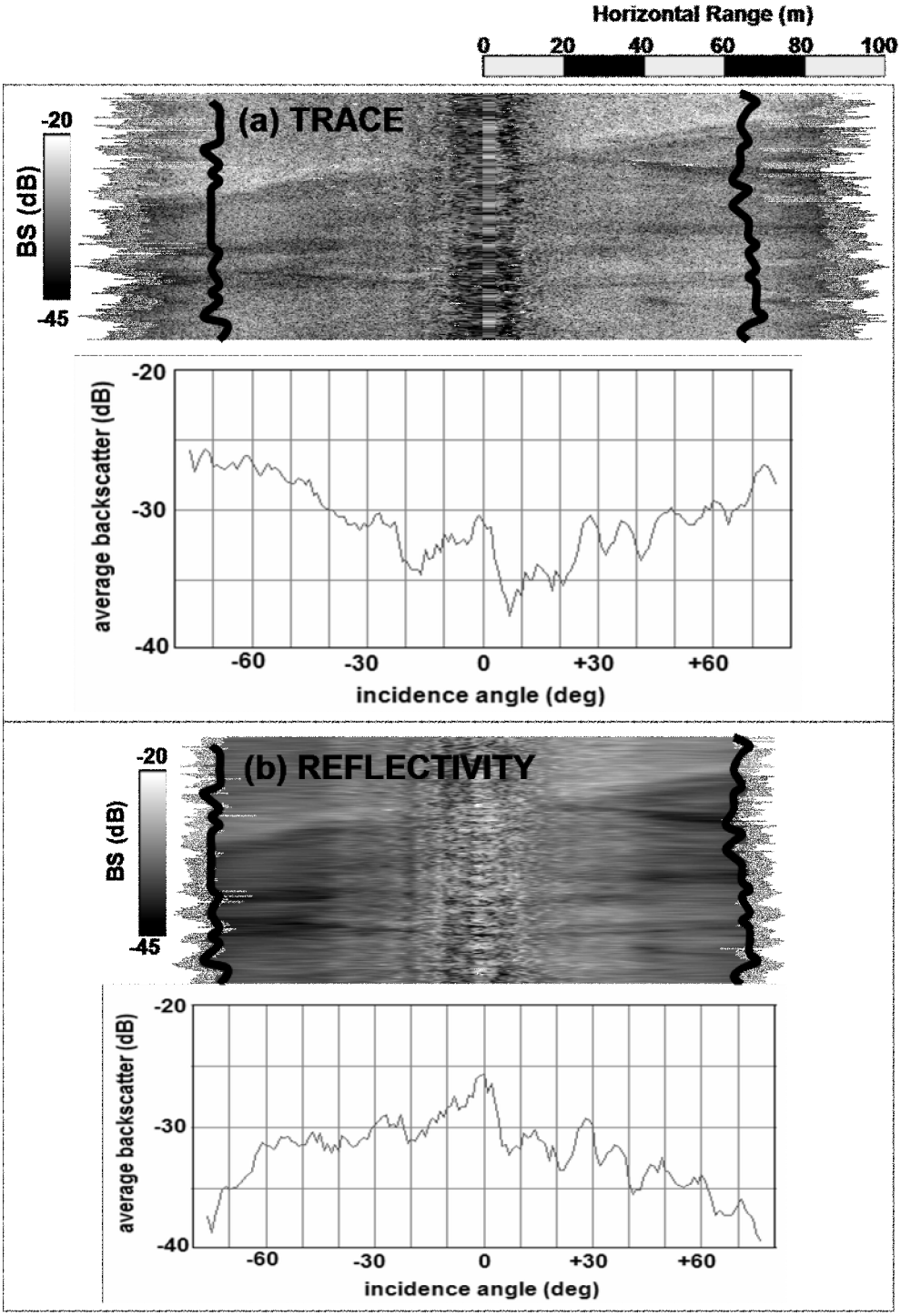

Figure 2.13 (Top Image) Full sidescan trace data logged in the sonar image amplitude telegram and its average backscatter taken with *getBeamPattern* software. (Bottom Image) Beam average reflectivity data logged in depth telegram. Notice better resolution and extended area coverage of full trace data. Average backscatter plots have inverted pattern because reflectivity data is not compensated for the angular response effect.

The ultimate aim of the real-time Simrad TVG (time-varying gain) is to remove the gross effect of angular response in the trace data, so that the backscatter values represent those that would occur if the seafloor were imaged only at the crossover angle (BSo). Ideally, a seafloor of uniform composition would exhibit a constant grey-scale across the swath. This makes it ideal for human interpretation and automated textural classification. As one can see in Figure 2.13 (top), for the case of the Brazilian data, the trace data response is still not flat. This can be attributed to two effects:

1. Inappropriate BSn/BSo Lambertian mode; and
2. Residual transmit and/or receive beam pattern signatures.

Some Brazilian data have been logged without the sidescan telegram. Therefore, only reflectivity is available. It still represents a possibility of extracting information of the seafloor if data is properly compensated. As observed in Figure 2.13, the reflectivity is able to represent most of the facies of the seafloor. However, only the mean and angular response can be derived as the textural data is corrupted in the within-beam-averaging.

Herein, we wish to empirically improve on the real time TVG to account for modeled beam pattern residuals.

2.4 OMG (beampatt) processing

The Ocean Mapping Group (OMG) has been developing in the last 15 years a series of software implementations with the objective of reducing artefacts found in the backscatter data of many multibeam sonar models.

As commented, for the specific case of Simrad sonars, the logged backscatter already has benefited from some compensations, but in a simplified way. Normalization is executed during data acquisition. For that, previous pings are used to infer the average bottom backscatter strength (nadir (BSn) and oblique (BSo)) and topographic flat model, which are to be used to estimate the best TVG to compensate the following pings. In addition, absorption coefficient receives a fixed value established before the survey.

To improve the backscatter quality, OMG software starts building an array of 180 values corresponding to the entire angular sector (+/-90^o with 1^o spacing) possible to be covered below the ship. The algorithm calculates average backscatter within each array bin (1^o spacing interval). For the average calculation, it uses the trace backscatter amplitudes (averaged by beam), which has been compensated using Simrad simplified model. During processing, a vertically-referenced frame centered at the transducer mean depth is used, therefore assuming that beam-pattern does not migrate with roll.

This vertically-referenced model can detect amplitude fluctuations occurring between specific roll-stabilizing receiver beamforming channels. Nevertheless, fluctuations due to imperfections in the transducer elements physical structure or transmit beam pattern would roll while ship moves and cannot be detected [Llewellyn, 2006]. For the EM1000, this has never been seen to be important.

The OMG extraction of bin averaged amplitudes is able to map Simrad “raw” data through beam pattern plots like that ones presented in Figure 2.14. Examples of shallow mode (a) and medium mode (b) for a specific EM1000 echosounder are presented, which demonstrate that several remaining artefacts (stronger amplitudes near nadir, small beam-to-beam oscillations and angular gaps) are still present. Notice that each mode (with

different pulse length and angular sector) has its particular beam pattern and artefacts to be compensated. The EM1000 stores the mode setting in the depth telegram, which permits automatic statistics sorted by mode.

These artefacts would produce along-track residuals in the sidescan/backscatter images, which complicate its geological interpretation. In addition, they will bias statistical or power spectral analysis executed for seafloor classification [Augustin and Lurton, 2005].

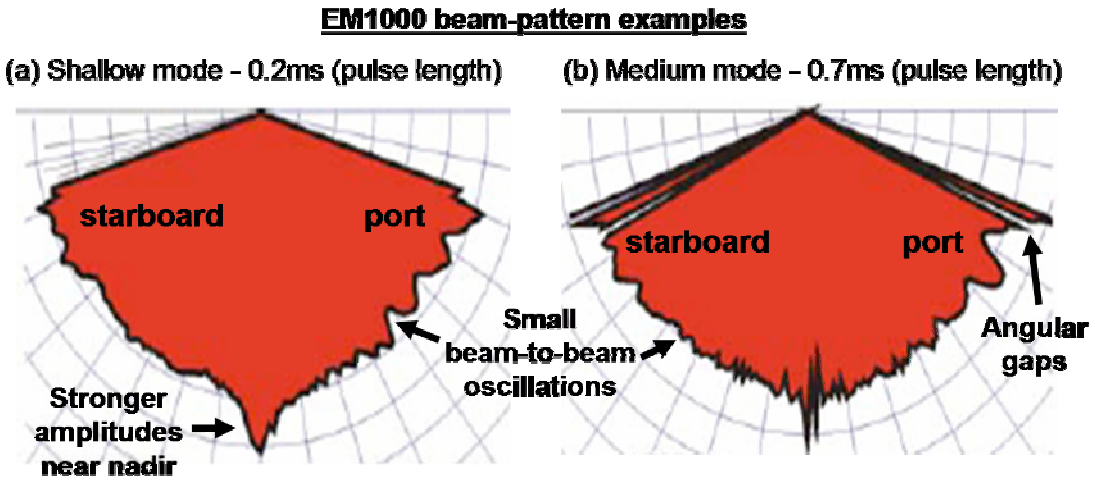

Figure 2.14 This EM1000 beam pattern examples of shallow mode (a) and medium mode (b) were generated with the OMG software. Algorithm gets along-track stacks of vertically referenced angles. Values represent averaged backscatter data (from sonar image telegrams, with Simrad corrections already applied) taken from each 1 degree angular interval. Notice that many artefacts are still present in both examples. [edited from Hughes Clarke, 2005].

In order to reduce the encountered artefacts related to the angular response and beam-to-beam oscillations, OMG software executes extra signal normalization.

For that, in the first step, the algorithm calculates the average of the amplitudes located inside arrays 25^{o} to 65^{o} and 115^{o} to 155^{o}, producing the results indicated by dashed line in Figure 2.15. Therefore, angular range used is extracted from 25^{o} and 65^{o}

incidence angles to each side. Other angular regions (close-to-nadir and outermost beams) are not considered for the average computations because they are more inclined to higher amplitude oscillations, which might bias the final average.

In the second step, the single backscatter amplitude of each bin series is subtracted from the final average. Therefore, the correction parameters (arrows in Figure 2.15) to be used further at each array bin can be determined. The corrections are established in logarithmic values (dB) permitting addition calculations, instead of multiplication used with linear values.

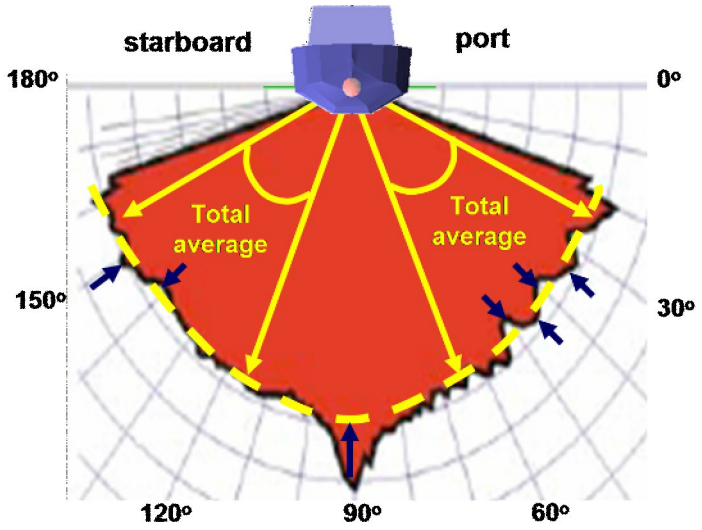

Figure 2.15 OMG software executes extra normalization to the backscatter signal logged in the sonar image telegram. For that, first step consists of getting the average (dashed line) of the amplitudes located inside arrays 25-65 and 115-155. In the second step, each beam series is subtracted from the average (arrows).

Figure 2.16 summarizes the steps previously described. The bottom curve represents the arrays averages computed from Simrad "raw" backscatter amplitudes (from the sonar image telegram). Horizontal line is the total average evaluated with the values that are comprehended inside 25° and 65° incidence (launch) angles to each side. Top curve are the correction values, which are the arrays amplitudes subtracted from the

total average. This correction values are used to accomplish the normalization executed by the OMG software.

In addition, OMG program permits the changing of the absorption coefficient parameter. Just to recall, this value is inserted in the operator unit before the survey. Post-processing of watercolumn properties can indicate other more appropriate absorption coefficient to be used, most probable occurring in estuarine areas.

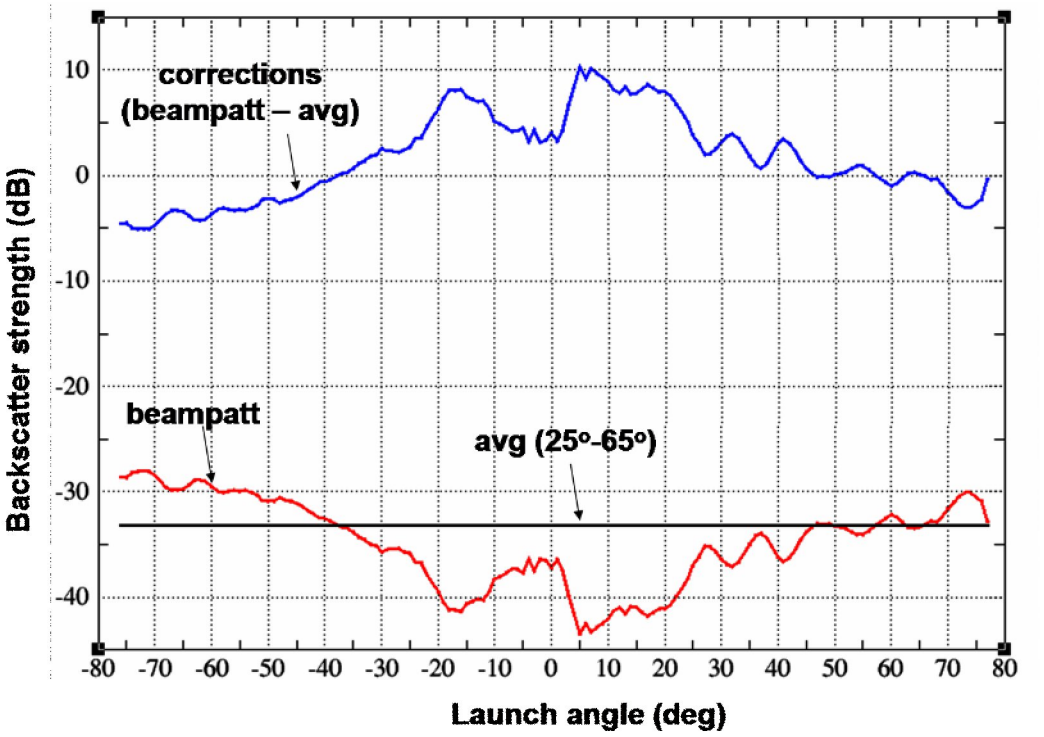

Figure 2.16 OMG (beampatt) software calculates the average amplitude values each 1.0 degree interval. Then, it takes the average (avg) between 25º- 65º degrees. (Corrections) that will be used later for backscatter normalization are calculated by subtracting beampatt from average curves.

The normalization process undertaken by OMG software demonstrates an improvement in the backscatter quality when sidescan/backscatter images are generated. Figure 2.17 shows one image produced with the Simrad "raw" amplitudes (a) and other with OMG processed amplitudes (b).

Raw amplitudes image presents many artefacts printed in the along-track direction and a strong contrast (black-white oscillations), while OMG processed image has one marked residual, which is the dark strip in the outermost beams.

Both images have a very strong noise in the near-nadir region, which is extremely difficult to be removed. This problem occurs because near-nadir angular response suffers high variations as sediment type changes. By taking average values for the entire survey line, the software fails to compensate every time a new sediment type is crossed. Besides that, in the inner regions, lesser samples (with greater across-track distance) are recorded and noisy backscatter data can bias the average. Also, as the angular response curve is usually so steep close to the normal incidence, small change in local seafloor slope causes strong fluctuation in backscatter.

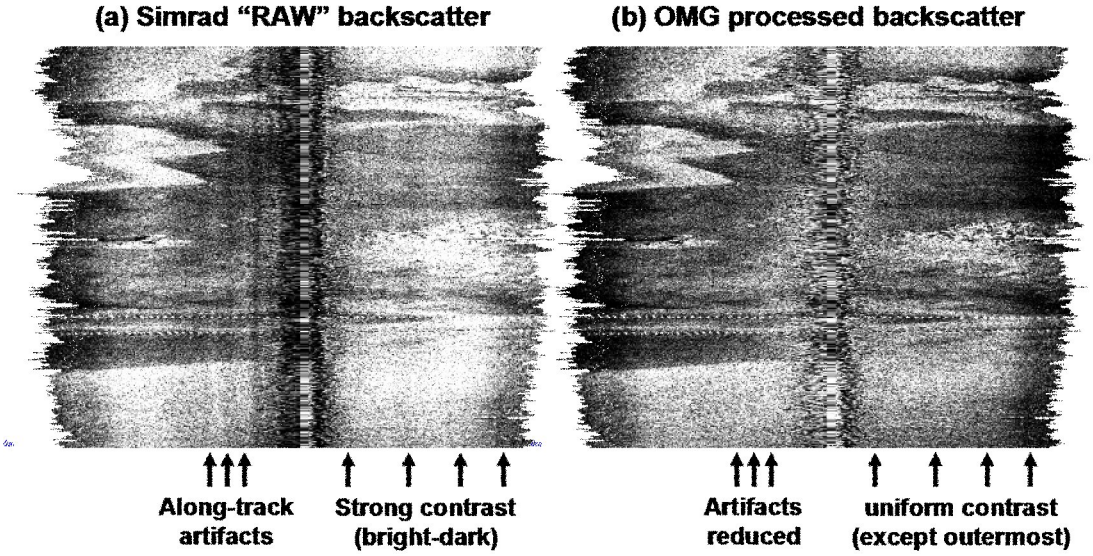

Figure 2.17 (a) Simrad "raw" backscatter image has many along-track artefacts, while (b) OMG processed backscatter image has mainly the outermost beams artefacts (darker strip). Central beams have different "texture", but on average the same normalized backscatter.

2.5 New implemented (tracepatt) processing

New software implemented was built to remedy the remaining residual after OMG processing. Therefore, the most evident problem to be solved concerns the outermost beams darker stripes.

An algorithm was built to investigate the traces (amplitude samples) pattern within the outermost beams and to calculate the corresponding corrections necessary for its normalization. For this reason, the derived file that stores these corrections has been named as *tracepatt*. Besides that, other motif was to use similar nomenclature as *beampatt*, which would facilitate OMG software users. The software itself was termed as traceBP.

The first function was developed to detect the outermost valid beams in each survey line being processed. Subsequently, procedures were undertaken to extract the backscatter strength estimates for that beam from the sonar image telegram and to organize them in a way that backscatter variations inside the beam should be understood.

To achieve that, inside each outermost beam, the launch angle of central sample is calculated. The central sample corresponds to the beam detection position, which is assumed to correspond to the boresite. Normally, it is equivalent to the zero-phase crossing of the bottom detection. Launch angles with relation to the boresite for the other samples are computed in the next step, so that they can be positioned with relation to the central sample (adopted as the reference). An array was created to cover 10^{o} to each side with relation to the central sample. The array uses 0.1^{o} intervals. Therefore, after each ping cycle, the calculated launch angles can address what is the indicated array spot

(within 0.1^{o} interval) to store any backscatter sample. At the end of the line, average values are calculated for each array bin.

To accomplish the procedures previously listed, the imaging geometry has been analysed as demonstrated in Figure 2.18. One can observe that the total number of samples within each beam is a function of the sampling interval, beam launch angle (θ) and depth. In the vertical incidence situation, the beam instantaneous footprint is limited by the across-track beam width. Otherwise, as the incidence angle increases, the beam pulse length is the main factor which restricts the instantaneous footprint. Therefore, higher incidence angles, as well as greater depths, are capable of increasing the number of samples stored inside each beam. The consequence of storing more samples is the tighter launch angle interval between samples.

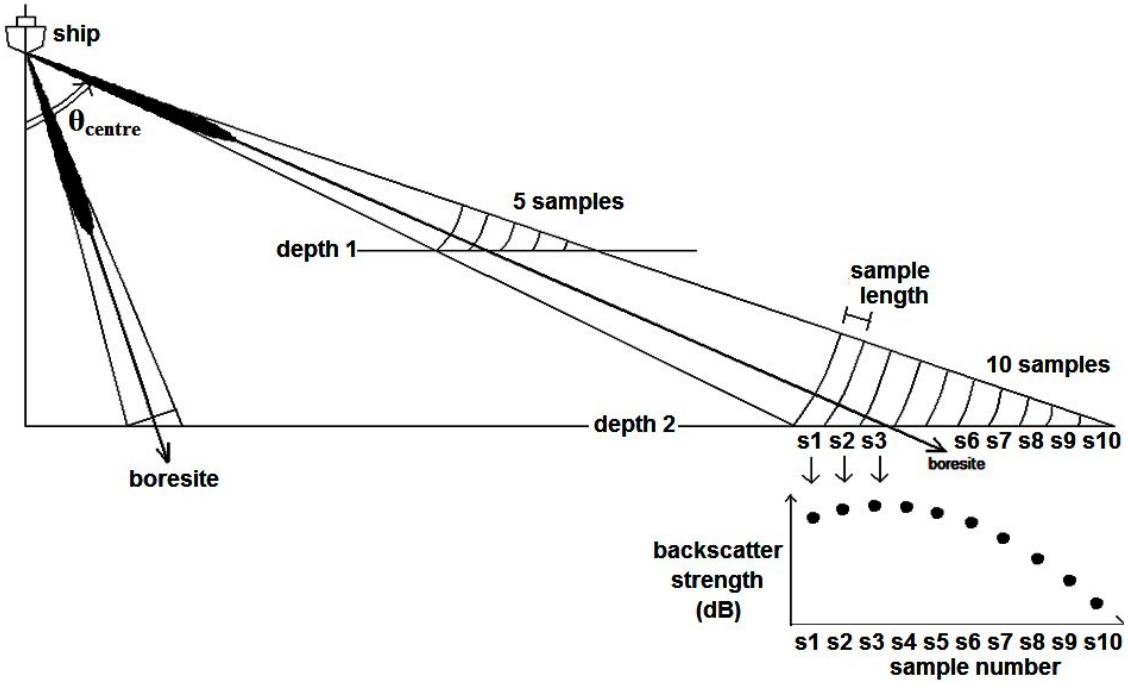

Figure 2.18 The imaging geometry. Inner beams are limited by beam width and outer beams store many instantaneous footprints (samples). The number of stored samples is a function of the beam launch angle and depth.

Equation 2.5 was used to compute the samples launch angles for the starboard side considering the geometry presented. For the port side, sample number and centre number have to be inverted in the formula.

$$\theta_{sample} = \left(\frac{depth \times \cos(\theta_{centre})}{depth + (SampleLength \times (SampleNumber - CentreNumber) \times \cos(\theta_{centre}))} \right) \quad \text{(Eq. 2.5)}$$

Results from data extraction produced plots similar to that one presented in Figure 2.19. Observe that central sample (in the boresite position) is used as the angular reference in the x-axis. Total measurable beam width has more than 4^o because amplitudes are recorded beyond the -3 dB limit. In the y-axis, backscatter amplitudes vary more than 10dB. In conclusion, this detected pattern with the amplitudes rolling down is the cause for the darker stripes in the backscatter image produced (Figure 2.17) after the OMG processing.

Least squares fitting matrix (Equation 2.6) was used to calculate the coefficients (a,b,c) of the quadratic function that best matches the shape of traces pattern curve, as indicated in Figure 2.19. Input values (x,y) are taken from the original curve. Coefficients of the quadratic function are stored in the *tracepatt* file. They are used for normalizing the curve in future processing steps, specifically at the time of backscatter images creation by *makess* and *EchoCalib* functions (available in OMG package).

$$\begin{vmatrix} Ymax \\ Ycen \\ Ymin \end{vmatrix} = \begin{vmatrix} Xmax^2 & Xmax & 1 \\ Xcen^2 & Xcen & 1 \\ Xmin^2 & Xmin & 1 \end{vmatrix} \times \begin{vmatrix} a \\ b \\ c \end{vmatrix} \quad \text{(Eq. 2.6)}$$

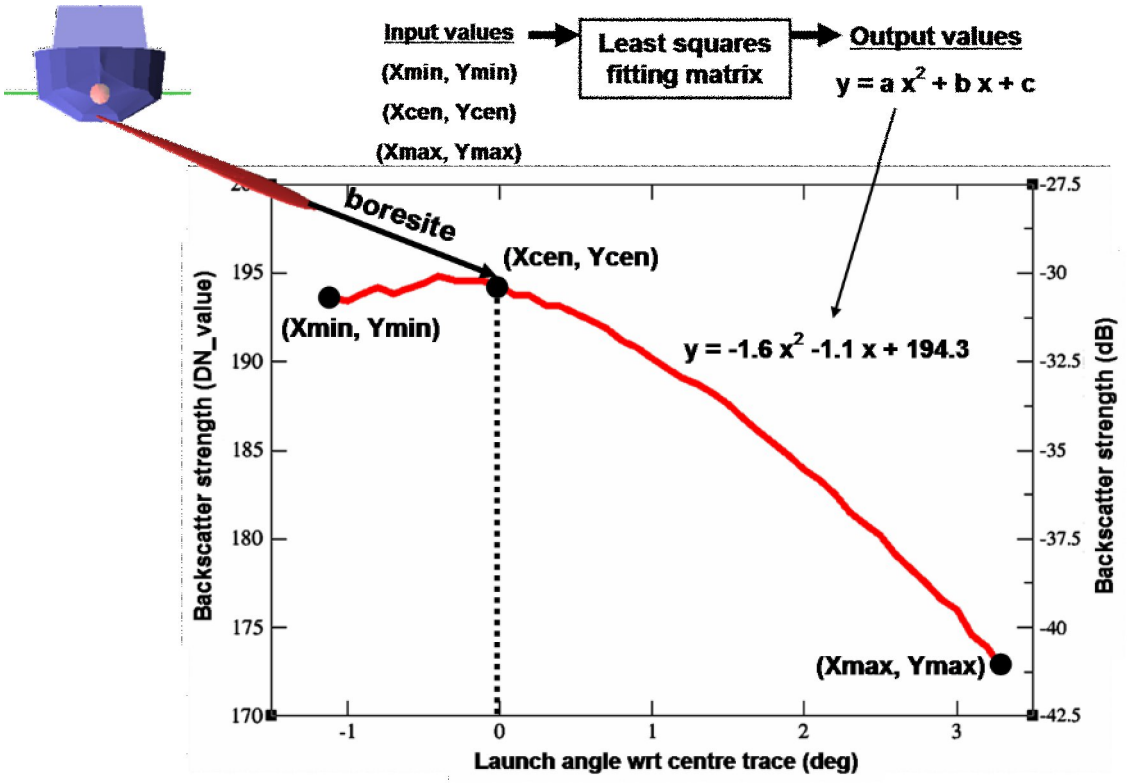

Figure 2.19 The detection of average amplitudes (taken each 0.1 degrees interval) variations in the outermost beams, which was termed as tracepatt. Beam boresite is taken as the launch angles reference (x-axis) to the other samples. Amplitudes variation are greater than 10dB, therefore information is logged beyond the -3dB limits.

Following the same procedure taken in Figure 2.17 when OMG (*beampatt*) processing improvements for the image were presented, Figure 2.20 shows the results when using the newly implemented *tracepatt* corrections.

The left image (a) is the previously obtained image, after OMG already implemented *beampatt* processing, which fails to compensate for the roll-off effect. Right image (b) shows the results after using new *tracepatt* corrections for the outermost beams amplitudes. Notice that the new process can improve the quality of the extended region beyond the centre of the outermost beams. Outermost beams herein represent up to 28% of the entire swath because the system has been operated with +/-75^{o} of angular sector.

This improvement was useful in the mosaicking steps that will be explained in the next chapter. In summary, as the ship surveyed the areas with 200% coverage, outermost beams with better quality will be able to replace the noisy close-to-nadir beams.

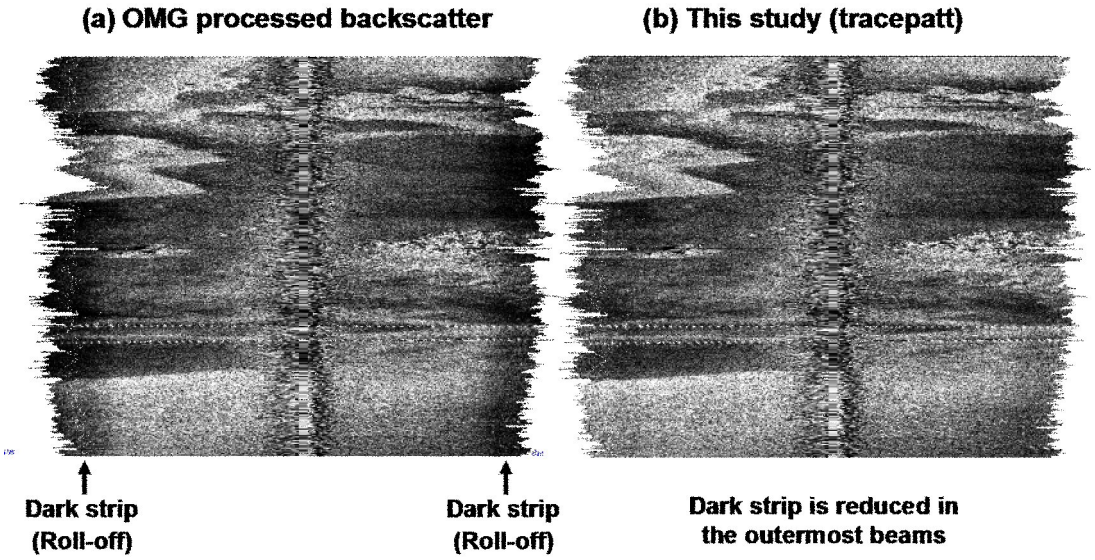

Figure 2.20 (a) OMG processed backscatter image has the outermost beams artefacts (dark strip). (b) New software implemented (tracepatt) reduces outermost beams problem.

As an extension of *tracepatt* implementation, the algorithm was adopted to work for all 60 beams. The results (this study) are plotted by the curve with many oscillations in Figure 2.21. In the same graphic, a straight curve represents the results from (OMG) *beampatt*.

As the intensities are just taken from Simrad's sonar image datagram in both situations, we are able now to compare results simultaneously. Differences are due to the intervals used in the averaging calculations for each case.

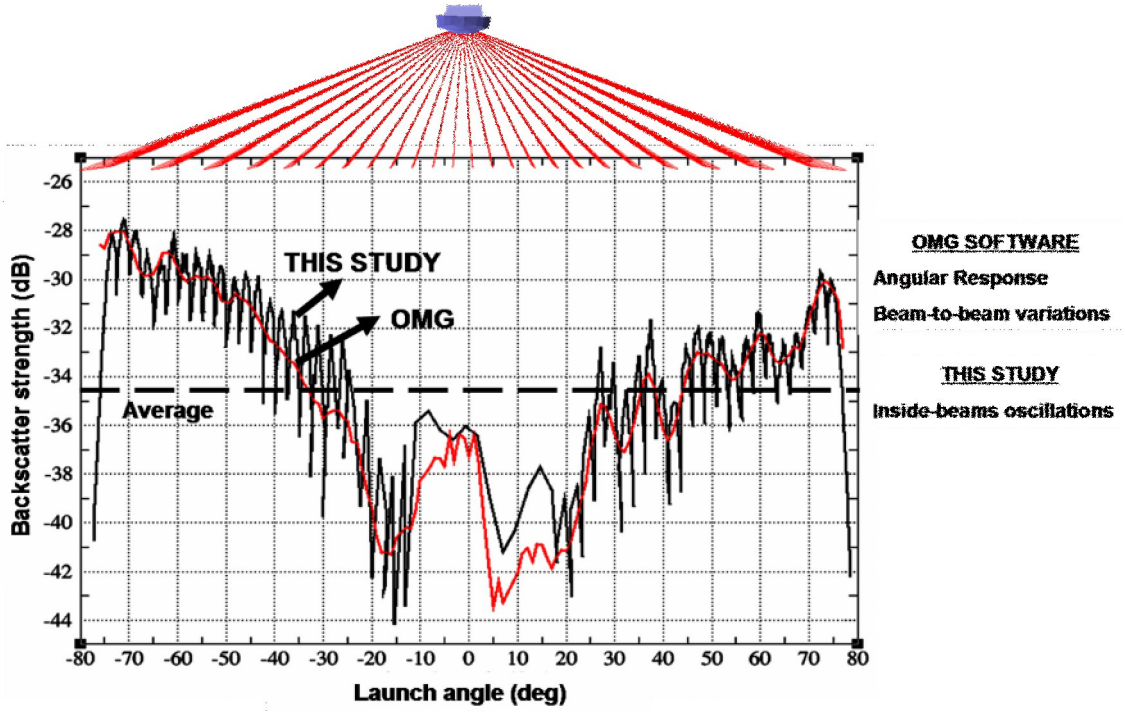

Figure 2.21 The backscatter strength presented here was taken from the Simrad's sonar image amplitude telegram. OMG (beampatt) software evaluates the backscatter averages for each 1.0 degrees interval. New implemented (tracepatt) works inside each beam and calculates the backscatter averages within 0.1 degrees intervals.

As commented, the straight curve shows the extraction of Simrad's "raw" amplitudes by the OMG *beampatt* algorithm, which averages the backscatter for each 1.0 degree interval. In following processing steps, this curve is normalize to the average (taken from 25^{o} to 65^{o} incidence angles) indicated by dashed horizontal line. This normalization reduces angular response and beam-to-beam variations.

The other curve with many oscillations represents the method implemented here, using the *tracepatt* algorithm, which works inside each beam and computes the averages for each 0.1 degree interval. Notice that each beam stores a range of 2 dB to 3 dB, but outermost beams are able to extend their range more than 10 dB. The *tracepatt* pattern was implemented for all the beams to reduce inside-beams oscillations. Therefore, it

would represent an improvement in the final power spectral analysis, which will be discussed later. Within +/-25^{o} of incidence, in the EABS mode, there are usually insufficient samples to define a good trace pattern. This is not important here, as this data is not used for classification. The algorithm establishes a minimum number of samples to accept an angular interval as valid, which solves overlapping problems between adjacent beams.

As commented before, the outermost beams present high amplitude variations (>10dB), which causes the roll-off artefacts printed in the backscatter images. The other beams oscillations (2 dB to 3 dB) are normally difficult to see in the noisy backscatter image. However, when one beam loses the seafloor tracking, the formed gap is filled by the adjacent pair of beams and stronger roll-off effects are also produced. Therefore, in this situation, inside-beam corrections (from *tracepatt*) will also be able to improve the backscatter image.

Figure 2.22 summarizes (at top images) artefacts reduction through the process. But, main focus (at bottom images) is on the backscatter data around a submerged pipeline consisting of a series of concrete blocks. The sonar commonly mistracks on the blocks and thus drops a beam or two. Without *tracepatt* (presented in the right images), previous images present low backscatter that are not real.

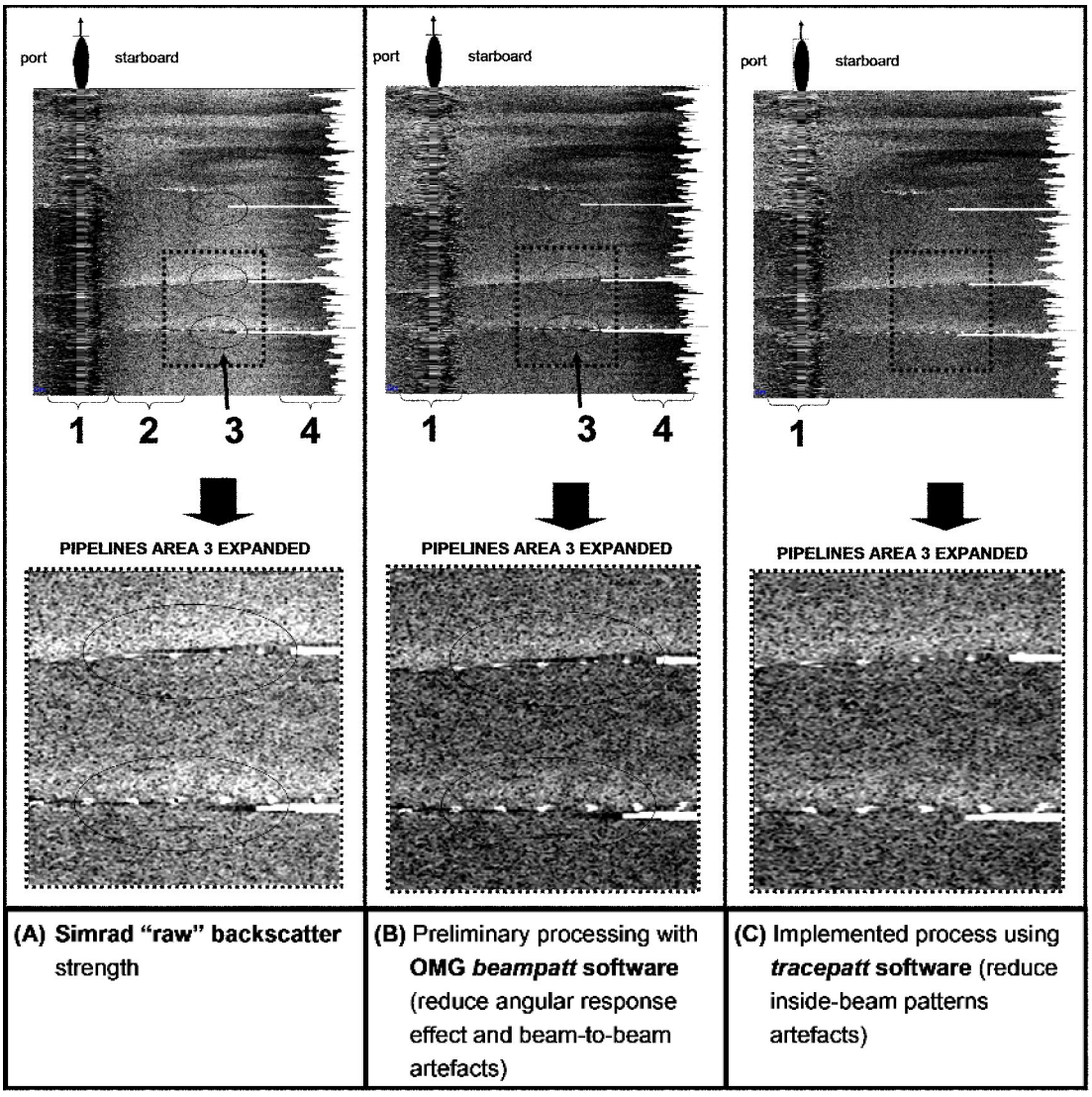

Figure 2.22 Backscatter maps taken from different processing steps.

(Fig. 2.22a): Raw backscatter presents plenty of artefacts: noisy inner region (artefact 1), strong beam-to-beam oscillations (artefact 2), losing beam tracking close to the pipelines and topographic slopes (artefact 3) and rolling down intensities in the outermost beams (artefact 4).

(Fig. 2.22b): Preliminary processing using *beampatt* software was able to reduce the strong contrast across the swath (between the 4 artefact regions described), normalizing the backscatter strength values accounting for the angular response and beam-to-beam artefacts. Notice that artefact 2 is also reduced.

(Fig. 2.22c): Implemented processing using *tracepatt* software worked mostly on the artefacts 3 and 4, related to the strong backscatter oscillation taking place within each beam. In the case of the outermost beams, strong variations are normally present. In the case of other beams, oscillations stronger than 2-3dB (more visible in the image) occur when the sonar loses the seabottom tracking and a gap is formed between the beams.

2.6 Filling the outermost beams "hopping" gaps

As a result of the beam hopping, the outermost beams coverage is strictly not completed. Therefore, there is the necessity of filling the hopping gaps to allow the usage of the maximum portion of the swath. It is executed at the end of the processing steps.

Figure 2.23a presents the Simrad “raw” intensities in the starboard outermost beam location with the hopping gaps already present. Figure 2.23b shows the results after reducing data artefacts with *beampatt* and *tracepatt* processing. The last image, Figure 2.23c, demonstrates the effect produced after filling the gaps between the pings. For that, the OMG *glfill* software was used. But, a new option was implemented here to replace the missing pixels with information from antecedent pings, instead of averaging the adjacent pings (original option in *glfill*). The idea was to avoid changes to the image spectral content resulting from averaging, which would bias the seafloor classification during power spectral analyses to be executed later.

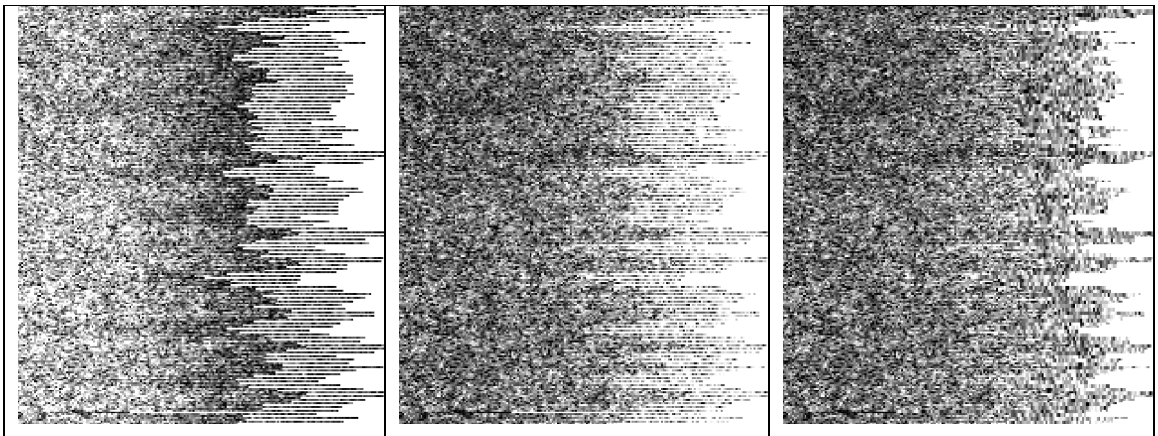

(a) Raw intensities map, with actual coverage of outermost beams. Presents the hopping gaps and backscatter roll-off (dark).	(b) Processed map, still presenting the original coverage (with the hopping gaps), but roll-off effect is normalized.	(c) Final map produced after filling the hopping gaps with antecedent pings values.

Figure 2.23 Process of filling the hopping gaps in the outermost beams.

2.7 NHo Taurus backscatter pattern

A small sample of data logged in 2001 has been processed during this study, just because in this specific survey the ship has collected data using both the EABS and EDBS modes. Therefore, the differences between the two modes should be understood.

First, EABS mode characteristics are presented in Figure 2.24.

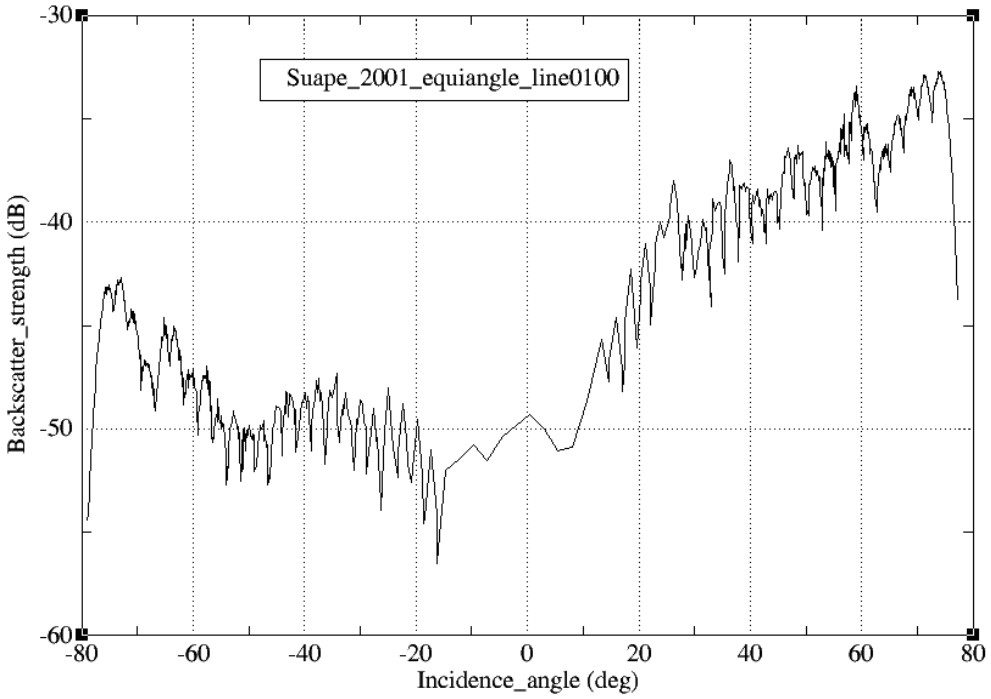

Figure 2.24 Backscatter strength logged in the EABS +/-75^{o} mode. Data from EM1000 multibeam installed on board the NHo Taurus during the survey in Suape, PE, Brazil, in October 2001.

As commented before, for the EABS mode, higher backscatter oscillations (>10dB) are in the outermost beams and smaller oscillations (~3 dB) are present in the other beams. Notice that backscatter amplitudes in the port side (-50 dB) are smaller than in the starboard side (-40 dB).

Figure 2.25 presents the corresponding backscatter image produced with the EABS data. The left image (a) shows the high contrast between starboard and port backscatter

intensities. The right image (b) presents more uniform contrast obtained after processing the data with the OMG software. Outer beams rolling-off intensities is the main problem to be solved.

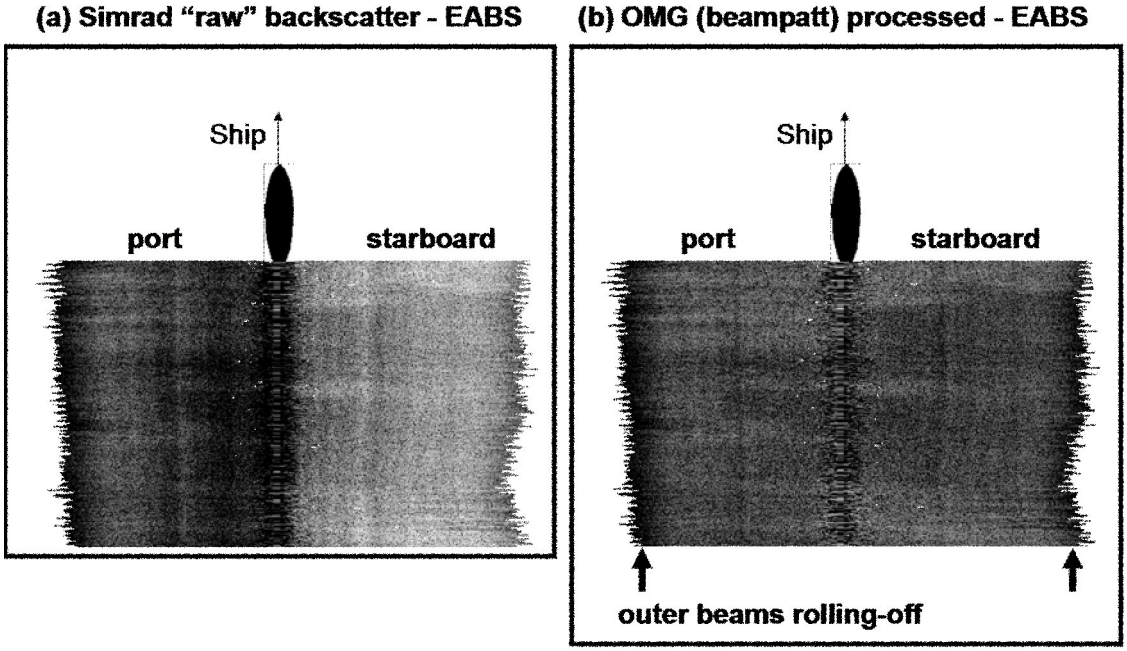

Figure 2.25 Comparison between (a) Simrad "raw" backscatter image and (b) OMG processed image. Data collected in the EABS +/-75^{o} mode. Survey of Suape Harbour, PE, Brazil, in 2001.

Second, EDBS characteristics are showed in Figure 2.26. For this case, higher oscillations (>10 dB) are in the intermediary incidence beams. Hellequin et al. [1997 and 2003] have analysed this case in detail and described the limitations to reduce artefacts within near-nadir region. Again, mean backscatter amplitudes in the port side (-50 dB) are smaller than in the port side (-40 dB).

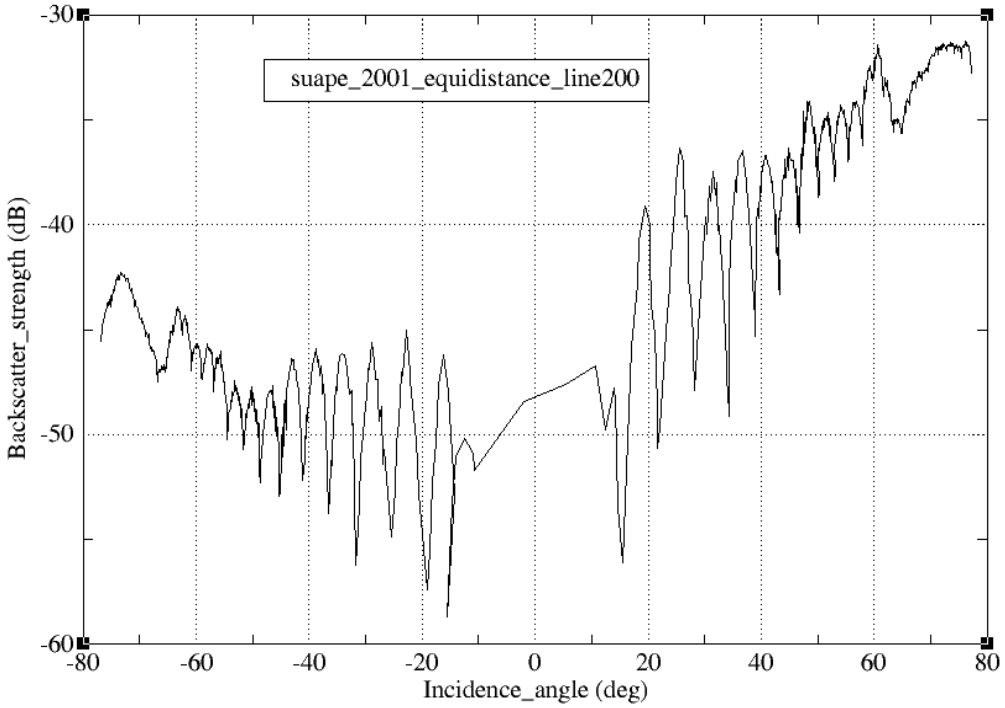

Figure 2.26 Backscatter strength logged in the EDBS +/-75° mode. Data from EM1000 multibeam installed on board the NHo Taurus during the survey in Suape, PE, Brazil, in October 2001.

Figure 2.27 presents the backscatter image produced with EDBS data. Again, the "raw" backscatter image (a) and processed image (b) are showed. For this case, contrast problems between starboard and port side are also solved after OMG processing. But, different artefact is detected, being related to the stripes at the intermediary incidence location (close to the nadir).

Therefore, for both modes (EABS and EDBS) used during Suape survey, port side presents weaker amplitudes than starboard side. This contrast causes strong artefacts in the "raw" backscatter images.

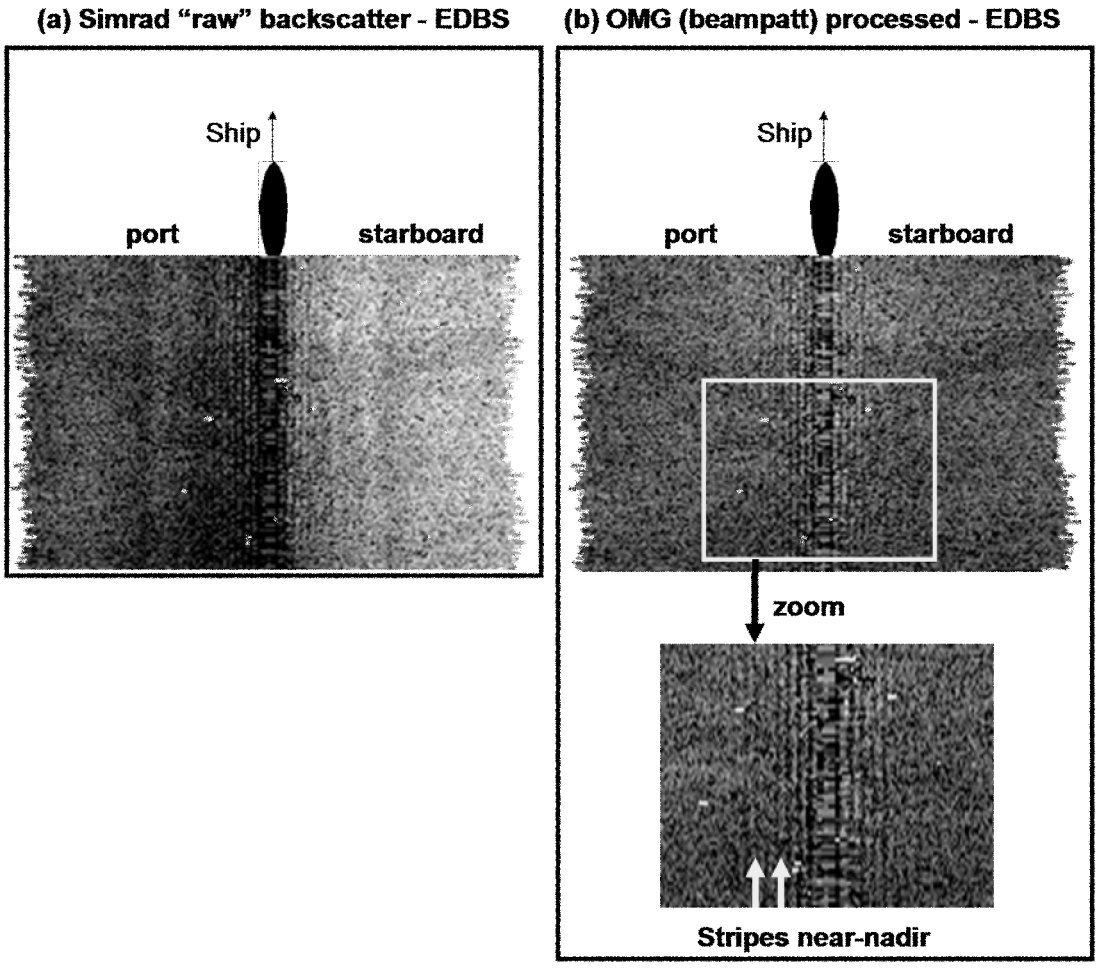

Figure 2.27 Comparison between (a) Simrad "raw" backscatter image and (b) OMG processed image. Data collected in the EDBS +/-75^{o} mode. Survey of Suape Harbour, PE, Brazil, in 2001.

EDBS and EABS raw images contrast has been solved with OMG normalization process. However, the processed backscatter values are probably biased towards the lower values from the port side. They are also used by the OMG *beampatt* software to calculate the backscatter average for data normalization. Therefore, absolute amplitudes must be analysed with care. For the purpose of seafloor segmentation although, we should expected that the relative backscatter distortions in each side have been

normalized to the same level, which is a true statement if we are analyzing a region with homogeneous sediment type.

Figure 2.28 presents (to the left) the normal situation with both sides (starboard and port) equally compensated (similar shapes) during data acquisition and (to the right) the biased situation (different shapes) verified here with one side weaker than the other.

In the normal situation, OMG software applies x and y corrections to normalize to the real average. In the biased situation, the incorrect side (starboard or port) cannot be defined. For data analysis, port side is assumed here to present the wrong values. Then, data is normalized (with 2x and y/2) inadequately to the wrong average. But, as commented before, assuming that seafloor is homogeneous, even the biased situation is able to properly show the same gray-level in the image after processing. Therefore, seafloor segmentation can still be executed.

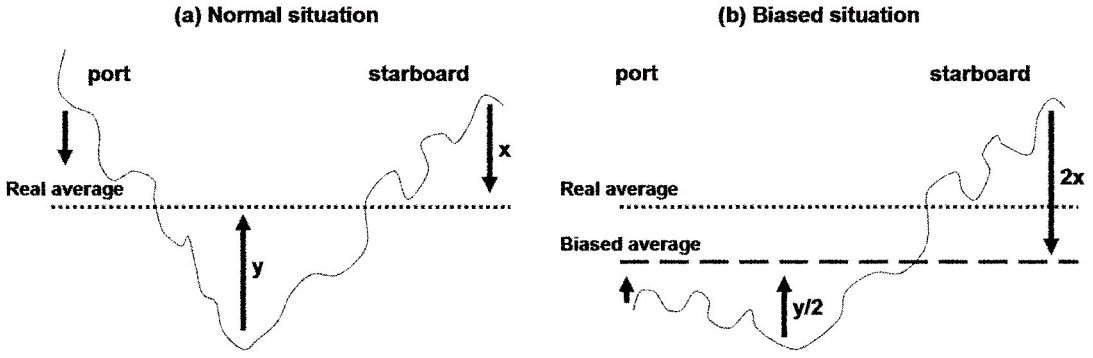

Figure 2.28 (a) Normal situation when amplitudes are equally distributed for both sides. (b) Biased situation when lower port side averages pulls averages downwards.

The main data used in this thesis (Figure 2.29) was collected in EABS +/-75^{o} mode in Barra do Riacho, ES, Brazil, in 2004. This data has backscatter patterns very different to that one previously analysed from the Suape survey (Figure 2.24). While the Suape data presented very weak backscatter in the port side, data from Barra do Riacho has

slightly smaller values in the opposite side (starboard side). In both cases, the backscatter increases with incidence angle suggesting a grazing angle response flatter than Lambertian.

Differences between surveys patterns can be related to the transducer changing executed in 2003, between the two surveys periods. But, most probable explanation should be the failure occurred in transceiver boards during the Suape survey.

Such a problem has to be checked later by comparison with other surveys data. To recognize changes to hardware, it should be necessary to combine and compare all 7 years of data. Where possible, data collected in the same area using different hardware and software combinations can be used to inter-calibrate. If overlapping data does not exist, a later attempt should be made to image all areas with single pass using a reference set of hardware and software configuration.

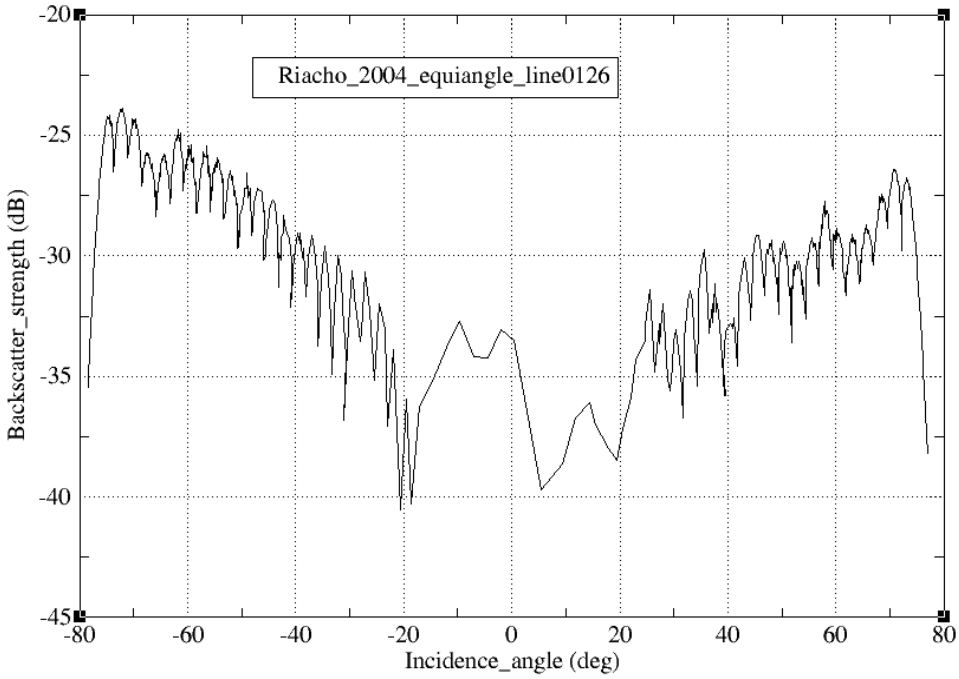

Figure 2.29 Backscatter pattern from Simrad "raw" amplitudes. Data collected in EABS +/-75^{o} in Barra do Riacho, ES, Brazil in 2004.

Chapter 3: BACKSCATTER MOSAICS

Backscatter mosaics are geographically-registered maps representing the spatial variability in seabed backscatter strength. Pixels in the map normally use gray-scale to represent the bottom backscatter strength.

The mosaicking process is executed when all the survey lines are organized in the same image (map) to represent the entire coverage of the seafloor. The process has to cope with overlapping data. Backscatter mosaics usually present along-track residuals in the survey line direction, which is caused because each single backscatter line already presents these artefacts printed at specific incidence angles, predominantly at nadir.

In this chapter, two subjects related to the backscatter mosaics will be discussed:

- First, an alternative mosaicking method adopted in this study will be explained. This method chooses to use the outer pixels to replace the inner pixels, which is the reverse of the traditional method. This takes advantage of the improvement in low grazing angle data developed in the previous chapter.
- Second, a parallel study that has been undertaken using digital image analysis techniques to reduce the along-track residuals in the mosaics will be described. This technique applies two-dimensional fast Fourier transform (2D-FFT) to the original mosaic, which brings the image to the frequency domain where the structured noise can be aggregate in on specific orientation sector for cleaning.

3.1 Mosaicking the outer beams with higher weights

During the mosaicking process, many survey lines are joined in the same map to represent the seafloor. As exemplified by the two lines in Figure 3.1, every time that one pixel from one specific line (survey line 1) occupies the same geographic position as another pixel in the adjacent line (survey line 2), software has to decide which pixel will remain in the image.

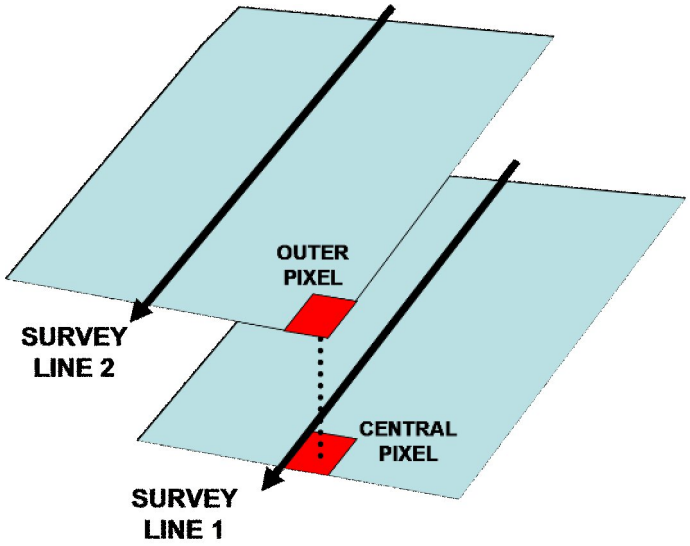

Figure 3.1 During mosaicking, the pixels from different lines can match the same geographic position. Therefore, one of them has to be chosen to be placed in the final map.

Most automatic sidescan mosaicking software has the ability to deal with inter-swath overlap. Because the outermost part of the swath is often noisy (and in the case of towed sidescan, least well geographically located), the default is to preferentially overlay inner swath data over outer swath data. This tends to retain the near-nadir backscatter variations, which have a very strong and sensitive dependence on seabed slope.

Figure 3.2 presents an example were two lines have to be mosaicked. Both inner and outer beams are noisy, so traditional decision is to keep the inner beams in final mosaics.

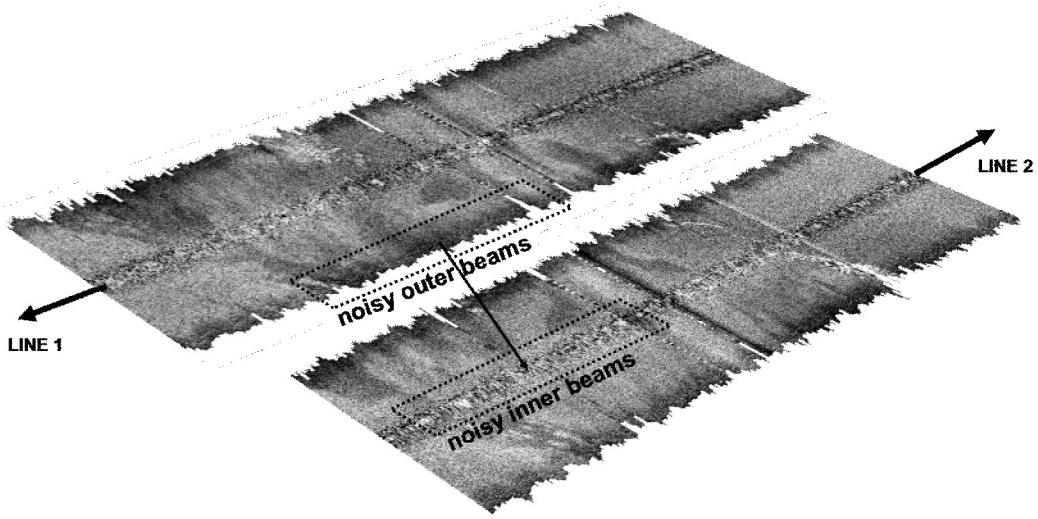

Figure 3.2 Each survey line usually presents backscatter artefacts (noise) in the inner and outer beams. Mosaicking process tend to give keep the inner beams (higher priority).

As 200% coverage has been collected and outer beam artefacts have been reduced, we have now the opportunity to replace the noisy inner beams (Figure 3.3).

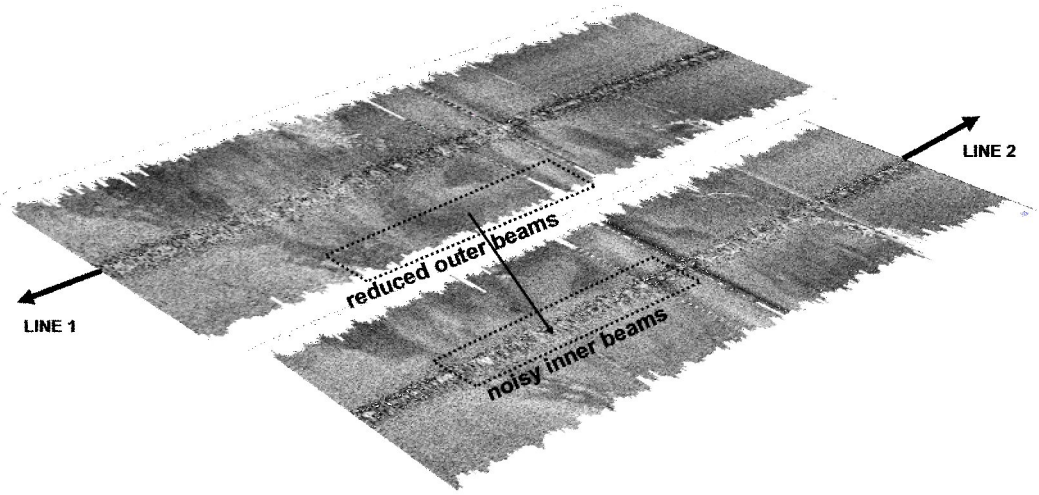

Figure 3.3 In this study, outermost beams rolling-off artefacts have been reduced. Therefore, the better quality outer beams (higher priority) can be used to replace the noisy inner beams.

In Figure 3.4, top diagram (a) presents the traditional method with inner beams having the higher weights, which is available in commercial softwares (auto-seam option). Notice that map pixels are filled with inner beams information (below the ship). Then, bottom diagram (b) demonstrates the weights established here giving more importance for the outer beams. A ramp function was created with the reverse weight function used by the auto-seam option. For this situation, map pixels are filled with low grazing angle data.

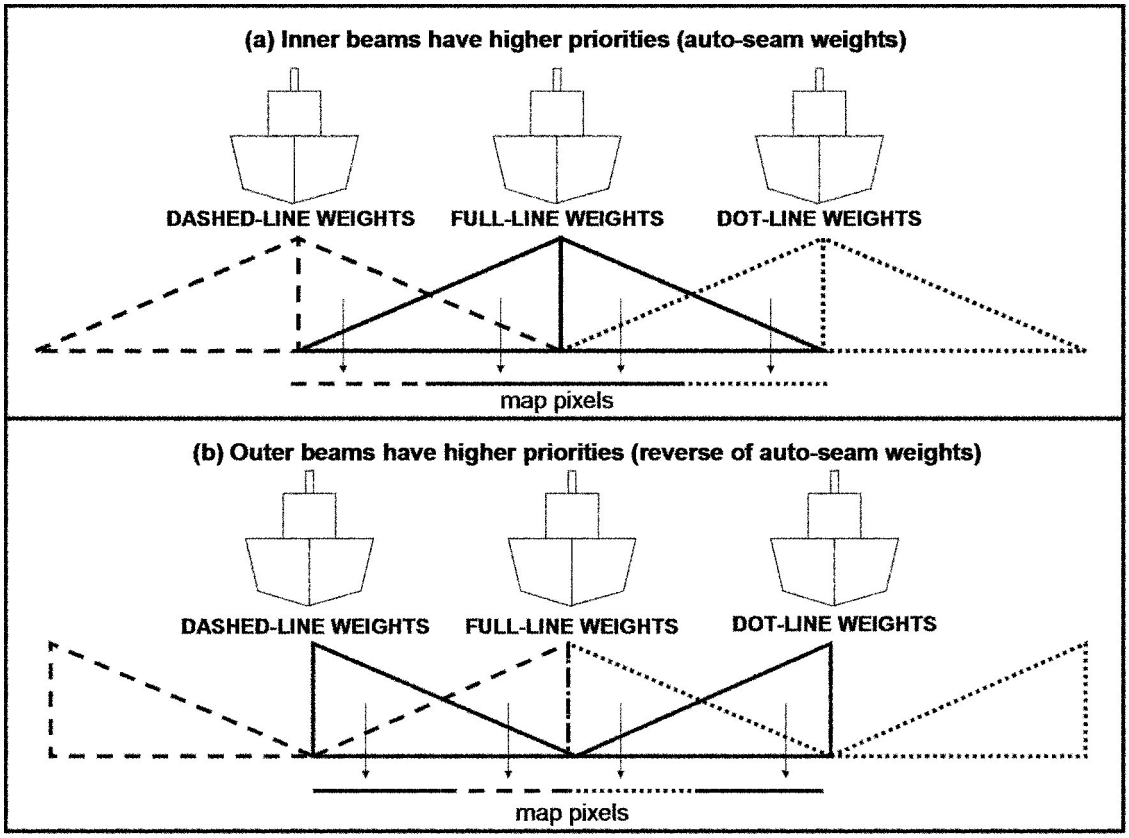

Figure 3.4 During mosaicking process, when backscatter data from adjacent survey lines occupy the same pixel (geographic position) in the map, algorithm has to decide which information has to be stored in the image. Situation (a) presents a traditional method ("auto-seam"), which gives higher priorities to the backscatter from inner beams. Situation (b) shows the weights used in this study, which intends to replace noisy inner beams by the outer beams that have been already reduced from inside-beams artefacts.

The image presented in Figure 3.5a was processed using the traditional mosaicking method (inner beams having higher priorities) and Figure 3.5b shows the results using reversed weights (outer beams having higher priorities).

The leftmost image (a) is dominated by the “nadir stripe”. Although the average variation in beam pattern across the swath has been compensated for, there is a markedly different texture at nadir that still draws the eyes. Part of the problem is that the shape of the near-nadir angular response curve is highly sediment dependent and thus averaging that over a survey line (crossing multiple sediment types) fails to account for local changes in the angular response. Also, the slope of the angular response curve is so steep, that small changes in seafloor slope, switch the echo from specular to oblique.

In the rightmost image (b), the outermost swath data of the adjacent line covers (replaces) the nadir region. Normally survey lines are spaced to achieve 200% coverage (considering the outermost beam boresite). As outermost beams record extended backscatter amplitudes beyond this range, coverage can achieve ~220%. A markedly-reduced contrast in the along-track striping in the image is evident. The line spacing, however, is not always achieving 200% coverage and occasional near-nadir data is retained. In this situation, along-track artefacts can remain in final mosaic image.

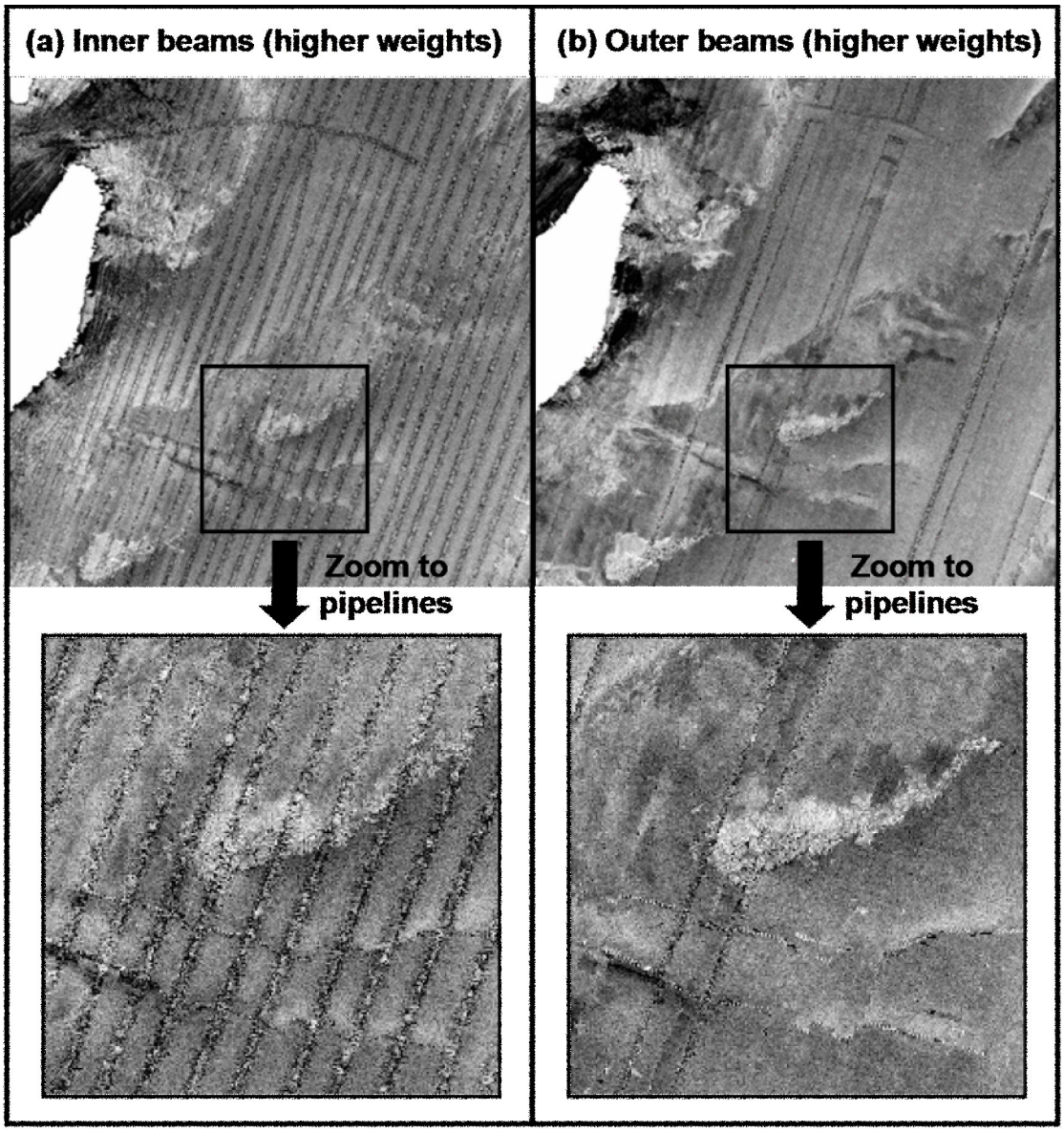

Figure 3.5 Backscatter mosaics from the harbour area prepared using two different weighting parameters: (a) higher weights to the inner beams. (b) higher to the outer beams, which has been implemented in this study and improved maps quality.

Without correcting for the roll-off in the outermost beam pattern, this would not be possible. Figure 3.6 presents two images that have been mosaicked with outer beams with higher weights. But, while image 3.6a has been reduced from rolling-off effect, the other image 3.6b has not been processed to remove these artefacts.

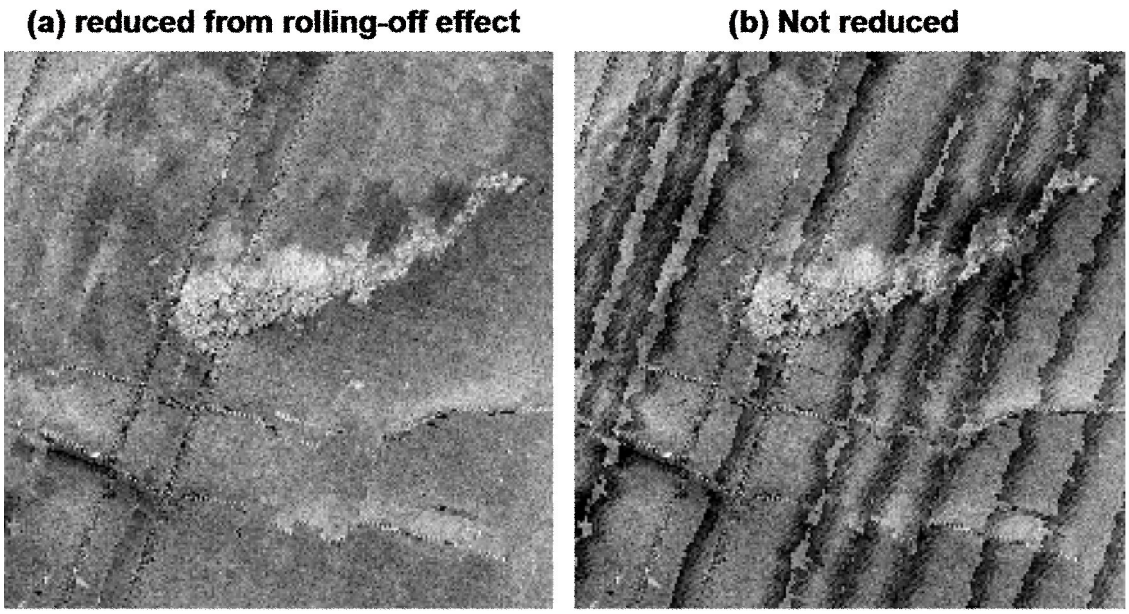

Figure 3.6 Both images were mosaicked with outer beams having the higher weights. (a) Left image has been previously processed to reduce the outermost beams rolling-off artefacts (with *tracepatt* software developed in this study). (b) Right image has not been processed to reduce rolling-off artefacts, so cannot be benefited by this weighting method.

3.2 Applying digital image analysis to reduce mosaic artefacts

Digital image analysis has one restoration technique especially designed for the structured noise [Parker, 1997], which is the noise constituted by several regularly spaced lines (Figure 3.7a). Normally, this noise occurs when electronic devices operate close to video screens.

Backscatter mosaics (Figure 3.7b) usually present along-track residuals printed in the same direction of ship's survey lines, which are very similar to the structured noise. For this reason, one parallel experiment has been undertaken to test this image restoration technique to reduce the mosaics along-track artefacts.

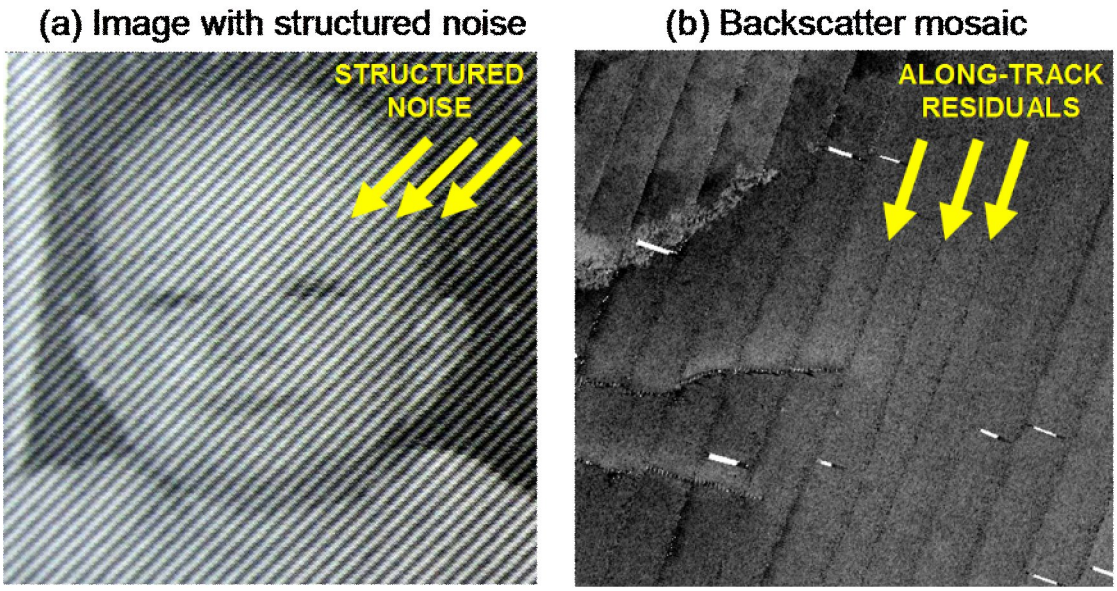

Figure 3.7 (a) The image [Parker, 1997] presents the structured noise, which reminds the (b) along-track residuals in backscatter mosaics.

The many steps involving this technique are described by Parker [1997] and are presented in Figure 3.8. First, the original squared image (128x128 pixels image in the left) is still in the spatial domain and presents the structured noise. Then, two-dimensional fast Fourier transform (2D-FFT) brings the original image to the frequency domain (centre image), where noise is isolated in two single spots to be filtered out with a box filter. The number of oscillations in the original image determines the noise location in frequency domain image, as described in the text at image bottom. At last (right image), an inverse two-dimensional fast Fourier transform (inverse 2D-FFT) is applied to bring the frequency image back to the spatial domain.

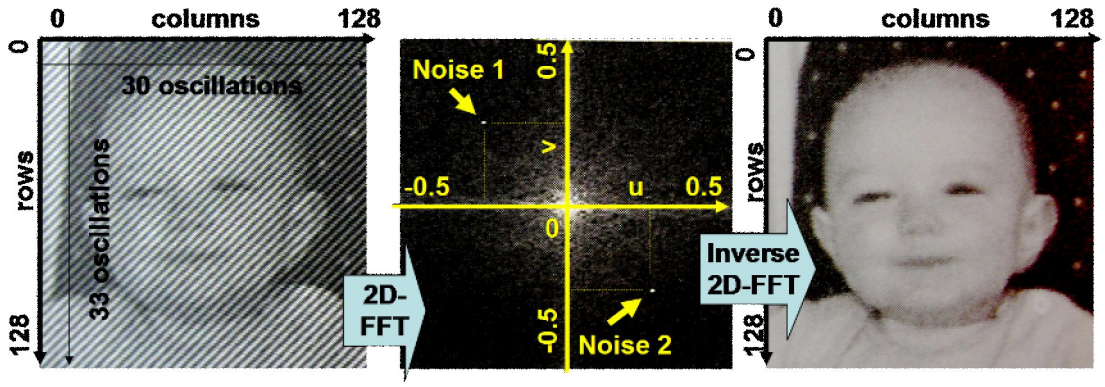

Figure 3.8 (left) The original image is in the spatial domain with the structured noise. (centre) The frequency domain image is generated when a two-dimension fast Fourier transform (2D-FFT) is applied to the original image. The noise is concentrated in two spots to be filtered out. (right) The image restored after transforming back to the spatial domain (with inverse 2D-FFT). [edited with images from Parker, 1997].

Parker [1997] already provides some programs to execute the described sequence. Mosaics were tested using the available software, but two modifications were implemented:

1. The *align* program [Parker, 1997], that is used to square the image, enlarges its size by adding rows and columns with zero value pixels to match a squared size (2^n). This algorithm was slightly changed here in order to resize the image to the smaller power of two instead, which provided a squared image (Figure 3.9 left) containing pixels with valid backscatter data only.
2. The *snr* program [Parker, 1997], which is the box filter used to filter the noise in image 3.8, cannot be used for the mosaics artefacts. They present different characteristics and new software termed *bsfilter* (backscatter filter) had to be implemented. The *bsfilter* program is explained in the following text.

After using the 2D-FFT algorithm available to convert the squared image (512x512 pixels) to the frequency domain (Figure 3.9), mosaic noise was concentrated in two angular sectors perpendicular to the survey lines direction. So, it has different characteristics to the single spots noise of previous example. The mosaic angular sector noise obtained after 2D-FFT represents the range of frequencies (fundamental frequency and its harmonics) that contribute to the image oscillations.

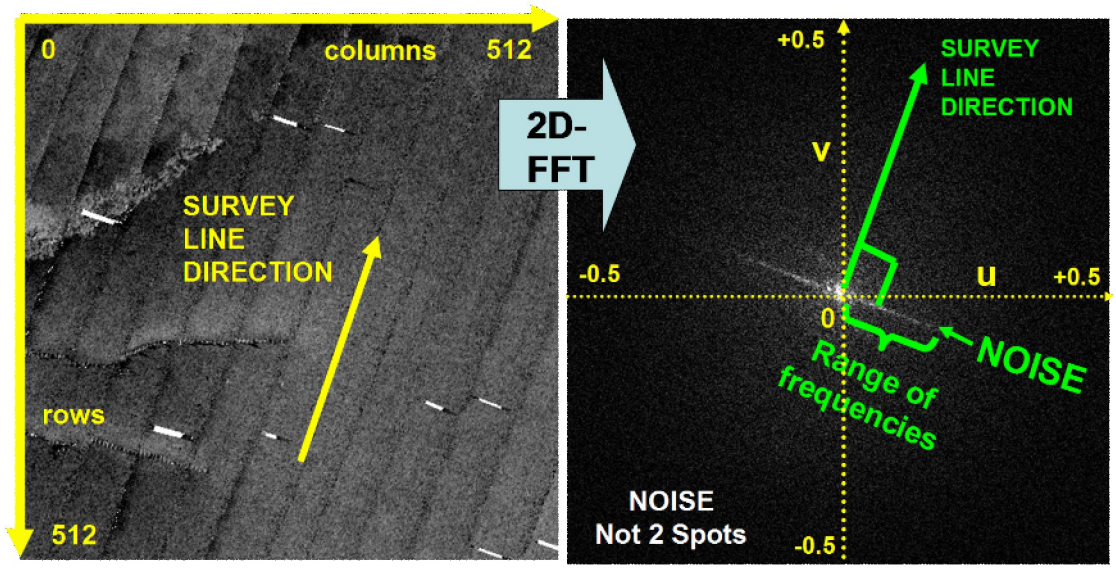

Figure 3.9 Backscatter mosaic converted to the frequency domain image. Noise is the result of the contribution of many frequencies (fundamental and its harmonics, from the 2D-FFT). It is located in a sector perpendicular to the survey lines direction.

In order to eliminate this specific noise, the *bsfilter* algorithm has been implemented here. Its command line has three arguments (survey direction, sector width and sector size) presented in the Figure 3.10, which allow the user to configure the filter.

Each command line argument has an effect in the filter, which is demonstrated by the illustrative lines drawn in the image. In this example, survey direction is 20º, which

orients the filter to the perpendiculars (110º and 290º). Filter is only represented here in the 110º direction. Sector width is 4º, then 2º to each side (108º-112º) of the filter direction. Finally, sector size is 0.4, which corresponds to 40% of the total horizontal radius.

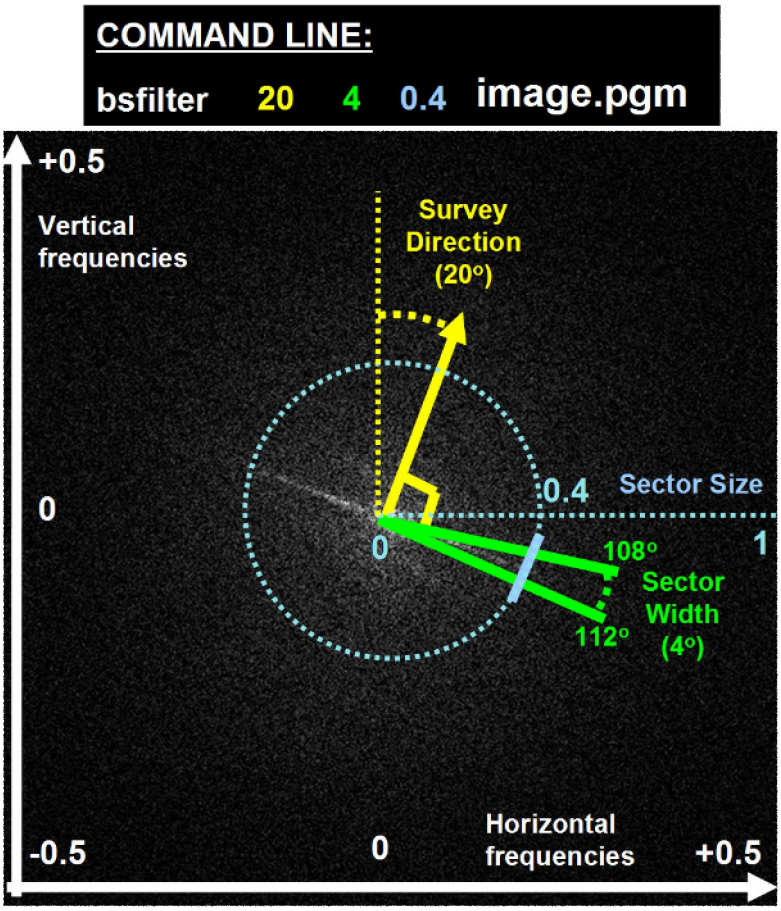

Figure 3.10 The bsfilter command line. User can choose survey direction (degrees), sector width (degrees) and sector size (percentage of horizontal radius) to reduce the noise printed in the spectral domain.

This program was evaluated with 9 backscatter mosaic images, which has been taken both from data being used in this thesis and from the internet. One advantage of this process is that no access to the original data is necessary, only the backscatter image. Also, it is important to point out that both multibeam and sidescan sonar images have

been tested and presented any improvement in their quality. Two processing results are presented below.

Figure 3.11 shows results for filtering applied to the mosaic produced with multibeam raw backscatter data. Original backscatter mosaic (left) has been filtered and produced the structured noise reduced image (right). Final image has better quality than the original, but still presents strong artefacts.

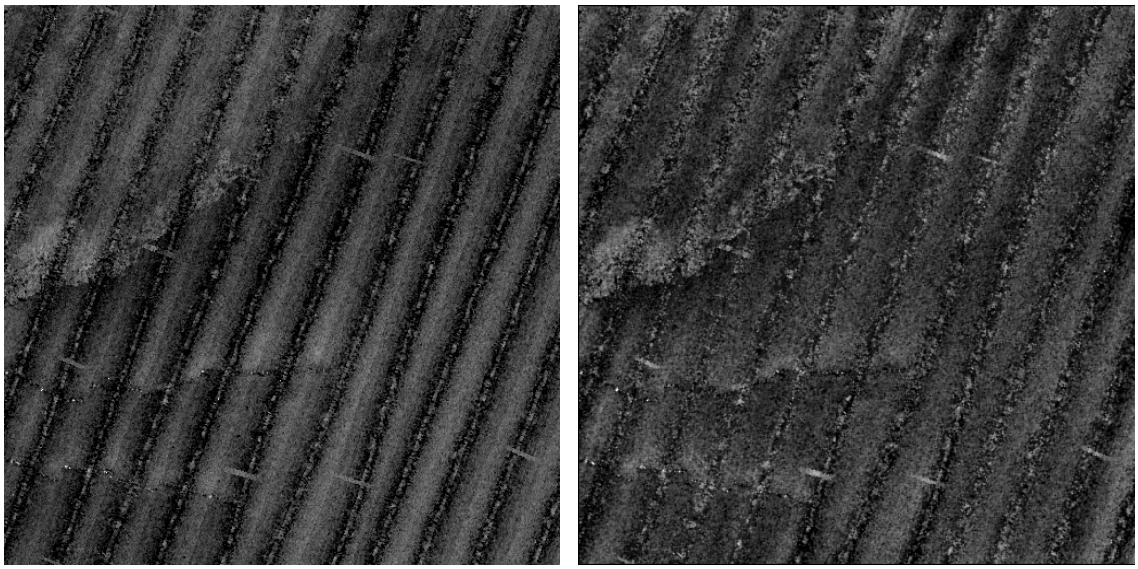

Figure 3.11 (left) Raw backscatter mosaic. (right) Structured noise reduced.

Then, same test was undertaken to filter a mosaic (for the same area) produced with data previously processed with OMG *beampatt* software (Figure 3.12 left). For this situation, filtering allowed image enhancement and produced a high quality image (Figure 3.12 right).

So, when analyzing both examples (Figure 3.11 and 3.12), we can say that spectral filter works better as a complimentary final step to be executed after the beam pattern suppression.

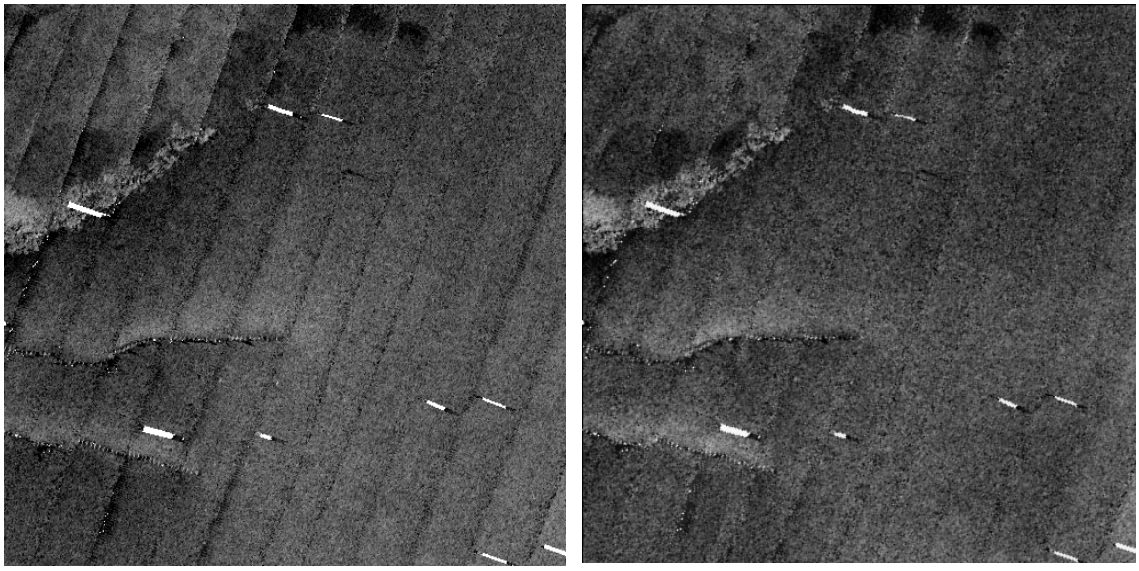

Figure 3.12 (left) OMG processed backscatter mosaic. (right) Structured noise reduced.

Whenever filtering directional noise, one has to be aware that there could be real natural geological features that have a similar wavelength and azimuth to the nadir artefacts. They will be removed also.

As surveys normally have multiple line directions and abrupt data boundaries, an additional concern is related to these situations when the spectral directional filter might fail. To evaluate these situations, the areas 1, 2, 3 and 4 indicated in Figure 3.13 were studied.

Area 1 has survey lines in three different directions, which are highlighted through the arrows. Direction 1 has several lines and directions 2 and 3 have just a few lines.

Areas 2, 3 and 4 are used to evaluate the borders situation. Each area covers different amounts of surveyed area. In area 2 (full-line box), valid data occupies ~80% of box area. In area 3 (dashed lines box), valid data is reduced to ~40%. Finally, in area 4 (small dots box), border situation is pushed harder and valid data corresponds only to ~10%.

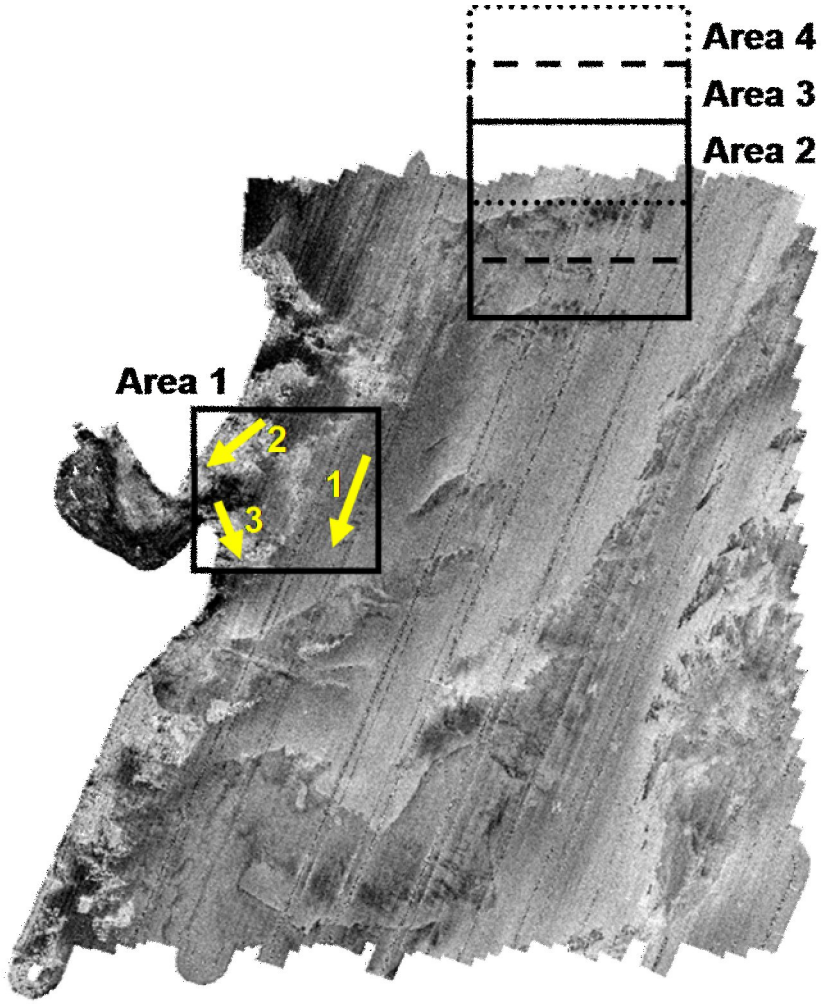

Figure 3.13 Backscatter mosaic from Barra do Riacho, ES, Brazil. Boxes illustrate areas chosen for software evaluation. Area 1 has survey lines in many directions and areas 2,3 and 4 are located at the image border.

Results of area 1 are presented in Figure 3.14. Direction 1 has many lines and marked noise in the frequency domain, which has been filtered. But, directions 2 and 3 have just few lines and are located in a rough seafloor region. Then, their signature cannot be detected in the frequency domain spectrum.

Algorithm works properly in direction 1 without affecting other directions, which represents a satisfactory result. Theoretically, any direction can be filtered independently.

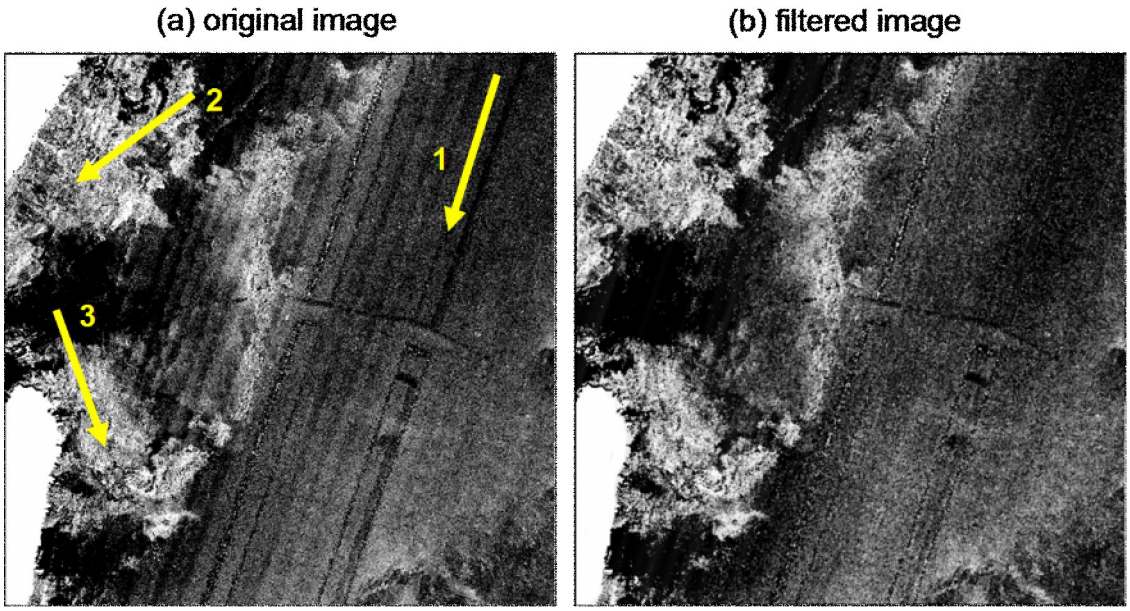

Figure 3.14 (a) Area 1 has survey lines in three directions. In the frequency domain, only the noise corresponding to direction 1 was detected. Other directions (2 and 3) cannot be detected, because they have few lines and are located in a rough seafloor region. (b) When *bsfilter* was applied for the artefacts in direction 1, resulting image presented higher quality.

Border experiment was evaluated for the three different areas (2, 3 and 4) and results are presented in Figure 3.15, which demonstrates that software was able to filter properly the along-track artefacts. Images to the left (a) are the original images and to the right (b) are the filtered images. Filtered images presented striping noise in the external area, but they have been stenciled out. A common area for both images was highlighted with ellipses. Apparently, the same improvement is achieved independently of the border situation considered. But, to optimize boxes arrangement, the 512x512 boxes should be adjusted to include the maximum percentage of data.

Therefore, *bsfilter* demonstrate to be a useful complimentary tool for reducing along-track artefacts present in backscatter mosaics.

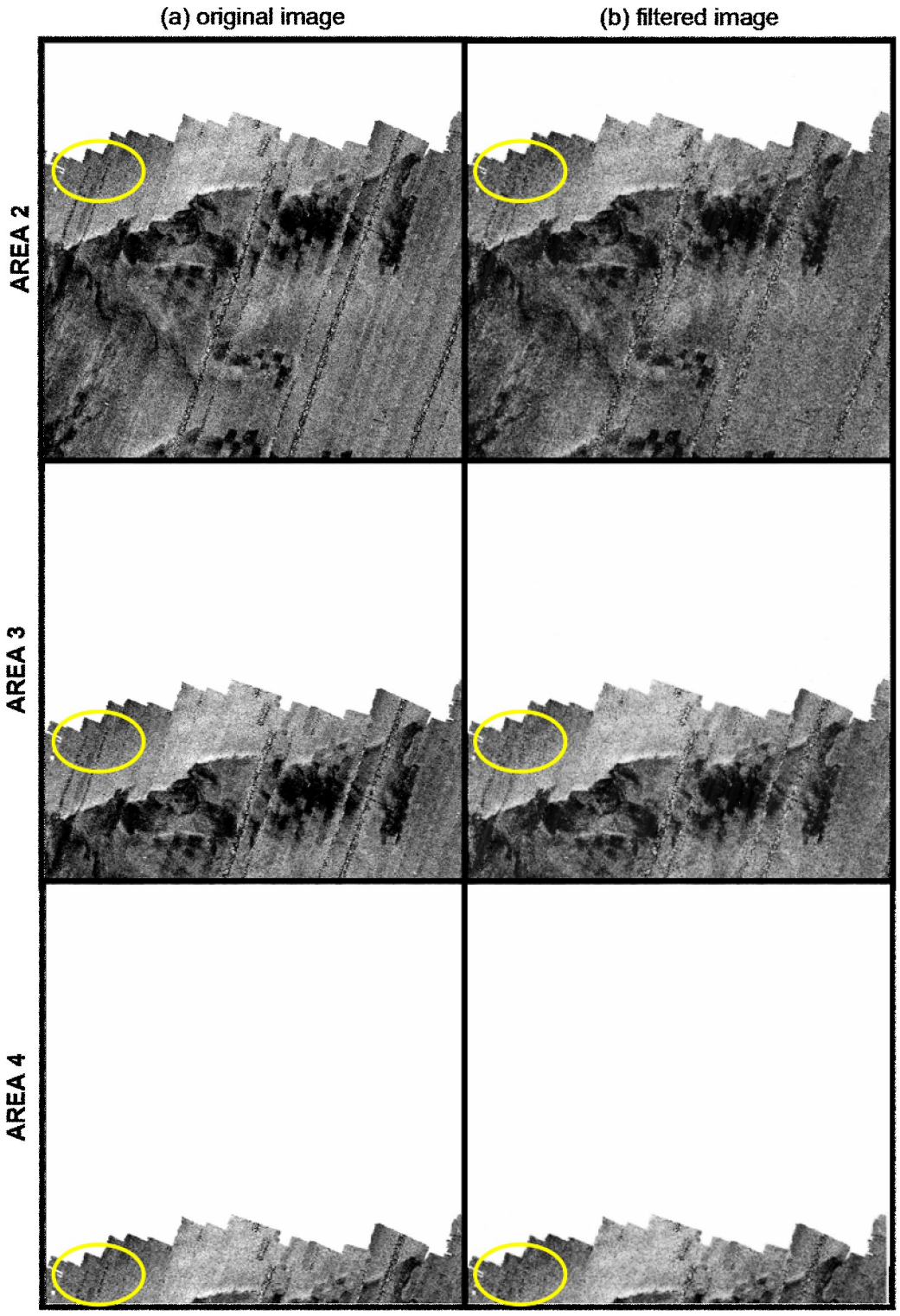

Figure 3.15 Border experiment for areas 2, 3 and 4 with different coverage. Left images (a) are the original and right images (b) are the filtered images. Ellipses highlight improvement obtained for a common region.

Chapter 4: EXTRACTING ATTRIBUTES TO AID IN SEAFLOOR CLASSIFICATION

Seafloor classification is the desired final product from backscatter analysis. First attempts to obtain seafloor properties with acoustical waves used single beam echosounders. Their normal incidence beams generate different echo-envelope shapes depending on the seafloor type [Lurton and Pouliquen, 1992]. Then, sidescan sonars had their low grazing angles backscatter studied. Finally, multibeam echosounders came with their geo-referenced beams producing an acoustical fan within intermediary incidence angles.

For the classification using multibeam backscatter, a variety of approaches have been experimented including textural methods with gray-level co-occurrence matrices (GLCM) [Pace and Dyer, 1979; Haralick, 1979; Reed and Hussong, 1989; Imen et al., 2005], angular response characterization [deMoustier and Alexandrou, 1991; Matsumoto et al., 1993; Hughes Clarke, 1994] and power spectral methods [Pace and Gao, 1988; Tamsett, 1993; Lurton et al., 1994; Hughes Clarke, 2004].

Textural methods tend to ignore the imaging geometry, working mainly on the mosaiced intensity data, thereby implicitly assuming that neither the grazing angle nor the imaging azimuth is important. Angular response characterization examines the variation with grazing angle, averaged over half a swath width, thereby implicitly only classifying regions larger than a typical swath width. In contrast to both of the other methods, power spectral classification works specifically along the ping azimuth, deliberately avoiding high grazing angle data and can be used to attempt to classify multiple sediment types within a single swath. Thus to use power spectral methods, one

needs to collect data at lower grazing angles, as was the case for the low aspect ratio sidescan systems.

For the case of typical hydrographic-purpose multibeam acquisition, however, the backscatter data collection has been usually restricted to high grazing angles, because bathymetric target detection requirements demand the better along-track coverage gained with the swath reduction. Furthermore, low grazing angles are more susceptible to the refraction and motion errors. As a result, most multibeam backscatter has been explored within smaller incidence angle sectors while sidescan sonar imagery explores the higher incidence angles. Some attempts to use power spectral classification at high grazing angles [Kavli et al., 1993 (built into the Simrad Triton software); and Quester Tangent, 2006] have been made, but are limited by the rapid changes in intensity due to seafloor slope variations approaching normal incidence.

Ideally, to take best advantage of power spectral classification, data should be collected out to lower grazing angles. The best solution is generally beyond the critical angle, which can be established through the ratios between the compressional (P-wave) sound speed of each specific sediment type and the water sound speed. As an example, for sediments with 1700 m/s of P-wave sound speed, the corresponding critical angle is ~61^{o}; for 1600 m/s, it is ~70^{o}. The reason that it is useful to collect data beyond the critical angle is that volume scattering phenomena is absent, because insignificant acoustic penetration takes place. So, roughness properties prevail and can be analysed separately. This allows a near equivalent classification to that achieved using low-aspect ratio sidescan sonars. Otherwise, inside the critical angle, surface and volumetric contributions are blended in the backscattered energy [Jackson and Briggs, 1992].

This lower grazing angle data has been collected by the Brazilian Navy with the EM1000 multibeam. And, this thesis research allowed the improvement of backscatter located beyond the critical angle, through the artefacts reduction explained in chapter 2. Therefore, valuable data is available now for power spectral analyses. But, the classification schema (described later) also uses the higher grazing angles (before the critical angle) to cover the entire area. Then, volume scattering is also present in some regions analyzed.

In this chapter, some seafloor classification methods already cited (textural analysis, angular response characterization and power spectral analysis) and others (probability density function and fractal analysis) are presented as a review. Afterwards, focus goes to the power spectral toolkit that has been created by the OMG [Hughes Clarke, 2004] to process conventional sidescan sonar data. Finally, some functions implemented here to enable the OMG toolkit to accommodate multibeam backscatter data will be described.

4.1 Overview of seafloor classification methods

4.1.1 Textural analysis

Textural analysis extracts seafloor classification parameters from the backscatter mosaics. It considers that low grazing angles backscatter is able to represent seafloor roughness. This information is printed as texture in the mosaic maps.

Haralick [1979] has produced an extensive review of image processing literature concerning the many approaches that had already been used for texture analysis. One of these approaches was the gray-level co-occurrence matrices (GLCM) method.

GLCM is able to provide statistics about the images with additional information relative to the pixels organization inside the image. For that, image is scanned in four directions (0^o, 45^o, 90^o and 135^o for example) and pixels are compared within fixed distances. It produces four (direction) matrices with NxN size (where N represents the original image gray-levels). Each matrix is evaluated through statistical processes to generate eleven feature vectors, which can be classified using pattern recognition [Pace and Dyer, 1979].

The first implementations worked with sidescan mosaics where the flat seafloor assumption was used. So, seafloor azimuthal anisotropy has not been considered. Therefore, the same area (sand waves for example) should present different textural patterns when imaged from different azimuthal directions. Other problems are referred to the angular dependence of bottom backscatter strength, which normally has not been considered.

With multibeam systems, bathymetric data is collected at the same time as backscatter data, which enables the construction of precise topographic models. They can be used to compensate the imaging geometry and enhance backscatter quality. This compensation is useful not only for the textural process, but for any classification process that will be described later.

In addition, more recent works started to consider the angular response effect [Imen at al., 2005], which should improve textural analysis performance.

4.1.2 Angular Response Characterization

Angular response is the term normally used to designate the dependency of the bottom backscatter strength to the incidence angles [Hughes Clarke, 1997].

As presented in Figure 4.1, beams can be transmitted within many incidence angles.

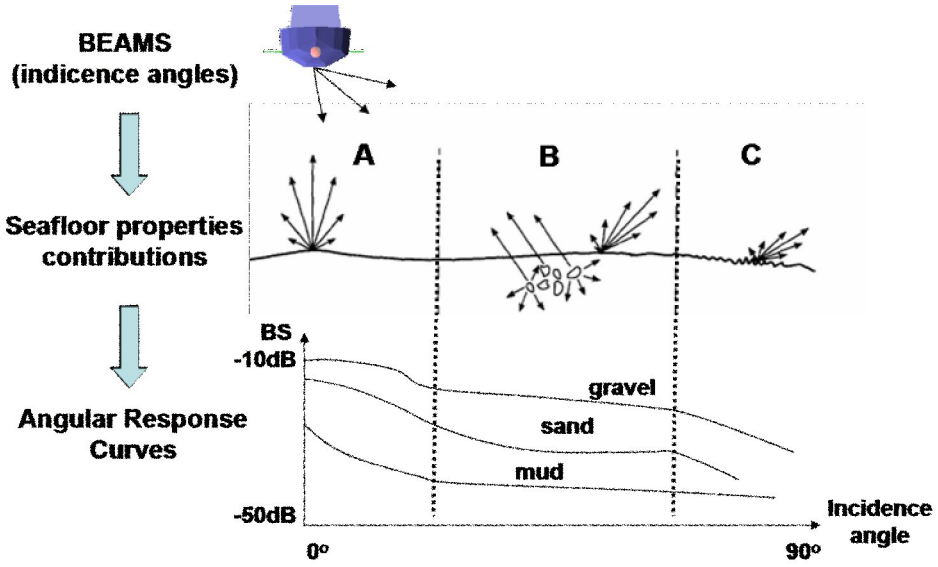

Figure 4.1 Angular response curves depend on beams incidence angles and seafloor types.

Seafloor physical properties contribute to the backscatter effect. These properties are related both to water-bottom interface (impedance and roughness terms) and to the volume inhomogeneities buried inside the seafloor (subbottom terms). Each property can present more contribution than the others to the backscatter strength depending on the ensonification (region A, B, C):

Region A) In normal incidence situation, response can be determined by the interface large scale roughness, through the tangent plane Kirchhoff theory [Jackson et al., 1986a].

Region B) In oblique incidence situation, small scale roughness (Bragg scattering) and volume scattering have important contribution [Augustin et al. 1996]. For low impedance sediments, volume scattering contribution becomes more relevant than the roughness [Hughes Clarke, 1997].

Region C) In very oblique incidence situation, small scale roughness prevails. This region is beyond the critical angle, where sound speed ratios between the water and seafloor are enough to prevent (through Snell's law) acoustic waves to penetrate in the seafloor.

Angular response curves are produced with the plotting of the backscatter strength for the entire angular sector. Their shapes, variances and magnitudes [Hughes Clarke, 1994] can be used as a seafloor classification tool.

One disadvantage of this classification method is that it requires areas with extensions at least half of the sonar swath width. Then, deeper regions demands larger areas with same sediment type to work properly. But, this method is useful to work together with others, as explained in the improvement provided for textural method.

4.1.3 Probability density function (PDF)

Bottom backscatter can be considered a stochastic process. Therefore, statistical analysis seems to be useful to represent it. To do this analysis, echoes at only a narrow range of grazing angles can be considered (else the variance is related to angular response as well as scatterers). De Moustier [1986] first applied this method to the vertical incidence multibeam (near-nadir) where coherent specular echoes are common. In

contrast, Stewart et al. [1994] applied this just for low-grazing angle (70^{o}-85^{o}) sidescan data. At those angles, coherent echoes are rare. For their case, however, rough basaltic rock ridges in the survey built inward facing facets that produced some coherent responses. Hellequin et al. [2003] describe the correlation between amplitude statistical distributions and incidence angles.

Probability density function (PDF) is used to draw the behavior of backscatter statistical distributions. Flat smooth surfaces tend to follow a Gaussian distribution (with echo coherent response) and rough surfaces have a Rayleigh distribution (with incoherent echo response), like presented in figure 4.2.

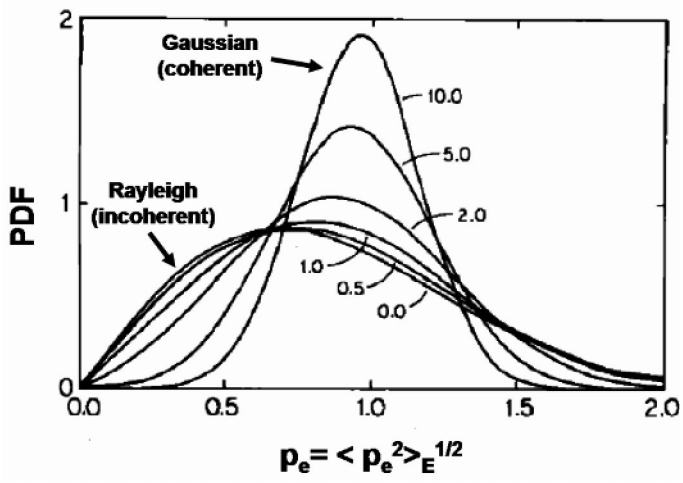

Figure 4.2 Probability distribution function (PDF). When analyzing the statistics of echo-amplitudes, flat smooth surfaces present a Gaussian distribution and rough surfaces a Rayleigh distribution. [edited from Stanton, 1984]

4.1.4 Fractal Analysis

Fractal concept is associated with geometrical objects satisfying 2 characteristics:

- Self-similarity: object can be portioned in smaller and smaller pieces, which (statistically) resemble the original object. If we consider a large

portion of the seafloor and start to divide in smaller areas to be studied in different scales, they will follow similar properties.

- Fractional dimension: object has two endpoints, but without defined length. Depending of the scale of measure (different rulers), object has different lengths.

Figure 4.3 presents one algorithm (box-counting) usually applied in fractal analysis. This figure is presented just to best explain how fractal works and the fractal dimension concept.

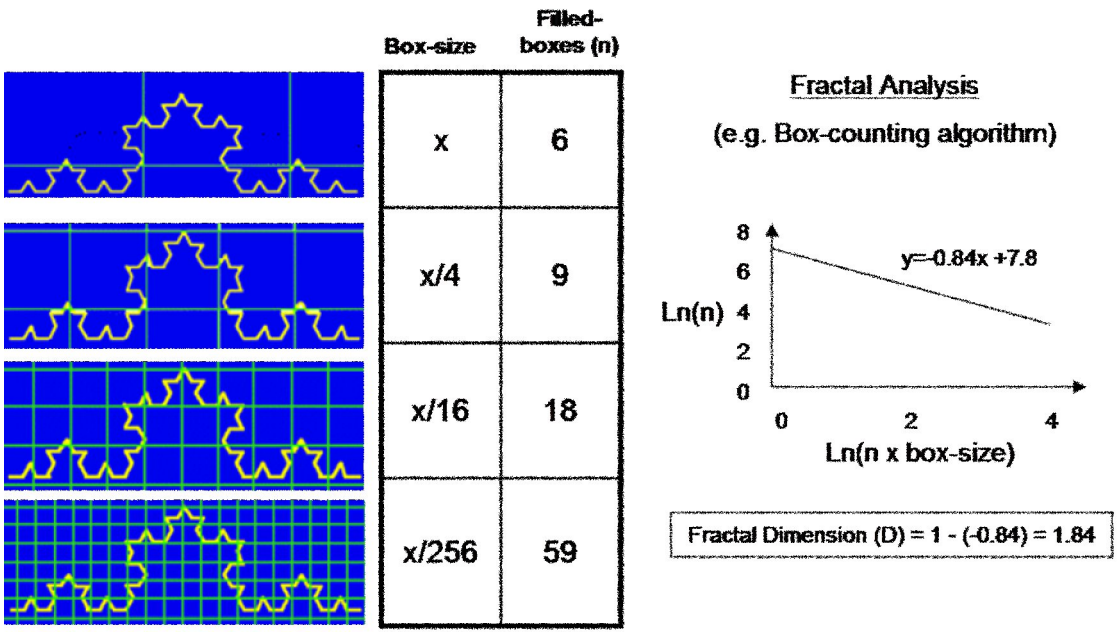

Figure 4.3 Box-counting algorithm used in fractal analysis. Image is analysed in many scales (box-sizes) resulting in different number of filled boxes. The negative slope in log-log space represents the fractal dimension [edited from University of Washington - Dept. of Radiology website].

Linnett et al. [1991] and Carmichael et al. [1996] used fractal analysis to measure seafloor properties from the backscatter oscillation. Instead of using the box-counting

algorithm, they used the perimeter-area measure technique. For their application, sidescan image is a surface where heights are represented by backscatter amplitudes. They considered the mean backscatter as the central surface and backscatter oscillations have the maximum distance (scale +/-ε) from this surface. Two "blanket" surfaces are built in the upper and lower levels +/-ε. The volume enclosed by the two blanket surfaces divided by 2ε gives an area A_ε. The ratio of change in this area A_ε within different scales ε represents the fractal dimension.

4.1.5 Power Spectral Analysis

For the power spectral analysis, 1D time (or range) series of backscatter intensities (linear or logarithmic) within delimited areas of the seafloor are processed through the Fourier transform method. Therefore, results are able to deliver energy content inside each area for different spectral bands.

Pace and Gao [1988] executed the first experiments with power spectral analysis for seafloor classification. They established some spectral features (classifier parameters), which are defined from ratios of energy content in different spectral ranges.

4.2 OMG seafloor classification toolkit

As commented before, Pace and Gao [1988] have experienced the power spectral method for seafloor classification. Their results with sidescan sonar backscatter suggested up to 97% success in classification. Significantly, they dealt with low-aspect ratio sidescan data and specifically avoided the near nadir backscatter data (which is only a small percentage of the swath).

OMG has developed two algorithms to work with power spectral analysis:

1. *sslook* option inside *jview* program allows the user to have a closer look in spectral contents for each line. This software was used just to verify if *tracepatt* corrections (implemented here) had satisfactorily enhanced the data quality for classification processes.
2. *classSS* program has been develop to process statistical and power spectral analysis of the data and deliver maps related to these analysis. This software was effectively modified here in this work to accommodate multibeam sonar geometry.

Both programs (*sslook* and *classSS*) usage will be described in the next sections.

4.2.1 Testing the usefullness of implemented process for power spectral analysis

After the end of processing steps and filling hopping gaps, the OMG *sslook* tool was used to enable a closer look in the validity of using the outer traces that were normalized and filled for classification.

The *sslook* tool [Hughes Clarke, 2004] automatically extracts a ground-range corrected intensity profile over a user-selected length and number of immediately-adjacent pings. For each profile, an FFT is performed to look at the power spectra. All spectra for the user-specified number of pings are averaged and the resulting average power spectra are then available for analysis [Pace and Gao, 1988].

Figure 4.4 presents the comparison between central beams (~50^o-68^o grazing angle) and outer beams (~68^o-75^o) spectral powers. In both examples (a and b), data have already been compensated for angular response effect with the *beampatt* software.

Therefore, as there are no real changes in the seabed type from the inner to outer swath, the two spectra should be near identical.

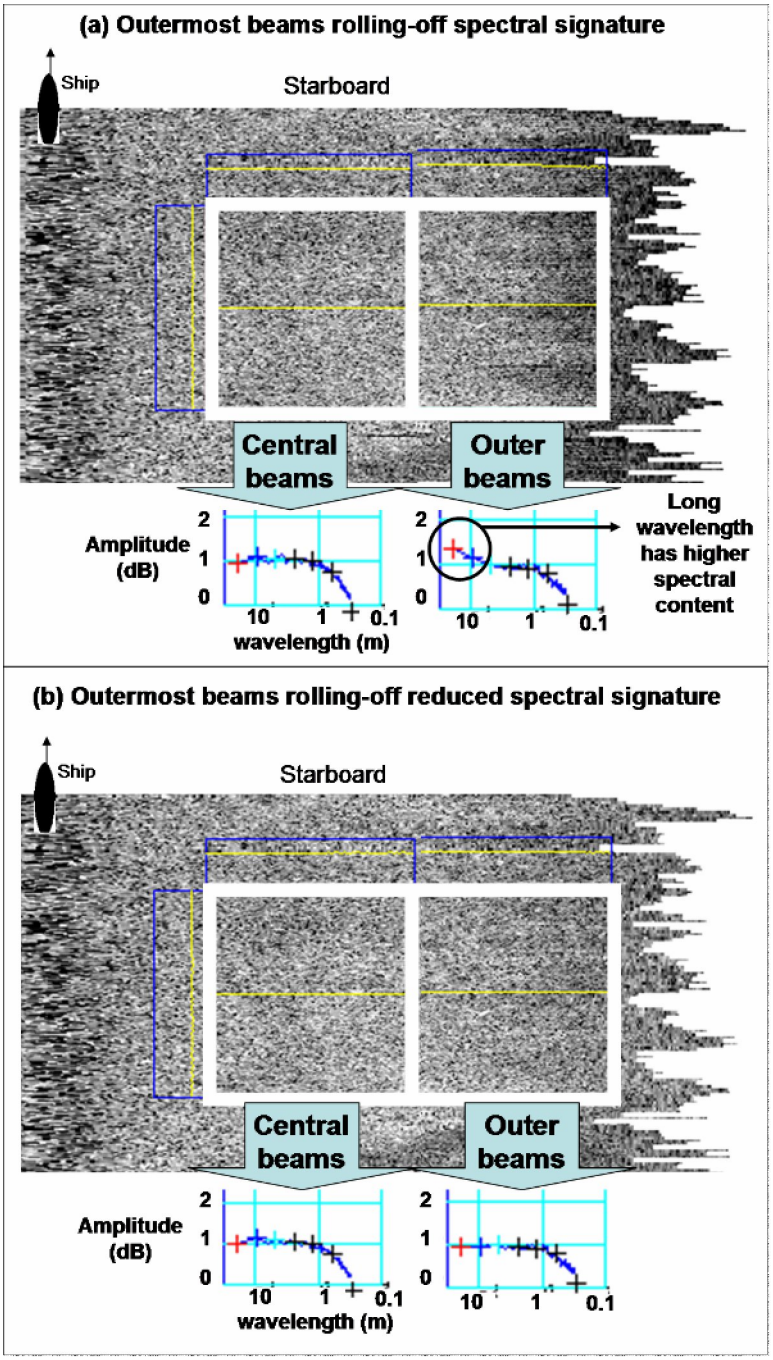

Figure 4.4 The OMG *sslook* software permits the selection of boxes where power spectral analyses is performed. (a) Backscatter presenting rolling-off effect was evaluated and spectral maps of outer beam present higher power for the wavelengths bigger than 10 m. (b) Rolling-off reduced backscatter situation, shows closer spectral power between central and outer beams.

In the top image (a), comparison was undertaken with data not normalized yet for the outermost traces rolling-off artefacts. By comparing regions of the seabed both in the central and outer beams, their spectral maps show that outer beams rolling-off is generating an apparent long wavelength (>10 m) signature that needs removing.

In the bottom image (b), the same analysis was evaluated for the backscatter that has been normalized with the *tracepatt* algorithm, so rolling-off was reduced. Results now present more similar spectral signatures between central and outer beams, indicating that equivalent textural signatures can now be obtained irrespective of the location of the terrain within the swath (still excluding near-nadir though).

4.2.2 Evaluating Backscatter analysis and producing classification maps

More recently, the OMG developed *classSS* software [Hughes Clarke, 2004] to deal with a keel mounted sidescan sonar situation. This software reproduces the Pace and Gao [1988] approach with the important addition of looking at the average backscatter strength. The Pace and Gao method had normalized all spectra to the peak level as the early sidescan sonar data had automatic gain control and thus the mean value had no classification significance.

A second important difference is that Pace and Gao worked with time series only. For low aspect-ratio sidescan, this is nearly equivalent to the ground range. But, for high-aspect ratio systems, the time series varies in ground range sampling. If we are to relate spectral bins to spatial variations (in metres), we must slant range correct the data. Speckle dimension is related to time sampling though and will be distorted in the ground-

range representation. Because of that, near-nadir regions (where time sample and ground sample ratios change rapidly) have been avoided.

In the classSS tool, the user chooses the number of pings (along-track size) and number of pixels (across-track size), which are the parameters to define classification boxes sizes (Figure 4.5). Inside each box, backscatter amplitudes are evaluated through statistical and power spectral algorithms.

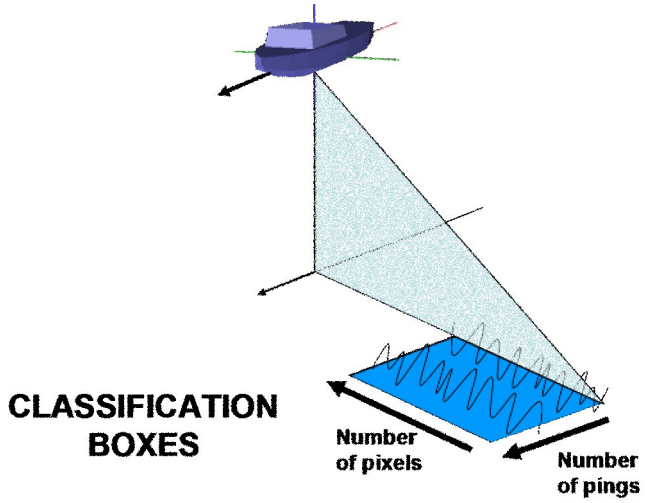

Figure 4.5 Classification box size is defined by the user, who chooses the number of pings and pixels.

Statistical analyses include backscatter average and standard deviation. Higher components (skewness and kurtosis) could be considered but are ignored herein. Power spectral analyses calculate energy concentration in seven different spectral wavelengths (the fundamental frequency and its harmonics).

This program was adapted in this study to accommodate the multibeam sonar characteristics, which works in a different angular sector than sidescan. As presented in Figure 4.6, sidescan sonars (a) are operated close to the seafloor and suffer small depth

(distance to the seafloor) variations. Therefore, the outer range is almost fixed, which permits the use of classification boxes at regular spacing. For the multibeam echosounder, depth variations and different angular sectors (wide (b) or narrow (c)) modify the outer range. So, classification boxes require more sophisticated positioning.

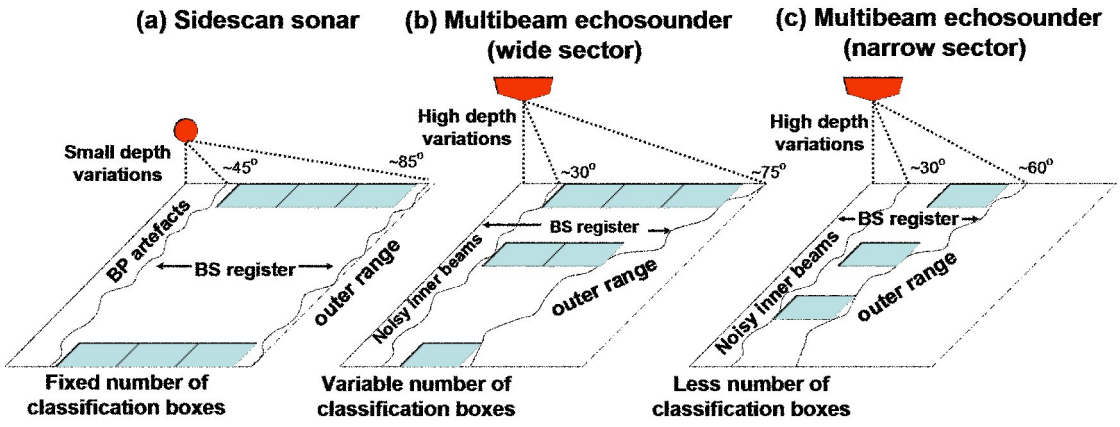

Figure 4.6 (a) Sidescan sonar is operated at regular distances to the seafloor. Their registers present regular range, which allows fixed number of classification boxes at regular spacing. (b and c) Multibeam echosounder operates fixed in the ship and can be operated with different angular sectors (wide or narrow). Their backscatter register are more susceptible for depth oscillations and requires more sophisticated boxes spacing.

Therefore, in this study, standard size classification boxes are still used for statistical and power spectral analysis, but the boxes are now dynamically repositioned for a geometry best suited for the multibeam echosounders.

4.3 Adapting classification boxes to work with multibeam

Software modifications implemented had to cope with the irregular swath width and higher aspect ratio of multibeam sonar backscatter. These modifications included a function to detect outer beams range to become the start point of the classification boxes creation, therefore accounting for depth oscillations during the survey. This facility ensures that outermost beam traces can be fully exploited. If outermost beams are not

properly compensated before, software allows the user to decrease external angular limit where classification boxes have to begin. As commented previously, the boxes have their size defined by the user (number of pixels across-track and number of pings in the along-track direction). The inner incidence angle limit can also be chosen to avoid the noisy close-nadir region. The number of classification boxes across the swath is therefore not constant. Rather it is dynamically varying to address just the most appropriate data.

In Figure 4.7 the boxes are represented in the backscatter strip before geo-referencing, having the compression effect in the along-track direction. The full-line registered in the top of the image is created to signal an invalid stack of pings eliminated from the classification procedures.

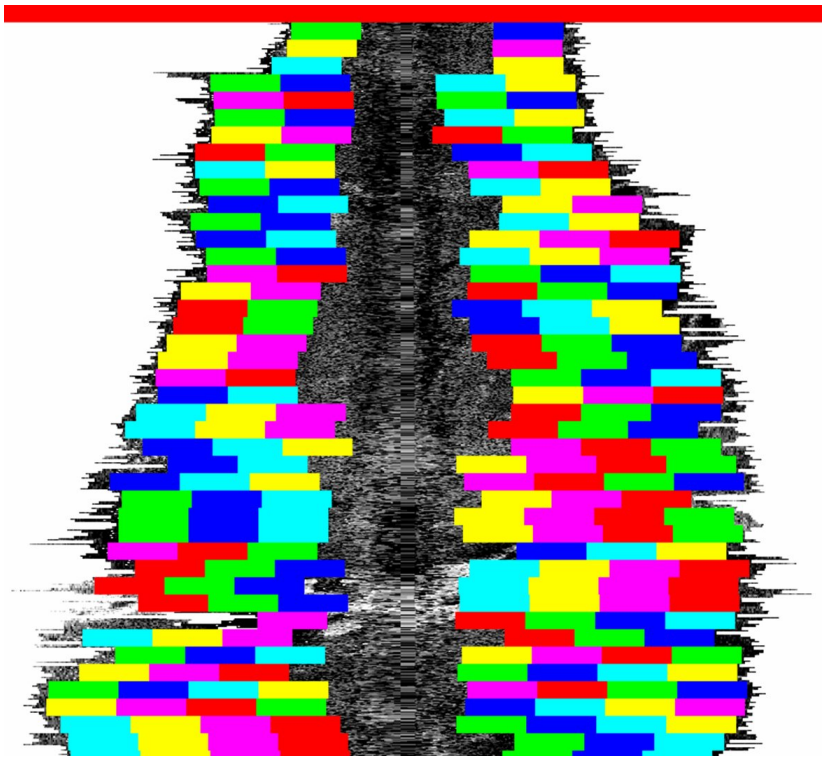

Figure 4.7 Classification boxes with outer limits of 75º and inner limits of 30º. Boxes across-track sizes of 128 pixels (each pixel with 0.15m) and along-track sizes of 16 pings (vessel at ~4m/s and ping rate ~3.3Hz). Boxes start position adjusts to the depth variations because outermost pixels are detected. Top full-line is a flag-out signal because of invalid ping occurrences, therefore stack is discharged. Note how the nadir-data with its unique textural characteristics is ignored.

During backscatter processing, pixels were generated with 0.15 m radial dimension to match the sonar pulse length that determines the across-track resolution. Power spectral boxes were created with 128 pixels, so each box has an across-track dimension of 19.2 m, corresponding to the maximum spectral wavelength that can be determined in this case. The along-track size is determined by the number of pings, which was established as 16 pings. Vessel average speed was ~4 m/s and ping rate of 3.3 pings per second, so along-track box dimensions are ~19.4 m. Therefore, classification boxes used were almost squared with sides approximately ~19 m.

These boxes were implemented to process statistical and power spectral with backscatter trace data, including the outermost beams but avoiding close-nadir region. As the outermost beams have been compensated, they were able to properly fill the gaps of inner beams of the adjacent lines. As the ship has surveyed to acquire 200% of area coverage, this schema permitted the creation of classification boxes for the entire survey area, as presented in illustrative image edited from real processed data (Figure 4.8).

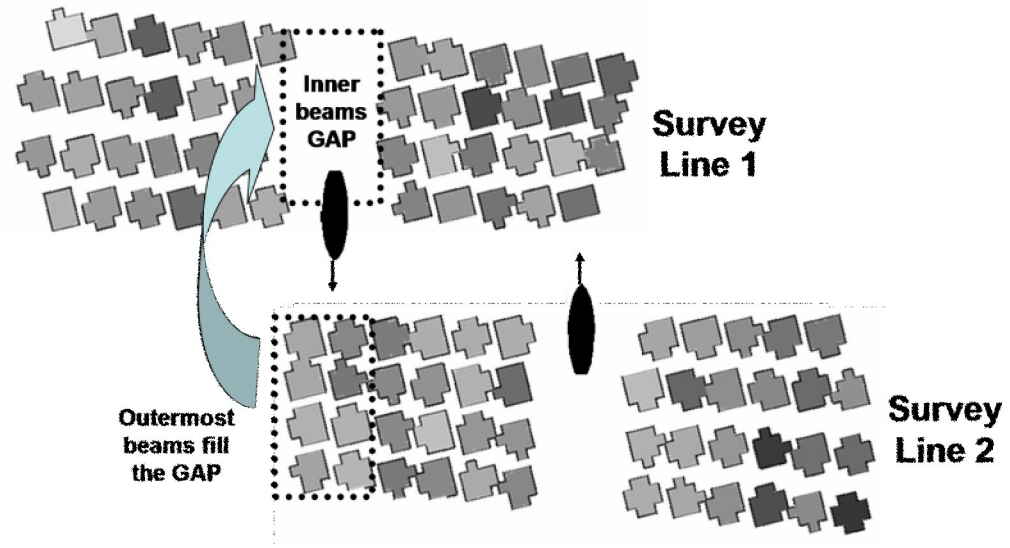

Figure 4.8 Outermost beams are able to fill the gaps created in the near-nadir region of the adjacent lines. Inner beams have been taken out from the statistical and power spectral analysis because they are more prone to have artefacts.

4.4 Seafloor classification processing results

The software was used to process all the survey lines. For each ~19x19 m patch (classification box), a series of parameters are extracted including the average backscatter strength, standard deviation and 7 representative spectral powers.

The first products delivered by the classSS software are the statistical maps (average and standard deviation) presented in Figure 4.9.

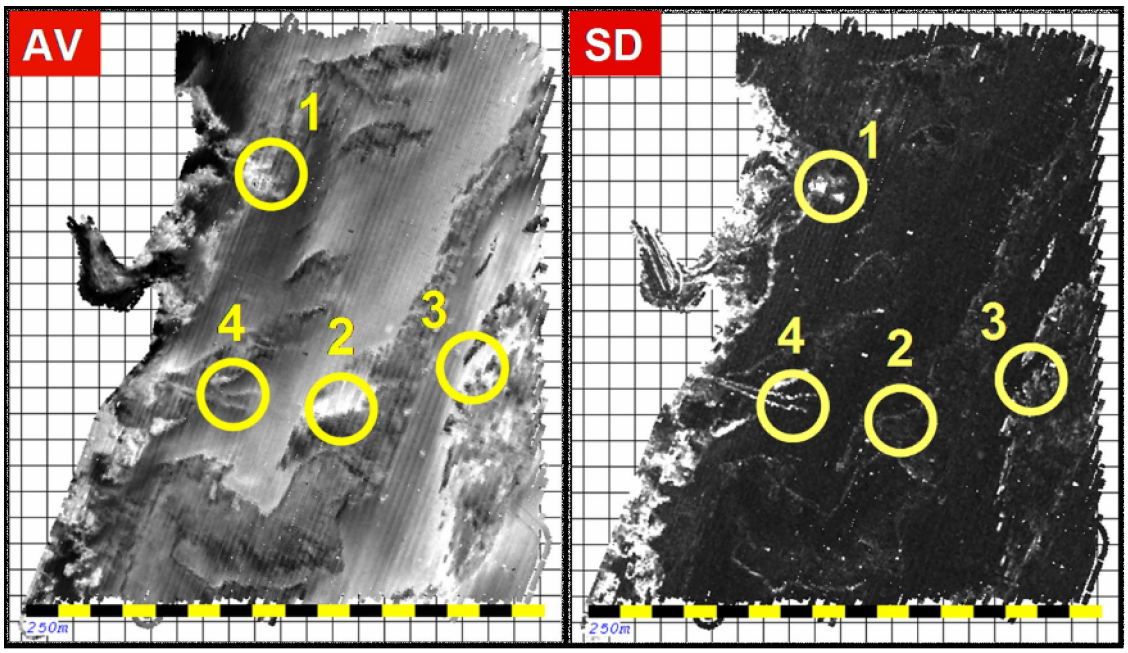

Figure 4.9 Statistical maps (average and standard deviation) produced during processing steps.

The average map for the entire surveyed area has four distinct regions highlighted: (1) shoreline, (2) intermediate, (3) offshore and (4) pipelines location. This is the prime output of most regional backscatter mosaics. It is only a valid classifier if radiometric and geometric corrections have been applied. Already, clear sediment boundaries are visible. However, based on the ground truth data, we know that multiple

sediment types can produce the same mean backscatter strength. We therefore wish to better separate these sediment types through the use of more degrees of freedom.

The standard deviation map was able to enhance regions with strong textural signature. The pipelines location (region 4) was highlighted when compared to the other maps (including to the sun illumination bathymetric map).

The other degrees of freedom available from this classification method derive from power spectral maps for 7 wavelengths (19.2 m, 9.6 m, 4.8 m, 2.4 m, 1.2 m, 0.6 m and 0.3 m). Each spectral map represents energy content (amplitude in dB), which proceeds from seafloor backscatter variations occurring in the specified wavelength. Backscatter variations are related either to topographic characteristics (changes in seabed slope) or seabed patchiness (changes in seabed type over the area).

Results demonstrated that power spectral maps can contribute to seafloor type segmentation. When comparing the areas under the number 1, 2 and 3 on Figure 4.9, one sees they have similar mean backscatter and cannot be segmented.

Analysing the power spectral maps in Figure 4.10 though, these regions can be properly segmented as having distinct characteristics. At 19.2 m wavelength, all the regions still are have energy content. But, at 9.6 m wavelength, the intermediate region 2 has lower energy. Continuing to the next 4.8 m wavelength, the offshore region 3 loses energy and only region 1 remains.

As one examines shorter wavelengths, more seafloor facies are segmented. In the sixth spectral map, at 0.6 m wavelength, no more distinction can be observed between the areas.

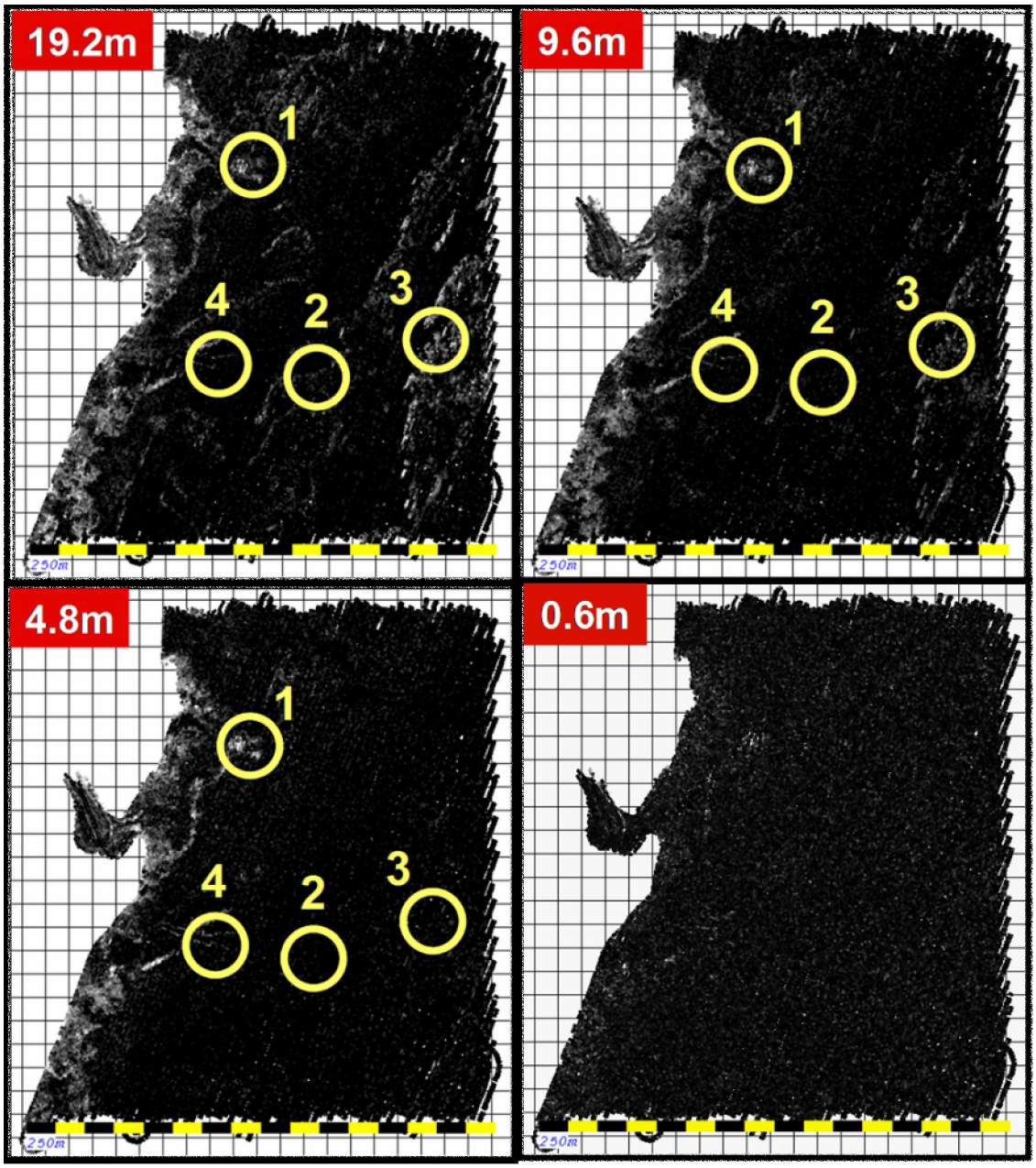

Figure 4.10 Power spectral maps showing energy concentration within different wavelengths.

Similar results were found by Hughes Clarke [2004] when wavelengths smaller than 0.8 m (~5x the pulse length) could no longer be used to segment different sediments. At this level, speckle phenomena compete with real patchiness in contributing to the backscatter variability. Therefore, as the pulse length is related to the minimum scale of

patchiness that can be detected, we should suppose that sonars with 4 times larger pulse lengths than the EM1000's sonar (0.15 m pulse length) should still produce equivalent spectral maps. This is an important result as many of the multibeam sonars automatically change pulse length with signal to noise and we wish the classification scheme to be equivalent at all pulse length settings.

Although the within-beam pattern correction is mostly used in the outermost beams, under conditions where inner beams occasionally mistrack, the backscatter data includes anomalous low backscatter zones in the place of dropped beams. Although this does not grossly alter the look of the data, these low backscatter zones can alter the spectral signatures, providing false spectral energy and wavelengths close to the beam spacing. By applying the within-beam correction to all beams, these inter-beam gaps are removed and the spectral signatures are more faithful.

These maps indicate the classification potential of the spectral information, but further analysis would be needed to delimit the exact location of each different seafloor type. For this task, an automated, but supervised classification is the most adequate, which should require the comparison with selected seafloor grabbed samples of the area. This would be the natural next step, but is beyond the scope of this thesis. Samples that are available were collected in 1983 in sparse locations. The produced backscatter and power spectral maps are able to provide the information to support the planning of a future seabed sampling survey, because they can indicate more efficiently the locations to collect new grabbed samples or photographic images.

Results were considered satisfactory as they enabled the production of maps covering the entire area with high-quality processing. Furthermore, Barra do Riacho

survey area has been divided in 8 sub-areas (Figure 4.11), which enabled the production of higher resolution maps.

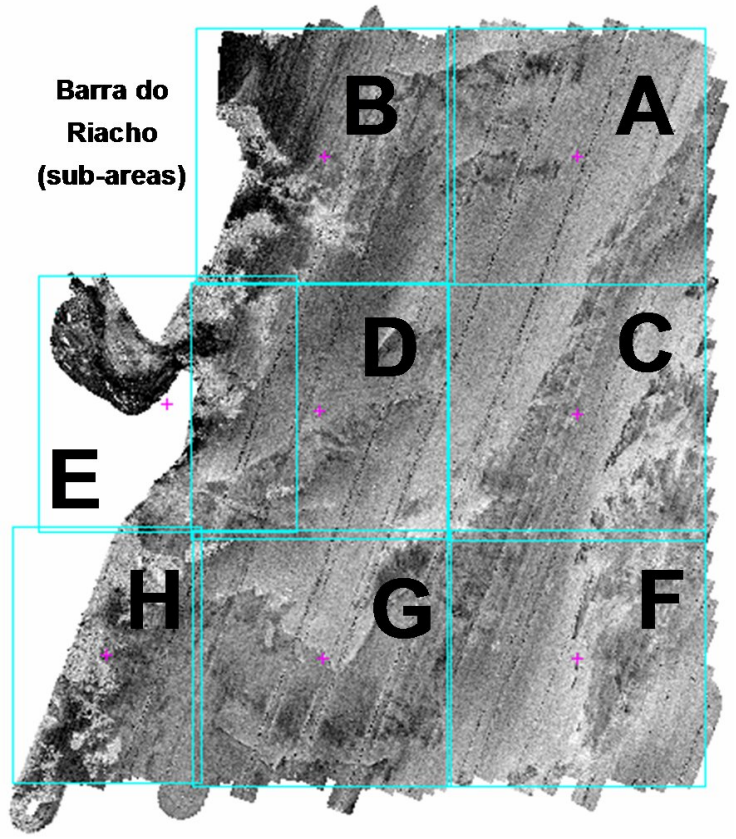

Figure 4.11 Barra do Riacho survey area has been dived into 8 sub-areas for the production of higher resolution maps (1x1m pixels).

Sub-areas maps were produced with 1m x 1m pixels. One example for area B is presented in Figure 4.12, which can be used while planning next surveys in this area. The following maps are presented for each sub-area:

- Bathymetry (BATHY) and backscatter strength (BS);
- Average backscatter (AV) and standard deviation (SD) from statistical analysis; and
- Spectral amplitudes for the larger wavelengths (19.2 m, 9.6 m, 4.8 m and 2.4m) from power spectral analysis.

This data presentation is intended to allow subjective comparison of different seafloor regions. It is suggested that it could be a standard product for aiding the surveyor in designing seafloor sampling locations.

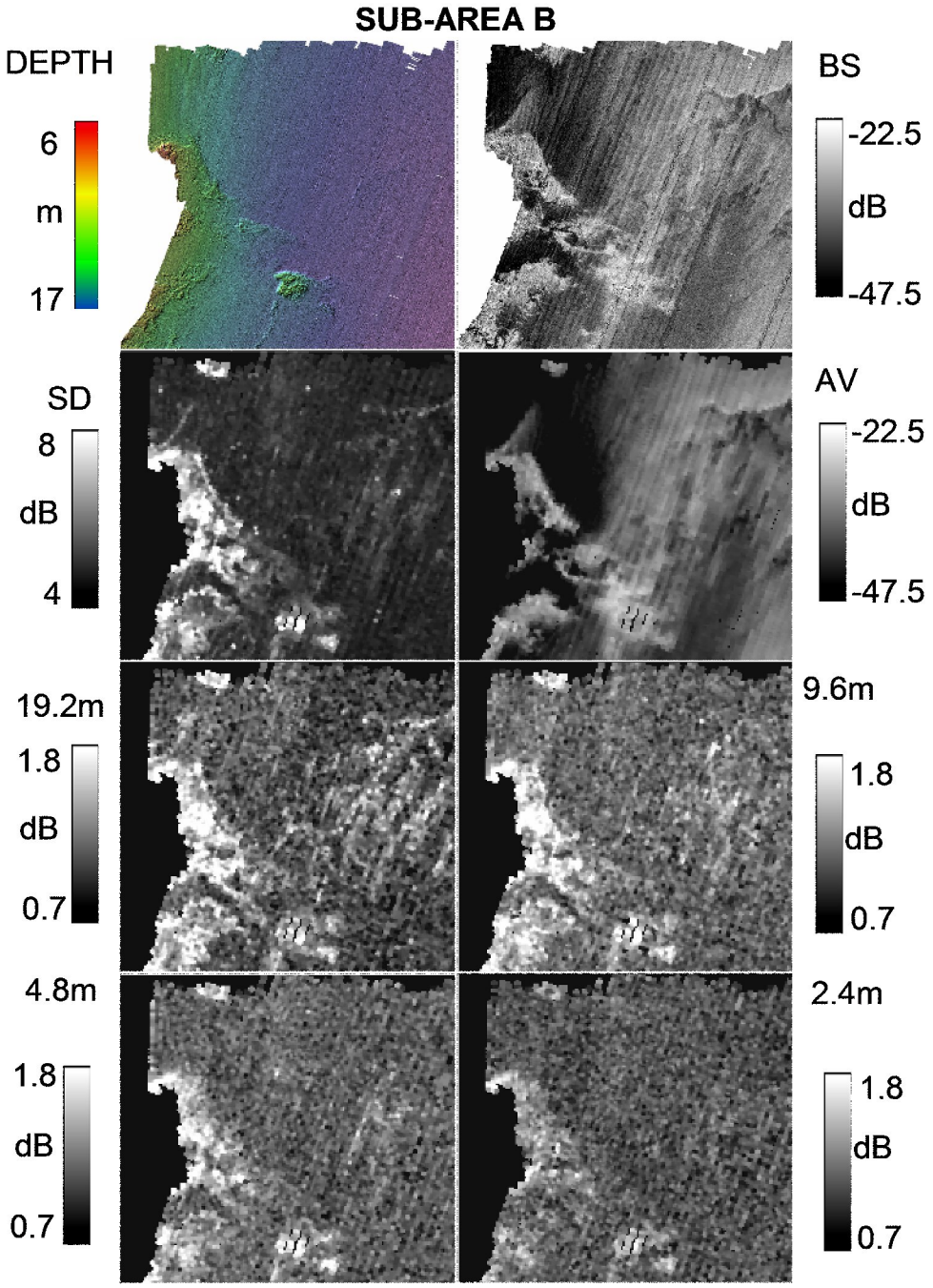

Figure 4.12 Example of maps produced at the end of processing for sub-area B.

Chapter 5: EM710 MULTI-SWATH MULTIBEAM

Modern sonars like the EM710 are starting to operate with multiple across-track swaths within each ping cycle, which can represent the end of the necessity of reducing swath width to get the better along-track coverage, as presented in Figure 5.1.

Figure 5.1a shows the effect of increasing the angular sector from 60^{o} to 75^{o}, when the larger two-way-travel time forces ping interval to increase. Therefore, along-track coverage density is reduced. In the other hand, wider angular sector (75^{o}) permits an increase in the across-track coverage and provides valuable lower grazing angle data. Figure 5.1b presents the sonar capable of transmitting multiple along-track swaths per ping and their ability to maintain simultaneous across-track and along-track coverage.

Therefore, with multiple swaths sonars, the extended outer traces logged should represent additional valuable data to be processed for seafloor classification purposes. When the outer beams launch angle is increased, the percentage of coverage of the seafloor with relation to the total swath is also increased.

With these perspectives, sample EM710 data were collected (with only one swath per ping at this time) and processed to bring a first overview of the possibilities that can be taken with this system. Data was acquired on-board Canadian Coast Guard Ship Matthew operating in the proximities of Halifax Harbour.

In this chapter, EM710 general characteristics are presented as well as the implemented algorithms, which allow the outermost beams artefacts reduction.

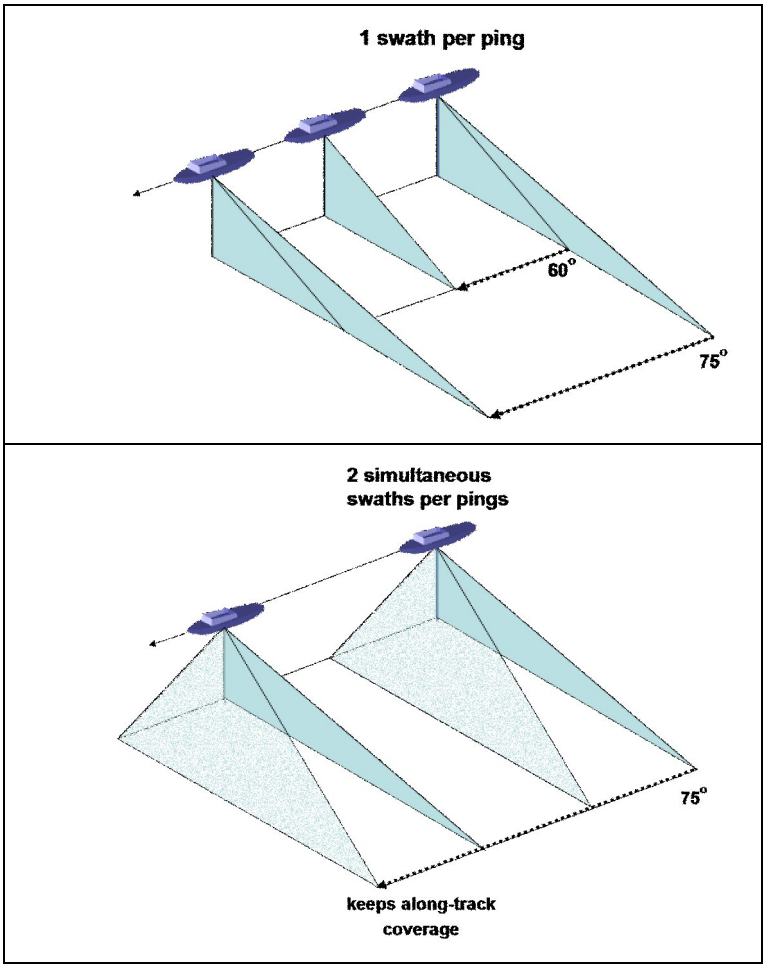

Figure 5.1 (a) Sonar with single across-track swath per ping cycle: The wider (75°) angular sector causes the reduction in ping frequency, which generates along-track gaps in the survey coverage. In the other hand, the narrow (60°) angular sector enables the ideal along-track coverage, but compromises the across-track coverage. (b) Sonar with multiple across-track swaths per ping cycle: the simultaneous swaths per ping permits to get both the along-track and across-track coverage when operating with wider (75°) angular sectors.

5.1 EM710 System description

EM710 sonar has operational frequencies between 70-100 KHz depending on transmitting sector. The system has three distinct transmission sectors, which can operate using different waveforms (continuous wave, continuous wave short or chirp).

Transducer arrays (used both for transmission and reception) can have small length (0.49 m) or large length (0.97 m), which enables beamwidths of 2^o and 1^o respectively.

Matthew uses the large arrays only. In addition, transmission has two sequentially positioned arrays, which produce a tighter transmit beam width of 0.5° like presented in Figure 5.2.

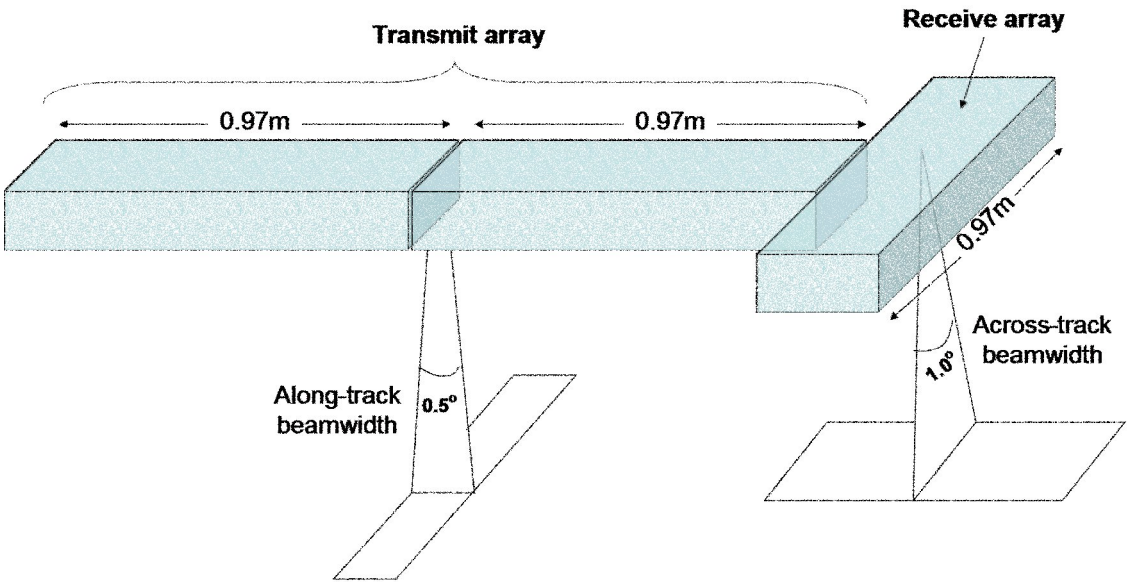

Figure 5.2 CCGS Matthew uses large transducer arrays (0.97m) only. Transmit total length is 1.94m, because two arrays are positioned sequentially. Therefore, it has transmit along-track beamwidth of 0.5° and receive across-track beam width of 1°.

Small arrays (2° RX beam width) have 128 beams, but can generate 200 beams when using high density mode. Large arrays (1° RX beam width) normally have 256 beams, but enable 400 beams in high density mode. When the 0.5° TX beam width is installed, system is going to provide two simultaneous swaths per ping cycle, which generates 800 beams (maximum number) in high density mode.

The transmission fan is electronically stabilized for roll, pitch and yaw. It is focused at the central expected range for each of the three sectors.

The receive beams are electronically roll stabilized and have dynamic focusing in the near field. Maximum transmission rate is up to 25 pings per second, which can be

undertaken in shallow depths. Equidistance beam spacing (EDBS) and equiangle beam spacing (EABS) modes are available.

Therefore, beam widths in this EM710 sonar are much tighter than the EM1000 sonar. But, EM710 still logs the outermost beams beyond the -3dB beam limits, which will extend their range as described in the next section.

5.2 Backscatter analysis and software implementations

The Figure 5.3 illustrates the beams pattern and the extended sector (~8%) reached when operating with only 65^{o} maximum launch angle.

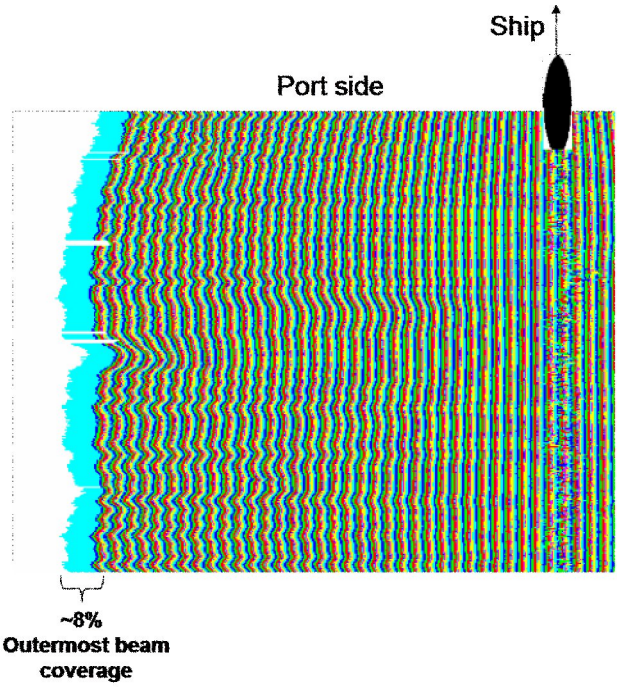

Figure 5.3 The EM710 beams operating in the EDBS +/-65^{o} mode with 0.5^{o} TX and 1^{o} RX beam widths. Outermost beams backscatter trace amplitudes correspond up to ~8% of the total swath.

The smaller extension of the coverage by using the outermost beam reflects both the more vertical incidence angle of the last beam (65º v. 75º) and the reduced RX beam

width (1.0º v. 3.3º). Using geometric calculation, outermost beams are expected to represent ~16% of the entire coverage when working on 75º.

The same processing steps applied for the EM1000 were followed for the outermost beams of the EM710 and results also demonstrated its validity. The pattern found for the port outermost beam is represented in Figure 5.4, where recorded data ranges over the beam -3 dB limits sector.

In this image also is presented the curve equation obtained with the least squares method as has been done for the EM1000. The parameters of the equation were used to normalize curve during processing.

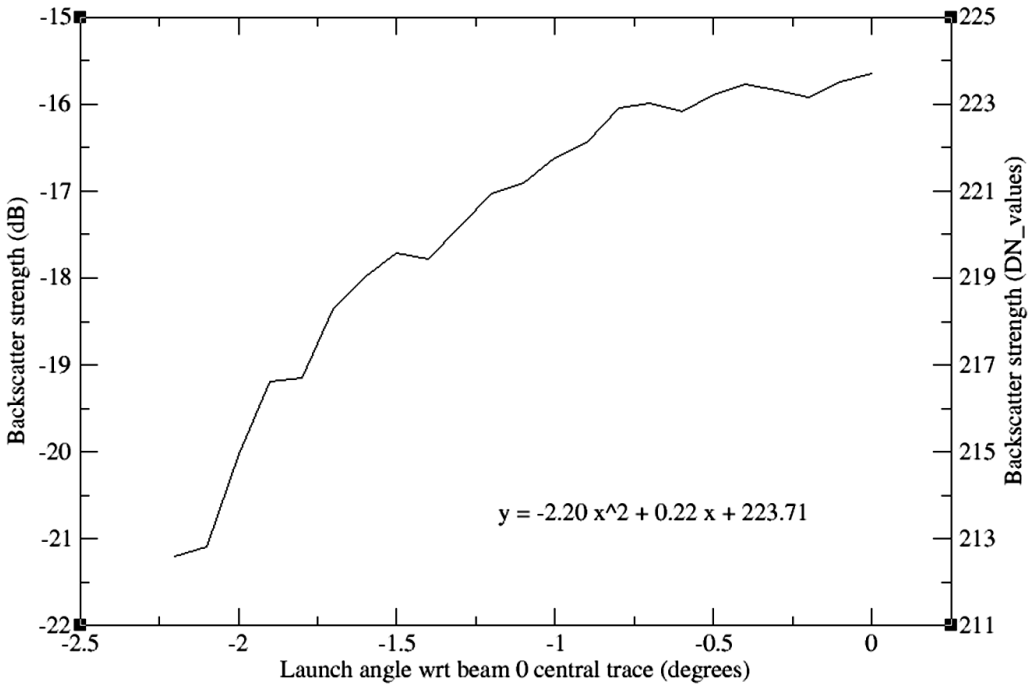

Figure 5.4 Port outermost beam average backscatter strength calculated for each 0.1 degree launch angle interval and quadratic equation obtained with least squares fitting method to be used for amplitude normalization.

Processing results are presented in Figure 5.5. Top image (a) is the raw backscatter. Centre image (b) was processed with *beampatt* software, which permitted to

reduce the artifacts 1, 2 and 3. Bottom image (c) was processed with *tracepatt*, which improved outermost beams quality (artifact 4).

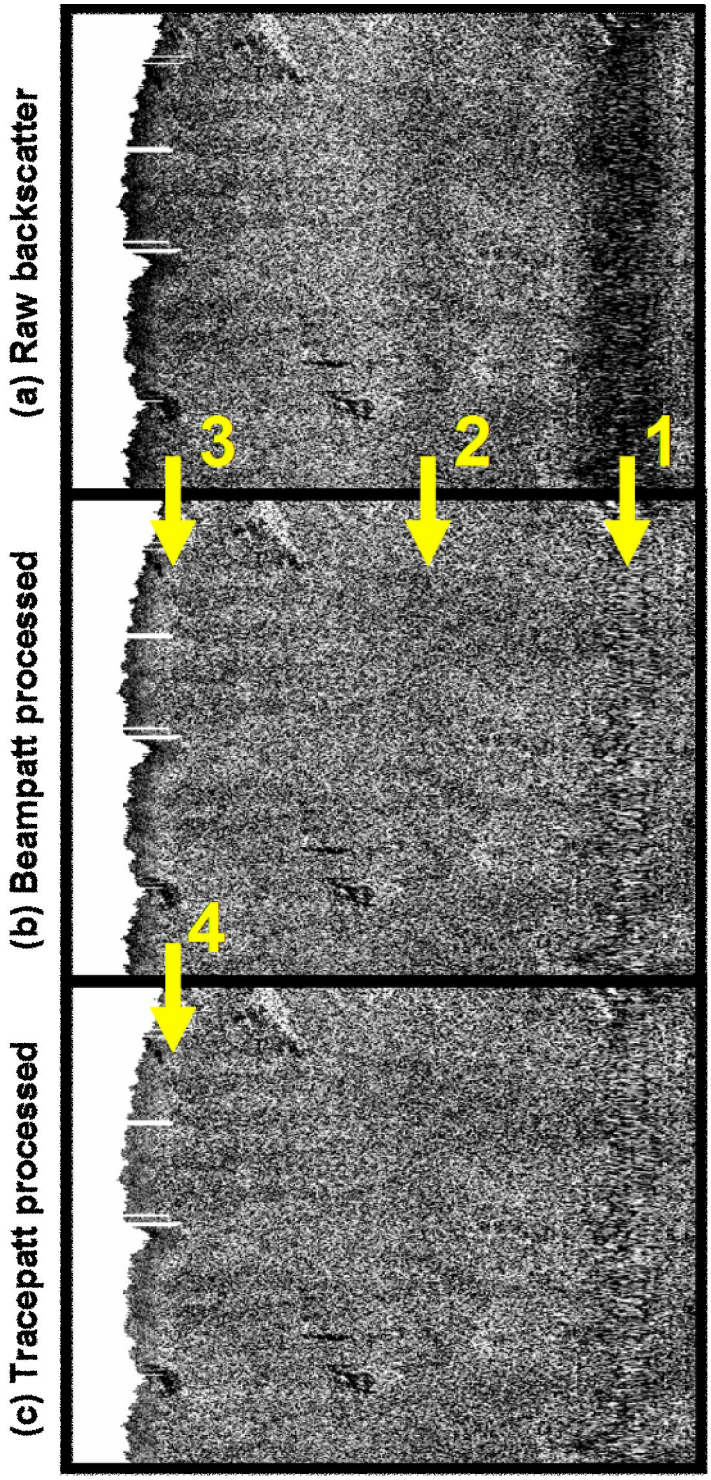

Figure 5.5 Results after each step of backscatter processing. Notice gradual image enhancement.

Chapter 6: CONCLUSIONS

The aim of this thesis was to enhance the EM1000 multibeam backscatter data processing. Data has been acquired by the Brazilian Navy since 1999 with sonar operated mostly in equiangle beamspacing (EABS) +/-75^{o} wide angular sector and survey lines spaced for 200% coverage.

The algorithm (*traceBP.c*) implemented here was able to normalize inside-beams directivity pattern. Special enhancements were obtained for the outermost beams, which record backscatter amplitudes beyond the -3 dB limits. Therefore, valid backscatter swath can now be extended up to 28%. In addition, other beams were benefited for reducing their usual small oscillations (2 dB to 3dB) or the greater oscillations (up to 10 dB) that occur when losing bottom tracking.

The recovered outer beams have been used to replace the noisy inner beams during mosaicking steps. To achieve that, a weighting function that applies higher weights to the outer beams was used, which is the reverse of traditional methods. Building on the improved mosaic quality, a parallel study was undertaken with image restoration techniques. In this study, a filter termed *bsfilter* (backscatter filter) has been implemented as a complimentary tool for reducing (in the spectral domain) noise in along-track direction normally present in the mosaics.

In an effort to take advantage of the improved and broader sidescan data, the OMG *classSS.c* classification algorithms have been adapted to accommodate the multibeam geometry. Modifications included a dynamically-located classification box scheme, which identifies and uses the most valuable region of the swath for statistical and power spectral analysis. As part of that, the software can detect outer swath range, utilize

full low grazing angle coverage and avoid noisy inner beams. Maps were produced to give more degrees of freedom for the seafloor characterization.

Finally, the EM1000 algorithms were implemented to process the outermost beams of the much newer sonar EM710. This newer sonar is going to use multiple swaths per ping cycle, which brings the possibility of using wide angular sectors in future surveys without compromising the along-track coverage.

REFERENCES

Alexandrou, D., C. de Moustier, and G. Haralabus (1992). "Evaluation and verification of bottom acoustic reverberation statistics predicted by the point scattering model." *The Journal of the Acoustical Society of America*, 91 (3), pp. 1403-1413.

Augustin, J.M., R. Le Suave, X. Lurton, M. Voisset, S. Dugelay, and C. Satra (1996). "Contributions of the multibeam acoustic imagery to the exploration of the sea-bottom." *Marine Geophysical Researches,* 18, pp. 459-486.

Augustin, J.M., and X. Lurton (2005). "Image amplitude calibration and processing for seafloor mapping sonars." *Proceedings of the Oceans'2005 Europe Conference*, 1, pp. 698-701, Brest, France, 20-23 June, 2005.

Beaudoin, J.D., J.E. Hughes Clarke, E.J.V.D. Ameele, and J.V. Gardner (2002). "Geometric and radiometric corrections of multibeam backscatter derived from Reson 8101 systems." *Proceedings of the Canadian Hydrographic Conference*, Toronto, Canada, 28-31 May, 2002.

Caris, (2005). "Caris HIPS/SIPS 6.0 User's Guide." Fredericton, Canada.

Carmichael, D.R., L.M. Linnett, S.J. Clarke, and B.R. Calder (1996). "Seabed classification through multifractal analysis of sidescan sonar imagery." *Proceedings of Radar, Sonar and Navigation*, 143 (3), pp. 140-148.

de Moustier, C. (1986). "Beyond bathymetry: mapping acoustic backscattering from the deep seafloor with Sea Beam." *The Journal of the Acoustical Society of America*, 79(2), p.316-331.

de Moustier, C., and D. Alexandrou (1991). "Angular dependence of 12-kHz seafloor acoustic backscatter." *The Journal of the Acoustical Society of America*, 90 (1), p.522-531.

Fonseca, L., and B. Calder (2005) “Geocoder: an efficient backscatter map constructor”. *Proceedings of the US Hydrographic Conference 2005,* San Diego, CA, USA, 29-31 March, 2005.

Francois, R.E., and G.R. Garrison (1982). “Sound absorption based on ocean measurements: part I: pure water and magnesium sulfate contributions.” *The Journal of the Acoustical Society of America*, 72 (3), pp. 896-907.

Francois, R.E., and G.R. Garrison (1982). “Sound absorption based on ocean measurements: part II: boric acid contribution and equation for total absorption.” *The Journal of the Acoustical Society of America*, 72 (6), pp. 1879-1890.

Hammerstad, E. (2000). “Backscattering and seabed image reflectivity.” Collected paper from Kongsberg, EM Technical Note.

Haralick, R.M. (1979). “Statistical and structural approaches to texture.” *Proceedings of the IEEE*, 67 (5), pp. 786-804.

Hellequin, L., X. Lurton, and J.M. Augustin (1997). “Postprocessing and signal corrections for multibeam echosounder images.” *Proceedings of the Oceans’97 Conference*, 1, pp. 23-26, Halifax, NS, Canada, 06-09 October, 1997.

Hellequin, L., J.M. Boucher, and X. Lurton (2003). “Processing of high-frequency multibeam echo sounder data for seafloor characterization.” *Journal of Oceanic Engineering,* 28 (1), pp. 78-89.

Hughes Clarke, J.E. (1994). “Toward remote seafloor classification using the angular response of acoustic backscattering: a case study from multiple overlapping GLORIA data.” *Journal of Oceanic Engineering*, 19 (1), pp. 112-127.

Hughes Clarke, J.E., L.A. Mayer, and D.E. Wells (1996). “Shallow-water imaging multibeam sonars: a new tool for investigating seafloor processes in the coastal zone and on the continental shelf.” *Marine Geophysical Researches*, 18, pp. 607-629.

Hughes Clarke, J.E., B.W. Danforth, and P. Valentine (1997). "Areal seabed classification using backscatter angular response at 95KHz." *Proceedings of the NATO SACLANT Conference CP-45*, Lerici, Italy, 30 June-04 July, 1997.

Hughes Clarke, J.E. (2004). "Seafloor characterization using keel-mounted sidescan: proper compensation for radiometric and geometric distortion." *Proceedings of the Canadian Hydrographic Conference*, Ottawa, ON, Canada, 25-28 May, 2004.

Hughes Clarke, J.E. (2005). "Acoustic backscatter data interpretation." UNB OMG/ UNH CCOM 38th Multibeam Sonar Training Course, Lecture Notes No. 20, Sydney, Australia, 18-23 July, 2005.

Hughes Clarke, J.E. (2005). "Sea bottom imaging with swath sonars." UNB OMG/ UNH CCOM 38th Multibeam Sonar Training Course, Lecture Notes No. 11, Sydney, Australia, 18-23 July, 2005.

Imen, K., R. Fablet, J.M. Boucher, and J.M. Augustin (2005). "Statistical discrimination of seabed textures in sonar images using co-occurrence statistics." *Proceedings of the Oceans'2005 Europe Conference*, 1, pp. 605-610, Brest, France, 20-23 June, 2005.

Intelmann, S.S., J.D. Beaudoin, and G.R. Cochrane (2006) "Normalization and characterization of multibeam backscatter: Koitlah Point to Point of the Arches, Olympic Coast National Marine Sanctuary Survey - HMPR-115-2004-03." Collected paper of the US Department of Commerce, Silver Spring, MD, USA, March, 2006.

Jackson, D.R., D.P Winebrenner, and A. Ishimaru (1986). "Application of the composite roughness model to high-frequency bottom backscattering." *The Journal of the Acoustical Society of America*, 79 (5), pp. 1410-1422.

Jackson, D.R., A.M. Baird, J.J. Crisp, and P.A.G. Thomson (1986). "High-frequency bottom backscatter measurements in shallow water." *The Journal of the Acoustical Society of America*, 80 (4), pp. 1188-1199.

Jackson, D.R., and K.B. Briggs (1992). "High-frequency bottom backscattering: roughness versus sediment volume scattering." *The Journal of the Acoustical Society of America*, 92 (2), pp. 962-977.

Kavli, T., M. Carlin, and R. Madsen (1993), "Seabed classification using artificial neural networks and other non-parametric methods." *Proceedings of the Institute of Acoustics, Acoustic Classification and Mapping of the Seabed*, 15(2), pp. 141–148.

Kongsberg Simrad, (2005). "EM710 multibeam echosounder, installation manual." Horten, Norway.

Linnett, L.M., S.J. Clarke, C. Graham, and D.N. Langhorne (1991), "Remote sensing of the sea-bed using fractal techniques." *Electronics & Communication Engineering Journal*, 3(5), pp. 195–203.

Llewellyn, K.C. (2006). *Corrections for the Beam Pattern Residuals in Backscatter Imagery from the Kongsberg-Simrad EM300 Multibeam Echosounder*. M.Eng. thesis, Department of Geodesy and Geomatics Engineering, University of New Brunswick, Fredericton, NB, Canada.

Lurton, X. and E. Pouliquen (1992). "Automated seabed classification system for echo-sonars." *Oceans'92 Conference IEEE*, 1, pp. 317-321, Newport, RI, USA, 26-29 October, 1992.

Lurton, X., S. Dugelay, and J.M. Augustin (1994). "Analysis of multibeam echo-sounder signals from the deep seafloor." *Proceedings of the Oceans'94 Europe Conference*, 3, pp. 213-218, Brest, France, 13-16 September, 1994.

Lurton, X. (2002). *An Introduction to Underwater Acoustics*. Springer-Praxis Publishing Ltd., UK.

Matsumoto, H., R.P. Dziak, and C.G. Fox (1993). "Estimation of seafloor microtopographic roughness trough modeling of acoustic backscatter data

recorded by multibeam sonar systems." *The Journal of the Acoustical Society of America*, 94 (5), pp. 2776-2787.

Miller, J.E., J.E. Hughes Clarke, and J. Patterson (1997). "How effectively have you covered your bottom?" *Hydrographic Journal*, 83, pp. 3-10.

Pace, N.G., and C.M. Dyer (1979). "Machine classification of sedimentary sea bottoms." *Transactions on Geoscience Electronics*, GE-17 (3), pp. 52–56.

Pace, N.G. and H. Gao (1988). "Swathe seabed classification." *Journal of Oceanic Engineering,* 13 (2), pp. 83-90.

Parker, J.R. (1997). *Algorithms for Image Processing and Computer Vision*. John Wiley & Sons, Inc., Canada.

Quester Tangent, (2005). "QTC Multiview user's manual." Sidney, Canada.

Reed, T.B., and D. Hussong (1989). "Digital image processing techniques for enhancement and classification of SeaMARC II side scan sonar imagery." *Journal of Geophysical Research*, 94 (B6), pp. 7469-7490.

Simrad Subsea, (1992). "EM1000 multibeam echosounder, product description manual." Horten, Norway.

Stanton, T.K. (1984). "Sonar estimates of seafloor microroughness." *The Journal of the Acoustical Society of America*, 75 (3), pp. 809-818.

Stewart, W.K., D. Chu, S. Malik, S. Lerner, and H. Singh (1994). "Quantitative seafloor characterization using a bathymetric sidescan sonar." *Journal of Oceanic Engineering*, 19 (4), pp. 599-610.

Tamsett, D. (1993). "Sea-bed characterization and classification from the power spectra of side-scan sonar data." *Marine Geophysical Research*, 15, pp.43-64.

Urick, J.R. (1983). *Principles of Underwater Sound.* 3rd. ed., Peninsula Publishing, USA.

BIBLIOGRAPHY

Ainslie, M.A., and J.G. McColm (1998). "A simplified formula for viscous and chemical absorption in sea water." *The Journal of the Acoustical Society of America*, 103 (3), pp. 1661-1662.

Alexandrou, D., and D. Pantzartzis (1990). "Seafloor classification with neural networks." *Proceedings of the Oceans'90 Conference*. Washington, DC, USA, 24-26 September, 1990.

Burczynski, J. (2001). "Bottom classification." Collected paper of the BioSonics Inc., USA. http://www.biosonicsinc.com/doc_library/docs/bottom_classification.pdf

Christensen, O., T. Thorsnes, L. Rise, K. Hovemoen, and A.Karlsen (2005). "Sediment classification by acoustic methods – ACOUSEC final report." Collected paper from the Geological Survey of Norway, report 2005.067.

Hamilton, E.L., and R..T. Bachman (1982). "Sound velocity and related properties of marine sediments." *The Journal of the Acoustical Society of America*, 72 (6), pp. 1891-1904.

Hou, T., L. Mayer, and C. de Moustier (n.d.) "Backscatter image normalization by best estimated grazing angles." Collected paper of the Center for Coastal and Ocean Mapping, University of New Hampshire, USA.

Huff, L.C., and L. Fonseca (2007). "A surprise occurrence in acoustic bottom backscatter measurements conducted in the eastern Bearing Sea." *Proceedings of the US Hydrographic Conference*. Norfolk, VA, USA, 14-17 May, 2007.

Masters, T. (1993). *Practical Neural Network Recipes in C++*. Morgan Kaufmann Publishers, USA.

Michalopoulou, Z.H., D. Alexandrou, and C. de Moustier (1995). "Application of neural and statistical classifiers to the problem of seafloor characterization." *Journal of Oceanic Engineering*, 20 (3), pp. 190-197.

Middleton, D. (1988). "S.O. Rice and the theory of random noise: some personal recollections." *IEEE Transactions on Information Theory*, 34 (6), pp. 1367-1373.

Parnum, I.M., P.J.W. Siwabessy, and A.N. Gavrilov (2004). "Identification of seafloor habitats in coastal shelf waters using a multibeam echosounder." *Proceedings of the ACOUSTICS'04 Conference*. Gold Coast, Australia, 03-05 November, 2004.

Preston, J.M., A.C. Christney, S.F. Bloomer, and I.L. Beaudet (2001). "Seabed classification of multibeam sonar images." *Proceedings from the OCEANS 2001 Conference*, Honolulu, USA, 05-08 November, 2001.

Preston, J.M., A.C. Christney, W.T. Collins (2004). "Automated acoustic seabed classification from swath images." Collected paper of the Iframer.

Smith, L.I. (2002). "A tutorial on principal component analysis." http://neurobot.bio.auth.gr/archives/000012a_tutorial_on_principal_components_analysis.php.

Sternlicht, D.D., and C.P. de Moustier (2002). "Near bottom sediment characterization offshore SW San Clemente Island." *Oceans'02 Conference IEEE*, v.4, pp. 2086-2092, Biloxi, MS, USA, 29-31 October, 2002.

Sternlicht, D.D., and C.P. de Moustier (2003). "Time-dependent seafloor acoustic backscatter (10-100 KHz)." *The Journal of the Acoustical Society of America*, 114 (5), pp. 2709-2725.

Sternlicht, D.D., and C.P. de Moustier (2003). "Remote sensing of sediment characteristics by optimized echo-envelope matching." *The Journal of the Acoustical Society of America*, 114 (5), pp. 2727-2743.

VITA

Candidate's full name: Aluizio Maciel de Oliveira Junior

Universities attended: University of New Brunswick
Fredericton, NB, Canada
September 2005 – July 2007
M.Sc.E. Geodesy and Geomatics Engineering

Directorate of Hydrography and Navigation
Rio de Janeiro, RJ, Brazil
January 1998 – December 1998
Extension Hydrography – Cat. A (IHO)

Navy School
Rio de Janeiro, RJ, Brazil
January 1991 – December 1994
B.Sc.E. Electronics

Conference Papers:

Oliveira Jr, A.M, and J.E. Hughes Clarke (2007). "Recovering wide angular sector multibeam backscatter to facilitate seafloor classification." *US Hydrographic Conference 2007,* Norfolk, VA, USA, 15-18 May 2007.